Heat expandable biopolymers for one-step production of foam core sandwich composites

PAR

Yonghoon YOON

acceptée sur proposition du jury:

Prof. C. Hébert, présidente du jury
Prof. J.-A. Månson, Dr J. C. Plummer, directeurs de thèse
Prof. S. Lundmark, rapporteur
Dr H. Kim, rapporteur
Prof. F. Sorin, rapporteur

EPFL

ÉCOLE POLYTECHNIQUE
FÉDÉRALE DE LAUSANNE

Suisse
2016

Acknowledgements

Abstract

The overall aim of this work has been to develop sustainable solid thermally activated foam precursors suitable for the in-line production of lightweight bio-based foam core sandwich structures with consolidated wood particle facings, using a non-inflammable, non-VOC (volatile organic compound) as a blowing agent. A preliminary study showed that expandable PLA (polylactide)/CO_2 could be prepared by impregnation of PLA, a commercially available bio-based polyester, with supercritical CO_2. However, the high processing temperatures, T, and pressures, P, associated with supercritical conditions resulted in premature foaming during the depressurization step, making it difficult to adapt this technique to the production of foam precursors in the particleboard process. In this thesis, PLA-based foam precursors were therefore prepared using impregnation in liquid CO_2 at moderate T and P. It was subsequently shown that the resulting heat-expandable materials could be successfully implemented in a simple one-step batch process for the manufacture of foam core particleboard, an important first step towards full implementation in a continuous process at the industrial scale.

The first part of the study involved determination of the optimum conditions for the impregnation of PLA with CO_2, so as to prepare foam precursors that were not only stable with respect to foaming at ambient T and P but also expanded readily at elevated T. Absorption and desorption of CO_2 from initially amorphous low and intermediate D-isomer content PLA was modeled using a concentration, c, dependent diffusion coefficient, $D[c]$, such that $D[c]=D[0]exp[Ac]$. The empirical constants $D[0]$ and A were obtained by modeling desorption results under various conditions. It was hence shown that CO_2 uptake by PLA at about 5 MPa and 10 °C was associated with a step-like concentration gradient, consistent with the morphologies observed in PLA specimens treated with liquid CO_2 for different times and then foamed. Further evidence in support of the model was obtained from observations of CO_2-induced crystallization in low D-isomer content PLA. The high melting temperature, T_m, of around 170 °C of the resulting crystalline phase nevertheless hindered subsequent foam expansion at T at and around 100 °C, i.e. the range of T associated with the particleboard process, which is turn fixed by the evolution of water vapor from the wood particles used to form the facings.

Crystallization could be avoided through use of fully amorphous PLA with an intermediate D-isomer content. Indeed, the significant reduction in the glass transition temperature, T_g, in the presence of high concentrations of CO_2, meant that amorphous specimens saturated under the chosen impregnation conditions, i.e. containing close to 40 wt% CO_2, tended to foam

spontaneously at room temperature, which is inconsistent with the stability requirements of the particleboard process. However, impregnation for a limited time, followed by partial CO_2 desorption at low T under conditions that could be inferred directly from the diffusion model, was shown to lead to solid foam precursors with a uniform CO_2 content of around 0.1 g/g. These were not only stable at room temperature, but contained sufficient CO_2 for the production of low density foams on heating.

The second part of the study was devoted to adjusting the thermal response of the precursors to better match the process conditions associated with the particleboard process, which imposed an expansion T of around 100 °C. This typically exceeded the effective T_g of the PLA/CO_2 by well over 40 °C, resulting in foam collapse during consolidation of wood particle facings. Fully amorphous PLA was therefore extrusion-compounded with poly(methyl methacrylate) (PMMA) in order to increase its T_g. The T_g of PLA-PMMA blends with a wide range of compositions was measured by differential scanning calorimetric (DSC) and the evolution of the corresponding α-transition was characterized by dynamic mechanical analysis (DMA). The uptake of liquid CO_2 during impregnation at 10 °C and 5 MPa was found to be dependent on PMMA content, but the subsequent desorption rates were comparable with those obtained for unmodified PLA. It was consequently possible to adapt the impregnation and conditioning procedure developed for unmodified PLA in order to prepare solid foam precursors from PLA-50 wt% PMMA blends, whose T_g better matched the processing window imposed by the particleboard process. The free expansion behavior of these precursors was investigated systematically as a function of T, and low density foams were successfully produced at foaming T of the order of 100 °C, as required by the particleboard process.

In a first attempt to produce fully sustainable foam precursors with comparable processing characteristics to the PLA-PMMA blends, based on previous observations of improved foaming characteristics in the presence of cellulose-based reinforcements during supercritical processing, the fully amorphous PLA was extrusion compounded either microcrystalline cellulose (MCC) or wood fiber (WF). In the present case, the high shear during processing broke up the WF somewhat, and the presence of residual moisture may also have led to hydrolysis of the PLA. Moreover, network formation and weak interfacial bonding as inferred from scanning electron microscopy (SEM) was argued to lead to significantly increased CO_2 desorption rates at high additive contents. It was nevertheless possible to obtain stable biocomposite foam precursors using suitable impregnation conditions, and foaming experiments were accordingly performed at different T. While the compression modulus at 25 °C of the resulting foams increased substantially as the additive content increased, severe shrinkage was observed during free expansion at 100 °C. Based on the results of relaxation measurements on the various compounds

and the predictions of the diffusion model, it was demonstrated that CO_2 retention times were too low in this range of T to sustain foaming over the times necessary to obtain structures that were stable with respect to viscoelastic recovery.

A possible way of stabilizing foam structures with respect to shrinkage was suggested to be to adjust the D-isomer content of the PLA in order to promote strain-induced crystallization during expansion, while reducing or suppressing crystallization during impregnation, which was shown previously to hinder foaming at and around 100 °C. A range of PLA with different D-isomer contents were therefore prepared by blending the low and intermediate D-isomer content PLA in the extruder, and DSC measurements confirmed a systematic decrease in the tendency to crystallize with increasing overall D-isomer content. Initially amorphous specimens of the blends were impregnated with liquid in CO_2 as previously, and the free foaming behavior investigated for fixed foaming times at different T. The resulting foam structures were found to vary markedly with the D-isomer content, 1.4 % D-isomer PLA showing limited expansion with a distinct semicrystalline skin-foam core structure, while substantial shrinkage persisted at 9.05 and 11.6 % D-isomer. However expansion of 3.95 % and 6.5 % D-isomer PLA at and around 100 °C resulted in low density foams ($\leq$ 100 kg/m^3), whose stability with respect to shrinkage could be attributed to strain-induced crystallization during the expansion step.

The final part of the work involved direct demonstration of the suitability of the various precursors for one-step foam core particleboard production, based on a batch process developed at Bern University of Applied Science (BUAS), Biel/Bienne, in which a layer of foam precursor was placed between two layers of wood particle mixed with a standard adhesive. A hot press was used to compress the resulting sandwich and consolidate the wood particle facings and then opened slightly to permit expansion of the foam core. By systematically adjusting the platen T, the process time and subsequent cooling rate, it was shown that PLA-50 wt% PMMA pellets impregnated with liquid CO_2 and conditioned to give a uniform CO_2 content of 0.12 g/g not only permitted straightforward handling but led to low density foam core particleboard with well consolidated wood particle facings and satisfactory adhesion between the facings and the PLA-PMMA foam core. The PLA-PMMA foam core itself had a density of about 100 kg/m^3 and showed superior mechanical properties to those obtained with commercial EPS (expandable polystyrene) foams with a comparable density, although limited adhesion at the boundaries of the original PLA-PMMA precursor pellets was suggested to lead to mismatch between the tensile and compression modulus of the PLA-PMMA foams. A first attempt was also made to use plaque-shaped foam precursors prepared from a commercial grade of PLA with an overall D-isomer content of 5 % and no additives. The 1 mm thick precursors, containing about 0.1 g/g of CO_2, showed easy handling at ambient T and P and highly promising foaming behavior, with little or

no foam collapse during foaming in the press. However, severe delamination was observed between the foam core and the wood particle facings owing to the lack of adhesion between the relatively crystalline skin of the expanded precursors and the wood particles. However, it is suggested that in future trials this problem may be overcome by incorporating an adhesive layer e.g. of fully amorphous (high D-isomer content) PLA at the surface of the precursor plaques.

In conclusion, a solid heat expandable foam precursor for the one-step particleboard process, based on a sustainable polymer matrix and a non-VOC blowing agent, has been successfully demonstrated. The accomplishments of this work, namely the establishment of processing windows for impregnation and *in situ* foaming of these materials under conditions consistent with the particleboard process, are expected not only to provide a firm basis for further development of a light weight particleboard process at the industrial scale, but also to open the way to further applications in e.g. insulation and packaging, in which *in situ* foaming in an open press would provide a simple means of producing lightweight PLA-based sandwich structures.

Keywords

Foam core particleboard, in-line foaming process, foam precursor, processing windows, polylactide, liquid CO_2

Résumé

Le but général de ce travail a été de développer un précurseur de mousse solide et durable, adapté à la production en ligne de panneaux sandwich légers avec des revêtements de bois aggloméré et un cœur de mousse de polymère. Ce précurseur doit être activé thermiquement et incorporer un agent moussant non combustible et non-VOC (composé organique volatil). Une étude préliminaire a montré que du PLA (polylactide)/CO_2 expansible pouvait être préparé par imprégnation du PLA, un polyester bio-sourcé commercial, avec du CO_2 supercritique. Cependant, les hautes températures, T, et pressions, P, associées aux conditions supercritiques provoquaient un moussage prématuré durant l'étape de dépressurisation, rendant cette technique difficilement adaptable à la production de précurseurs de mousse destinés à la fabrication de panneaux sandwich. Dans cette thèse, un précurseur de mousse, expansible à la chaleur, a donc été préparé par imprégnation de PLA avec du CO_2 liquide à T et P modérées. Il a été démontré par la suite que ce matériau pouvait être intégré avec succès dans un procédé de fabrication en une seule étape de panneaux de bois aggloméré à cœur de mousse. Cela représente un premier pas important vers son implémentation dans un procédé continu à l'échelle industrielle.

La première partie de l'étude a été consacrée à la détermination des conditions optimales d'imprégnation du PLA avec le CO_2, afin de préparer des précurseurs stables par rapport au moussage à T et P ambiantes, mais expansibles à haute T. L'absorption du CO_2 par du PLA initialement amorphe ayant une teneur en D-lactide faible ou intermédiaire, et sa désorption, ont été modélisées en utilisant un coefficient de diffusion, $D[c]$, dépendant de la concentration de telle sorte que $D[c]=D[0]exp[Ac]$. Les constantes empiriques $D[0]$ et A ont été déterminées en modélisant la vitesse de désorption dans différentes conditions. Il a été ainsi montré que l'assimilation du CO_2 par le PLA à 5 MPa et 10 °C environ était associée à un gradient de concentration sous forme de marche, ce qui était cohérent avec la morphologie de disques de PLA immergés dans du CO_2 liquide pendant différentes durées, et moussés par la suite. D'autres preuves à l'appui du modèle ont été obtenues à partir d'observations de la cristallisation induite par le CO_2 dans des disques de PLA de faible teneur en D-isomère. Cependant, la haute température de fusion, T_m, d'environ 170 °C de la phase cristalline limitait l'expansion ultérieure du PLA aux T autour de 100 °C, c'est-à-dire la plage de T caractéristique du procédé de fabrication de plaques de bois aggloméré, en raison de l'évaporation d'eau provenant des particules de bois.

La cristallisation pouvait être évitée en utilisant du PLA totalement amorphe avec une teneur en D-lactide intermédiaire. En effet, la réduction importante de la température de transition vitreuse, T_g, en présence de concentrations élevées de CO_2, impliquait que des disques de PLA saturés dans les conditions d'imprégnation choisies, c'est-à-dire contenant près de 40 wt% CO_2, avaient tendance à mousser de façon spontanée à la température ambiante, et ainsi ne remplissaient pas les besoins de stabilité du procédé de fabrication de bois aggloméré. Cependant, il a été démontré qu'une imprégnation de courte durée, suivie d'une désorption partielle du CO_2 à basse T d'une durée qui pouvait être déduite directement du modèle de diffusion, conduisait à des précurseurs de mousse solides avec une teneur en CO_2 uniforme d'environ 0.1 g/g. Ces derniers n'étaient pas seulement stables à la température ambiante mais contenaient également suffisamment de CO_2 pour la production de mousses de faible densité par chauffage.

La deuxième partie de l'étude était consacrée à une meilleure adaptation du comportement thermique des précurseurs aux conditions de mise en œuvre des revêtements d'aggloméré, qui imposaient une T d'expansion de 100 °C environ lors de la préparation des panneaux sandwich. Cette T dépassait typiquement de plus de 40 °C la T_g effective du PLA/CO_2, provoquant un affaissement de la mousse durant la phase de consolidation de l'aggloméré. Le PLA amorphe a donc été mélangé par extrusion avec du poly méthacrylate de méthyle (PMMA) afin d'en augmenter la T_g. La T_g de mélanges PLA-PMMA avec une large gamme de compositions a été mesurée par calorimétrie différentielle à balayage (DSC) et l'évolution de la transition α correspondante a été caractérisée par analyse mécanique dynamique (DMA). Il s'est avéré que l'assimilation du CO_2 liquide durant l'imprégnation à 10 °C et 5 MPa était dépendante de la teneur en PMMA, mais les vitesses de désorption obtenues par la suite étaient comparables à celles obtenues pour le PLA non modifié. Il a donc été possible d'adapter le procédé d'imprégnation et de conditionnement développé pour le PLA non modifié, afin de préparer des précurseurs à partir de PLA-50 wt% PMMA, dont la T_g correspondait mieux à la fenêtre de mise en œuvre imposée par les revêtements d'aggloméré. L'expansion de ces précurseurs a été étudiée systématiquement en fonction de T, et des mousses de faible densité ont été produites avec succès à 100 °C, conformément aux besoins du procédé de fabrication des panneaux sandwich.

Dans une première tentative de produire un précurseur de mousse entièrement bio-sourcé avec des caractéristiques de transformation comparables à celles des mélanges PLA-PMMA, et basé sur l'observation antérieure que le moussage du PLA imprégné avec du CO_2 supercritique est amélioré par la présence de renforts cellulosiques, le PLA amorphe a été mélangé par extrusion avec de la cellulose microcristalline (MCC) ou des fibres de bois (WF). Dans le cas présent, le cisaillement élevé durant l'extrusion provoquait une dégradation mécanique importante des WF et la présence d'humidité résiduelle conduisait vraisemblablement à l'hydrolyse du PLA. En outre,

la formation d'un réseau continu de contacts entre les fibres, et l'adhésion faible aux interfaces mise en évidence par microscopie électronique à balayage (SEM), provoquaient une augmentation importante de la vitesse de désorption de CO_2 lorsque la teneur en renfort était élevée. Il a été néanmoins possible d'obtenir des précurseurs de mousse bicomposite stables en utilisant des conditions d'imprégnation et de conditionnement appropriées, et de procéder à des tests de moussage à différentes T. Tandis que le module de compression à 25 °C des mousses obtenues augmentait considérablement avec le taux de renfort, une forte recouvrance élastique était observée suite à l'expansion libre à 100 °C. Sur la base de mesures de relaxation sur les différents mélanges et des prédictions du modèle de diffusion, il a été montré que les temps de rétention du CO_2 étaient trop courts dans cette gamme de T pour permettre la stabilisation des mousses par rapport à la recouvrance élastique.

Il a donc été proposé de stabiliser les structures de mousse par rapport à la recouvrance en ajustant la teneur en D-lactide du PLA de manière à obtenir une cristallisation induite par déformation pendant l'expansion, tout en réduisant ou en supprimant la cristallisation pendant l'imprégnation, qui avait pour effet de limiter le moussage à T autour de 100 °C comme il avait été démontré auparavant. Des PLA contenant des taux de D-lactide différents ont donc été préparés en mélangeant par extrusion un PLA de faible teneur en D-lactide et un PLA de teneur en D-lactide intermédiaire. Des mesures de DSC ont confirmé une réduction systématique de la tendance à cristalliser lorsque la teneur en D-lactide augmentait. Des disques préparés à partir de ces mélanges, et initialement à l'état amorphe, ont été imprégnés avec du CO_2 liquide et conditionnés suivant la méthode établie précédemment, et leur expansion libre a été étudiée en fonction de T pour un temps d'expansion fixe. La structure des mousses obtenues variait sensiblement en fonction de la teneur en D-lactide. Le PLA 1.4 % D-lactide montrait une expansion limitée avec une structure cœur expansé-écorce semicristalline, tandis qu'à 9.05 et 11.6 % de D-lactide une recouvrance importante était observée. Par contre, à 3.95 % et 6.5 % de D-lactide, le moussage à 100 °C conduisait à des mousses de faible densité (≤ 100 kg/m^3) d'une stabilité accrue, attribuée à une cristallisation induite par déformation pendant l'expansion.

La dernière partie du travail avait pour but une démonstration directe de la pertinence des différents précurseurs développés au cours de ce travail à la production en une étape de panneaux sandwich, basée sur un procédé développé par la Haute École Spécialisée Bernoise (BUAS), Bienne, dans lequel une couche de précurseur de mousse est placée entre deux couches de fibres de bois mélangées avec un adhésif standard. Une presse chauffante a été utilisée pour comprimer ce sandwich et consolider les revêtements d'aggloméré. Ensuite la presse est légèrement ouverte pour permettre l'expansion du cœur. En ajustant systématiquement la T du plateau, la durée de l'étape de compression et la vitesse de refroidissement ultérieure, il a été montré que des granulés

PMMA de PLA-50 wt%, imprégnés de CO_2 liquide et conditionnés afin d'assurer une teneur uniforme en CO_2 de 0.12 g/g, non seulement étaient facile à manipuler, mais permettaient aussi la fabrication de panneaux de faible densité avec des revêtements d'aggloméré bien consolidés et une adhésion satisfaisante entre les revêtements et le cœur de mousse PLA-PMMA. Le cœur de mousse PLA-PMMA lui-même avait une densité d'environ 100 kg/m^3 et possédait des propriétés mécaniques supérieures à celles obtenues avec des mousses de EPS (polystyrène expansible) commercial de densité comparable, bien que l'adhésion plutôt faible entre les granulés de PLA-PMMA conduisait vraisemblablement a une disparité entre les modules de Young et de compression de la mousse PLA-PMMA. Une première tentative a aussi été réalisée avec des précurseurs de mousse sous forme de plaque préparés à partir d'un PLA commercial avec une teneur en D-lactide de 5 % sans adjuvants. Les précurseurs, d'une épaisseur de 1 mm, contenant environ 0.1 g/g de CO_2, se sont révélés faciles à manipuler aux T et P ambiantes et avaient un comportement très prometteur au niveau du moussage, avec peu ou pas recouvrance élastique dans la presse. Cependant, des délaminages importants entre le cœur de mousse et les revêtements d'aggloméré ont été observés en raison d'un manque total d'adhésion entre la peau relativement cristalline des précurseurs expansés et les fibres de bois. Toutefois, il serait possible dans des tentatives futures de surmonter ce problème en incorporant une couche d'adhésif, p.ex. du PLA totalement amorphe (d'une teneur en D-lactide plus élevée) à la surface des plaques du précurseur.

En conclusion, un précurseur de mousse solide et expansible à la chaleur, adapté à la fabrication de panneaux sandwich en une seule étape, et basé sur une matrice de polymère durable et un agent moussant non-VOC, a été démontré avec succès. Les réussites de ce travail, à savoir la détermination de fenêtres de mise en œuvre pour l'imprégnation et le moussage *in situ* de ces matériaux dans des conditions représentatives de celles du procédé de fabrication des panneaux, fourniront non seulement une base solide au développement futur de panneaux sandwich légers au niveau industriel, mais ouvriront aussi la voie à des applications futures dans des domaines tels que l'isolation ou l'emballage, où le moussage *in situ* dans une presse ouverte serait un moyen simple de produire des structures sandwich légère à base de mousse de PLA.

Mots-clés

Panneau d'aggloméré à cœur de mousse, procédé de moussage en ligne, précurseur de mousse, fenêtres de mise en œuvre, polylactide, CO_2 liquide

Contents

Chapter 1

Introduction

1.1 Motivation and challenges

Over the past few decades, an increased need for wood composites has emerged as a result of two main driving forces: the demand for engineered wood products with characteristics superior to those of solid timber and the desire to reduce raw materials costs. Wood-based composite panels are widely used in the furniture, building and packaging industries. The densities of particleboard (PB) and medium density fiberboard (MDF) are 550 - 650 and 550 - 800 kg/m^3, respectively, but the panel industry requires lighter materials for two main reasons: (i) a strong increase in wood prices in recent years, as shown in Figure 1.1 [1], (ii) a need for easier handling and reduced transport costs owing to the development of the take-away furniture market and trade via internet. However, while many attempts to produce replacements for natural wood have achieved lower densities [2–5], the mechanical properties of the resulting products typically do not reach the levels associated with conventional particleboard, and the complex process steps tend to increase production costs.
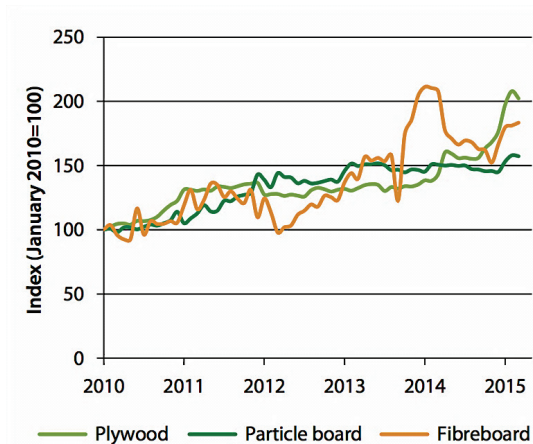
Figure 1.1 Monthly price change for wood-based panels [1].

The main purpose of the present research is to develop a novel sustainable foaming system for lightweight foam core particleboard compatible with an in-line production process in which foaming and consolidation of the particleboard take place in a single step. It is thus hoped to achieve industrial viability through simplified manufacture and hence reduced production costs. To accomplish this goal, new solid-state foam precursors based on a bio-sourced polymer matrix and a non-VOC blowing agent have been investigated. Process windows have been defined for the *in situ* foaming of these precursors during particleboard consolidation, enabling the development of industrially viable lightweight particleboard through materials, process and performance optimization.

This work is of both environmental and industrial interest, implying reduced consumption of wood and fossil-based resources to give equivalent or superior properties. However, it has also involved significant challenges. One of the most important of these is defining the composition of precursor system. Sufficient amounts of blowing agent (BA) must be introduced into the precursor matrix to ensure dense, homogeneous pore nucleation at the process temperature, but the precursor should remain stable with respect to foaming and loss of the BA during storage and handling. High solubility and low diffusivity of the BA in the matrix are therefore critical. However, green BAs, e.g. water, N_2 and CO_2, have poor solubility in most commercial plastics, and high solubility may imply excessive softening of the matrix owing to plasticization effects. The thermal properties of the matrix are also clearly of major importance for the heat resistance and long-term stability of the final product.

1.2 Approach

As set out in Section 1.1, the objective of this thesis was to develop an ecologically friendly foaming system for economically viable ultra-light foam-core particleboard production. The production cost of the foam core precursor should ideally be below 2 €/kg for an overall panel thickness of 13-19 mm [6], and the foaming step should be compatible with the conventional in-line particleboard process. The foam precursor is therefore required to take the form of a solid pellet or granulate. Moreover, to meet safety requirements and to satisfy the increasing demand for sustainable technology, the foaming system should be based on a non-flammable, non-VOC

BA and a bio-sourced and/or biodegradable matrix. Pelletized poly(lactide) (PLA) based matrices were initially chosen for study, modified by melt compounding where necessary. The BA was CO_2, introduced into the foam matrix in liquid form at 10 °C and 5 MPa, i.e. conditions of relatively low temperature and pressure [7,8]. Foaming of expandable solid polymer precursors in a semi-open mold for green foaming systems such as PLA/CO_2 has not so far been described in any detail in the literature. A knowledge of the time-temperature-pressure dependence of the solubility and diffusivity of the BA in the polymer matrix is particularly important for determining the conditions under which foaming is likely to be possible for a given process and process geometry. Understanding and defining process windows therefore necessitated careful characterization of the matrix and its compatibility with BA. The concentration dependent diffusion behavior of CO_2 in PLA has been modeled numerically, and the results validated experimentally [8].

While it has been possible to adapt amorphous high D-isomer content PLA/CO_2 processing methods to produce solid precursors that are compatible with the particleboard process, the relatively low softening temperature of amorphous PLA severely limits its usefulness in structural applications. Moreover, the processing window for the foaming of amorphous PLA in an open press shows only limited overlap with those of typical skin layer materials, restricting both the choice of these latter and the extent to which foaming conditions may be optimized. In a first approach to overcoming these difficulties, blending with poly (methyl methacrylate) (PMMA) has been investigated. PMMA has a significantly higher glass transition temperature, T_g, than PLA, and PLA/PMMA blends are known to be at least partly miscible [9]. The thermal, mechanical and foaming behavior of a range of such blends has been studied, based on the same methodology as for the pure PLA.

PMMA nevertheless has the disadvantage of being a synthetic petroleum-derived material. As an alternative route to a fully sustainable PLA-based foam material with improved properties, incorporation of natural cellulose fiber (wood fiber (WF) and microcrystalline cellulose (MCC)) has been investigated as a means of reinforcing the foam cell, as was demonstrated previously at LTC by Boissard *et al*. for PLA foams prepared using a supercritical process [10].

The possibility of using crystallisable PLA with a low D-isomer content was also investigated, given the superior heat resistance of this material compared with that of fully amorphous PLA. In

the open literature, low density foams have been demonstrated using PLAs with a range of isomeric contents [11], but in the present case, premature crystallization during impregnation was found to prevent expansion in the temperature range of interest for the particleboard consolidation. The focus was therefore on the feasibility of obtaining semicrystalline PLA foaming precursors whose processing windows matched those of a single step particleboard consolidation in a hot press, via careful control of the degree of crystallinity at each processing step through a suitable choice of D-content and processing parameters.

The final stage of the project was the optimization of the structure and physical properties of foam core sandwich structures based on the various precursors by tailoring the process parameters, and assessment of their potential for scale-up using a semi-industrial scale hot press under conditions representative of the particleboard process. This part of the work was carried out in close collaboration with the project partner, Bern University of Applied Science (BUAS).

1.3 Organization of this report

The organization of this thesis is shown schematically in Figure 1.2. Chapter 2, which describes the state of the art, covers both foam core particleboard and processing of bio-based foam materials. This provides the fundamental concepts required for subsequent chapters. The experimental approach is defined in Chapter 3, along with the selected foam precursor materials (polymers, blowing agent and fillers), and the processing and characterization techniques. The diffusion behavior of CO_2 and the influence of crystallization on CO_2 diffusion are discussed Chapter 4. Chapter 5 then describes the foaming behavior of PLA-PMMA blends. Efforts to develop fully sustainable PLA biocomposite foams with cellulose based reinforcements and PLA with controlled D-isomer contents are presented in Chapter 6 and Chapter 7, respectively. The implementation of the materials in the particleboard process is described in Chapter 8 and, finally, the overall conclusions and outlook are given in Chapter 9.
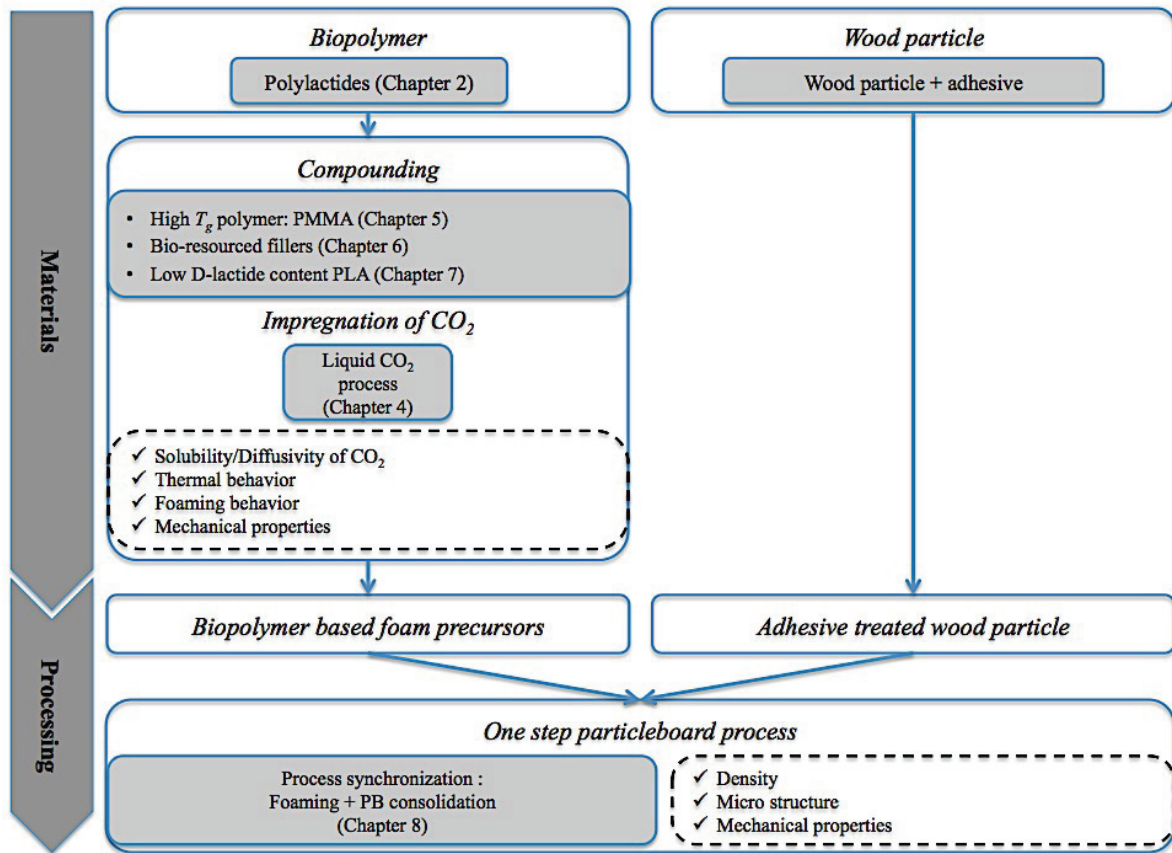
Figure 1.2 Outline of the approach adopted in this thesis and the organization of the work.

Chapter 2

State of the art

This chapter begins with a short introduction to wood composites, for which efforts to achieve low density wood composite panels are briefly surveyed, and foam core sandwich structures are highlighted as one of the most promising routes to lightweight panels. This is followed by a general discussion of polymer foaming, existing foam core particleboard technology and PLA foaming. The aims of the chapter are to establish not only the significance of this thesis work, but also the characteristics and processing windows of typical skin and core layer materials, providing a foundation for the experimental approach to the development of novel foam core precursors, including materials selection and process optimization, to be presented in subsequent chapters.

2.1 Introduction

Low-density wood composites

As briefly discussed in Section 1.1, there has been increasing interest in the development of lightweight wood composites for a wide range of applications such as furniture, building and packaging materials. A variety of techniques have been used in an attempt to produce cost effective lightweight wood composites, for example, using alternative wood species or agricultural residues [2,4,12], new adhesive systems, increased resin contents and optimized board density profiles [3,13–16]. Although the composites produced by the aforementioned methods lead to significant density reductions, important properties such as the internal bond (IB) strength and bending strength tend to be compromised. On the other hand, sandwich panels with faces from thin particleboard or medium density fiberboard (MDF) and cores made from honeycomb paper [5], very light wood species [12] or foams [17,18] have been demonstrated to meet many property requirements while offering substantial weight reduction. However, high production

costs owing to multiple production steps have restricted application of these materials. Recently, in an effort to reduce costs, a novel one-step process for the production of foam core particleboard was proposed using commercial polymeric foaming materials such as expandable polystyrene (EPS) and expandable micro spheres (MS) [19–25].

General notions regarding foaming

Natural cellular materials have been used wherever a high strength to density ratio is required, examples being wood, cork and bone. Man-made cellular materials are increasingly employed in consumer and industrial goods in the form of foamed ceramics, metals and polymers [26].

Foaming typically occurs when dissolved or physically incorporated gas molecules generate bubbles in a softened matrix material. This is usually a result of abrupt changes in external conditions such as temperature and pressure, or changes in the material itself, preventing a smooth response of the system. This type of foaming may therefore be regarded as a transition from a metastable state to a stable state [27], and the degree of super-saturation of the gas in the polymer matrix is often the primary driving force for cell nucleation and growth [26].

It follows that polymeric foams are typically manufactured from at least two materials: a polymer matrix and a blowing agent (BA), which are associated either physically or chemically. The polymeric matrix may be thermoplastic or thermoset depending on the chain connectivity. BAs can be categorized into two types, based on the gas generation mechanism: physical blowing agents (PBAs) and chemical blowing agents (CBAs).

PBAs do not alter the composition of a given system, but may change its physical state. They may be introduced into the polymer matrix using three main methods: (i) physical blending, (ii) physical dissolution, (iii) chemical reaction or encapsulation. Physical blending and dissolution are most common for high output production such as foam extrusion. Under high pressure, a gaseous PBA may be compressed into a sub- or supercritical state [28]. It is then blended or dissolved in either the solid polymer or polymer melt, depending on temperature, to form a metastable polymer/gas system. This metastable system may then be foamed using a pressure drop and/or temperature increase to initiate cell nucleation and growth.

CBAs generate gas molecules by reaction or thermally induced decomposition. A wide range of CBAs have been commercialized for extrusion and injection foaming. However, processing is not necessarily straightforward. Because chemical reactions may generate excessive heat, the thermal behavior of the polymer and heat management may be crucial to process optimization. However, the main disadvantage of CBAs with respect to PBAs in the present application is that they usually result in relatively high foam densities, i.e. 500 - 700 kg/m^2 as opposed to 100 - 500 kg/m^2 for foaming with PBAs [26].

In a PBA assisted process, foaming may be divided into 4 steps, depending on the interaction between the gas and polymer: (i) gas diffusion and dissolution; (ii) cell nucleation; (iii) cell growth; (iv) stabilization. In this thesis, the PBA was allowed to diffuse into the solid polymer in a pressure chamber. Cell nucleation was then initiated in the resulting polymer/gas precursors by increasing the temperature in order to soften the polymer matrix. Once the initial pores were formed, they grew as additional gas molecules diffused from the matrix. The foaming temperature was maintained for a predetermined expansion time and the cellular structure was finally stabilized by cooling to below the softening temperature, i.e. the glass transition temperature or melting temperature of the polymer. This foaming procedure is shown schematically in Figure 2.1.
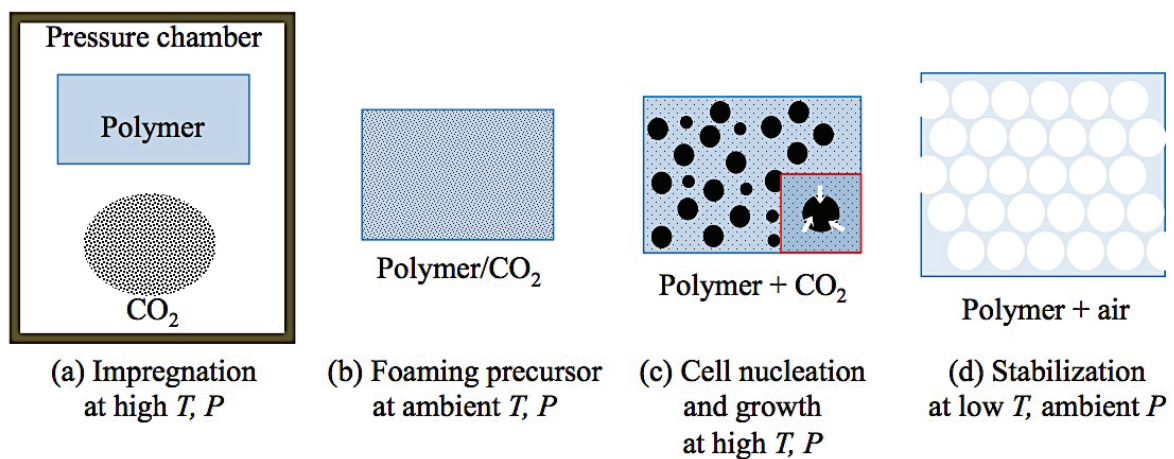
Figure 2.1 Schematic of the foaming procedure employed in this thesis.

The diffusion process may be described by Fick's second law

$$\frac{\partial C}{\partial t} = \nabla(D\nabla C) \qquad (2.1)$$

such that the change in gas concentration with time, $\frac{\partial C}{\partial t}$, is a function of concentration gradient, ∇C, and D is the diffusion coefficient or "diffusivity". Table 2.1 gives examples of the measured solubility, the maximum gas content and calculated diffusivity of CO_2 in different polymers under different conditions.

Table 2.1 Solubility and diffusivity of CO_2 in different types of polymer matrix.

	Solubility [wt%]	Diffusivity [cm^2s^{-1}]	Test conditions
PLA [29]	16.4	6.7	5.52 MPa, 25 °C
PS [30]	0.8	N/A	6.90 MPa, 25 °C
Polyvinylchloride (PVC) [31]	8.6	1.7	5.52 MPa, 25 °C

Numerous variables influence gas diffusion in polymers, but temperature, pressure, crystallinity of the polymer and the interaction between gas and polymer are generally considered to be the most important parameters for a given diffusing species. The diffusion rate increases as the temperature increases because the gas molecules acquire sufficient energy to move from one equilibrium state to another [30,32]. Increased pressure can also promote gas diffusion in a solid polymer, but results in reduced diffusivity in a polymer melt owing to reduced free volume [33,34]. Crystalline phases are known to have lower gas permeability than the amorphous phases so that the diffusion rate is typically reduced as the degree of crystallinity increases [8,31,35]. Finally, specific intermolecular interactions may retard diffusion. For example, the carbonyl group of PLA and CO_2 show strong Lewis acid-base bonds which lead to slower diffusion [34].

For a given system, the solubility, S, depends primarily on pressure, P, and temperature, T. The gas concentration, C, is then given by Henry's law:

$$S(T) = \frac{C}{P} \qquad (2.2)$$

Determining the solubility is of particular importance for the optimization of the gas concentration with respect to the processing variables during the impregnation step, and materials properties such as the crystallization behavior of the polymer, specific interactions between the gas and polymer and the presence of additives [28,30,35–41].

The cell density, the number of cells per unit area or volume and the cell distribution are established at the nucleating step. Three types of nucleation are generally considered: (i) homogeneous, (ii) heterogeneous and (iii) mixed nucleation [26]. According to Colton J *et al.* the homogeneous nucleation rate, N_{Homo}, may be expressed by [42]

$$N_{Homo} = C_0 f_0 exp\left(\frac{-\Delta G_{Homo}}{kT}\right) \qquad (2.3)$$

$$\Delta G_{Homo} = \frac{16\pi\gamma^3}{3\Delta P^2} \qquad (2.4)$$

where C_0 is the concentration of the gas dissolved in the matrix, f_0 is a frequency factor for the gas molecules, ΔG_{Homo} is the free energy for homogeneous nucleation, k is the Bolzman constant, T is temperature, γ is the interfacial tension and ΔP is the pressure difference. According to this equation, the gas concentration and interfacial energy at the gas-polymer interface are important parameters for homogeneous nucleation.

The activation energy for heterogeneous nucleation is lower than for homogeneous nucleation and it typically occurs when additives are present. The heterogeneous nucleation rate is given by

$$N_{Het} = C_1 f_1 exp\left(\frac{-\Delta G_{Het}}{kT}\right) \qquad (2.5)$$

$$\Delta G_{Het} = \Delta G_{Homo} S(\theta) \qquad (2.6)$$

$$S(\theta) = \frac{1}{4}(2 + cos\theta)(1 - cos\theta)^2 \qquad (2.7)$$

where C_1 is the concentration of heterogeneous sites, f_1 is the frequency factor and θ is the wetting angle between the gas and the additives.

Mixed nucleation is the combination of the both nucleation mechanisms. Because heterogeneous nucleation is associated with a low activation energy, it may consume of the blowing agent prior to homogeneous nucleation. The reduced gas concentration, C'_0, and the modified homogeneous nucleation rate, N'_{Homo}, is then given by

$$C'_0 = C_0 - N_{Het} t n_b \qquad (2.8)$$

$$N'_{Homo} = f_0 C'_0 \exp\left(-\Delta G^*_{Homo}/kT\right) \qquad (2.9)$$

where t is time, n_b is number of gas molecules in a bubble formed by heterogeneous nucleation and ΔG^*_{Homo} is the free energy after change by heterogeneous nucleation. The overall nucleation rate, N, is then

$$N = N'_{Homo} + N_{Het} \qquad (2.10)$$

The concentration difference between the interior and exterior of the bubble is the major driving force in cell growth [26]. The blowing agent diffuses from the gas-rich polymer/gas phase towards the cell nuclei. The main force opposing cell expansion are viscoelastic forces and the surface tension of the polymer. The diffusion rate should be high enough to overcome these forces, but if it is too high, the blowing agent will tend to escape from the system before foaming and/or stabilization is complete. Therefore, care must be taken in choosing process parameters that affect the diffusion rates, and in particular the temperature and the overall specimen dimensions.

The resulting cellular structure is frozen at temperatures below the glass transition temperature, or the melting temperature of the polymer in cases where crystallization during foaming contributes to stabilization [11,43,44]. It is significant in this respect that small gas molecules such as CO_2 may substantially modify the thermal behavior of polymer matrices through plasticization. Thus the glass transition temperature decreases and crystallization rates increase at a given temperature depending on the CO_2 content and its evolution during foaming [8,35,45].

One well-known PBA-based polymeric foaming material is expandable polystyrene (EPS), which is composed of polystyrene (PS) as the matrix and typically 4 to 7 % n-pentane as the blowing agent. Amorphous PS with a glass transition temperature of around 100 °C is used to form 0.2 mm to 3 mm diameter EPS beads and the blowing agent is added during the polymerization step. A chest molding technique is widely employed to foam EPS beads and is generally carried out in

two steps: pre-expansion and molding. In the pre-expansion step, the beads are treated with hot air and/or steam to adjust their density to around 64 kg/m^3 and the cavity of the mold is then filled with the pre-expanded beads. Steam at a temperature of about 110 °C is introduced into the mold, inducing further expansion of the beads [46]. Although EPS products with a wide range of foam densities, from 8 to 64 kg/m^3, are used in various applications [46], the hazardous nature of the blowing agent, which is a volatile organic compound (VOC) and is explosive at concentrations of more than 1.3 % by volume [17], makes it unsuitable for a particleboard process that makes use of an open press (see 2.2.1). Efforts to develop EPS beads using water as a blowing agent have been described in the literature [47–49]. However, premature loss of the blowing agent was reported and the resulting foam densities are relatively low.

Another PBA assisted foaming material of potential interest for foam core particleboard consists of expandable microspheres (MS). As shown in Figure 2.2, the MS in question are hollow polymeric beads containing a blowing agent. Typically, the shell material is a copolymer of acrylonitrile (AN) and other monomers such as methyl methacrylate (MMA), methyl acrylate (MA), and methacrylonitrile (MAN) [50]. The polymer composition is crucial for the foaming process through it influence on the gas barrier properties and thermal behavior of the shell. The blowing agent is isobutene, with a boiling point of -11.7 °C. When the MS are heated, the thermoplastic shell softens and the low boiling point hydrocarbon increases the internal pressure leading to a density of as low as 25 kg/m^3 [51]. This foaming technology is available on the market but a major limitation with regard to the particleboard process is that it again relies on an inflammable VOC as the foaming agent [17]. Moreover, neither EPS nor expandable MS are bio-based or biodegradable.
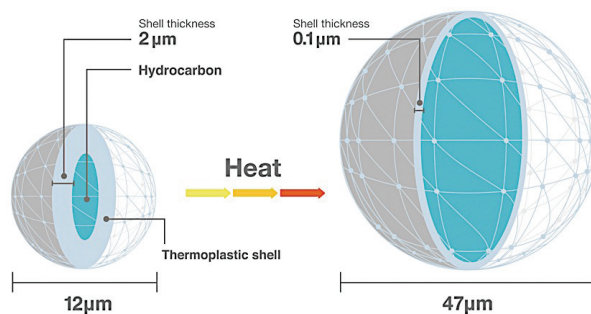
Figure 2.2 Schematic of the expansion mechanics of expandable microspheres (MS) [www.akzonobel.com].

2.2 Foam core particleboard

In Section 2.1, lightweight wood composites were briefly introduced and foam core particleboard was suggested to be the most promising method to achieve density reduction and satisfactory mechanical performance. Moreover, a general description of polymer based foaming was given and the limitations of petroleum-based matrices and inflammable or toxic blowing agents were explained. In what follows, a new process for the production of foam core particleboard by a single step process will be introduced.

2.2.1 Fabrication of foam core particleboard from one step process

Although a strong demand for lightweight panels has been identified [18] and various strategies for weight reduction in furniture have been tried over the last few decades, there are still no economically viable lightweight panels on the market for standard furniture parts of 13 to 19 mm thickness.
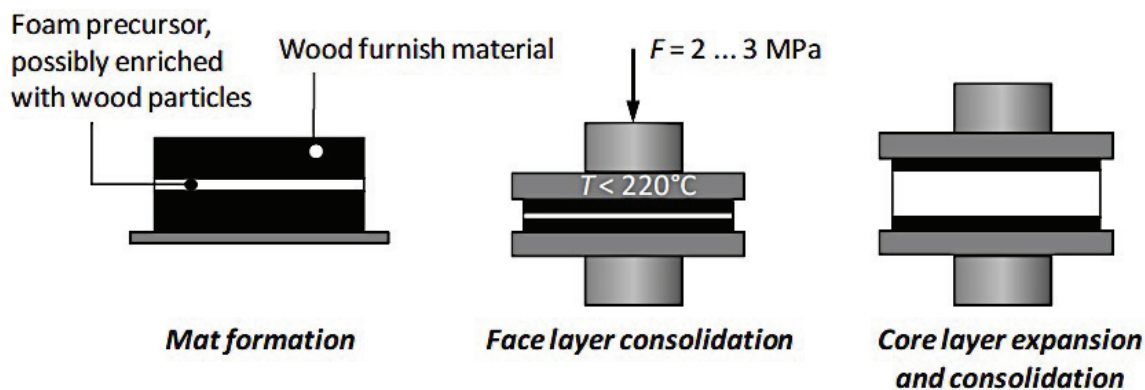
Figure 2.3 Concept of the in-line foam core particleboard process [18].

The lack of lightweight solutions has been the driving force for the development of the in-line foaming technology for manufacturing the foam core particleboard [17,18,52]. Figure 2.3, shows a model one-step process based on the conventional and relatively cost-efficient particleboard process. A three layered mat is formed from adhesive-treated wood particle surface layers and a

foam precursor core layer. Consolidation and foaming take place in a hot press. When the temperature of the core layer has reached the level needed to activate the foam precursor, the press is slightly opened to give room for the core material to expand. Finally, the panel is cooled to stabilize the foam. The inventors used EPS and MS as the core layer materials, and were able to achieve a core density of 120 to 180 kg/m^3, resulting in an average panel density of 300 to 500 kg/m^3 depending on the thickness and formulation of the surface layers. Adequate interfacial wetting was also obtained as shown in Figure 2.4. The specific mechanical properties of the panels were demonstrated to be significantly better than the requirements of conventional particleboard (Figure 2.5) [17]. Further investigation showed these panels can be machined and post-processed [18].

Figure 2.4 Micrographs of the interface between wood particles and foams (A: EPS, B: MS) produced by the in-line foaming process [17].
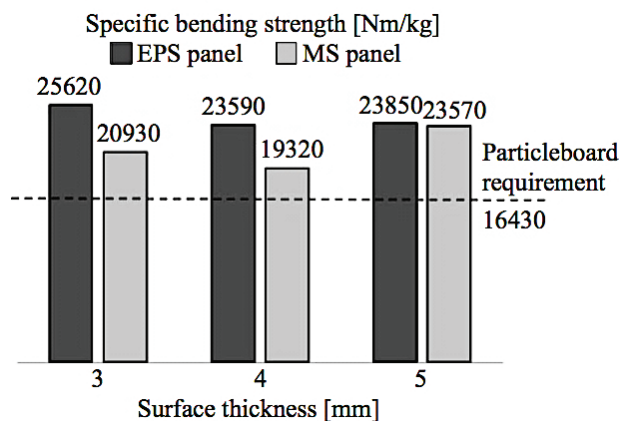
Figure 2.5 Specific bending strength of foam core particleboard with different core materials (EPS and MS), and surface thicknesses [17].

Figure 2.6 shows a proposed continuous production process based on the same concept, but using a double belt press. The adhesive treated wood particles and foam precursors would be introduced on a movi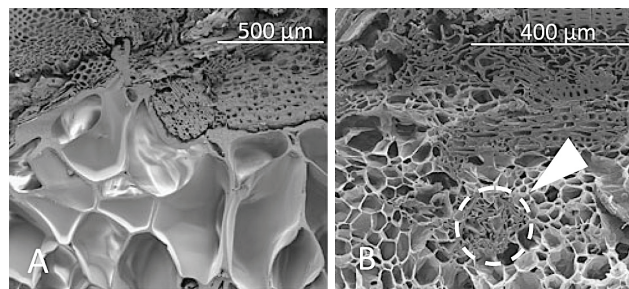ng belt in order to form the three-layered mat. The mat would be densified, and skin layer consolidation, core layer foaming and cooling would subsequently take place in-line

A feasibility study conducted by the University of Hamburg in cooperation with a producer of wood-based panel manufacturing machinery, a chemical company and a panel producer came to the conclusion that the in-line foaming technology is economically feasible, provided that the cost of the precursor is below 2 €/kg [6].
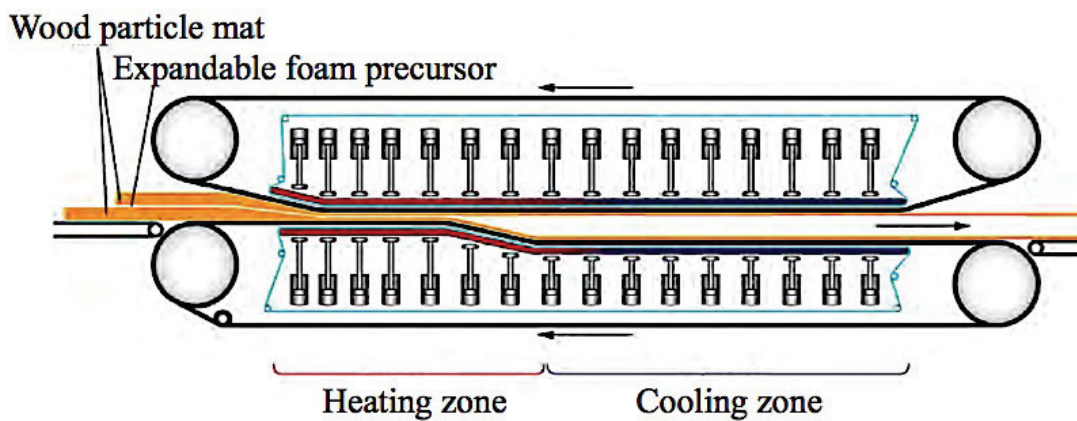
Figure 2.6 Concept for continuous production of foam core panel [53].

2.2.2   Particleboard process windows

In the conventional particleboard panel production process the temperature is known to be around 100 °C in the central plane of the panel. This is a consequence of water evaporation from the wood particle/adhesive system. The wood particles contain moisture levels typically up to 2 wt% and the widely used urea-formaldehyde based adhesive system is based on an aqueous solution [54]. Conduction is the main heat transfer mechanism at the interface between the hot press platens, which are generally heated to well above 100 °C, and the outermost surfaces of the particleboard, but water vapor transport is known to be the main heat transfer mechanism from the platens to the inside of particleboard [55], limiting the core temperature to around 100 °C in the initial stages of the process.

Thoemen *et al.* proposed the heat accumulation in the wood composite during hot pressing to be described by [56]

$$-\nabla q - H_V m_{ev} = c_u \rho_u \frac{\partial T}{\partial t} \qquad (2.11)$$

where q is the conductive heat flux, H_V is the latent heat of sorption from the vapor to the bound water state per unit mass [Jkg^{-1}], m_{ev} is the evaporation rate in the units of kg m^{-3} s^{-1}, c_u and ρ_u are the specific heat and density of the wood-facing at a given moisture content, respectively.
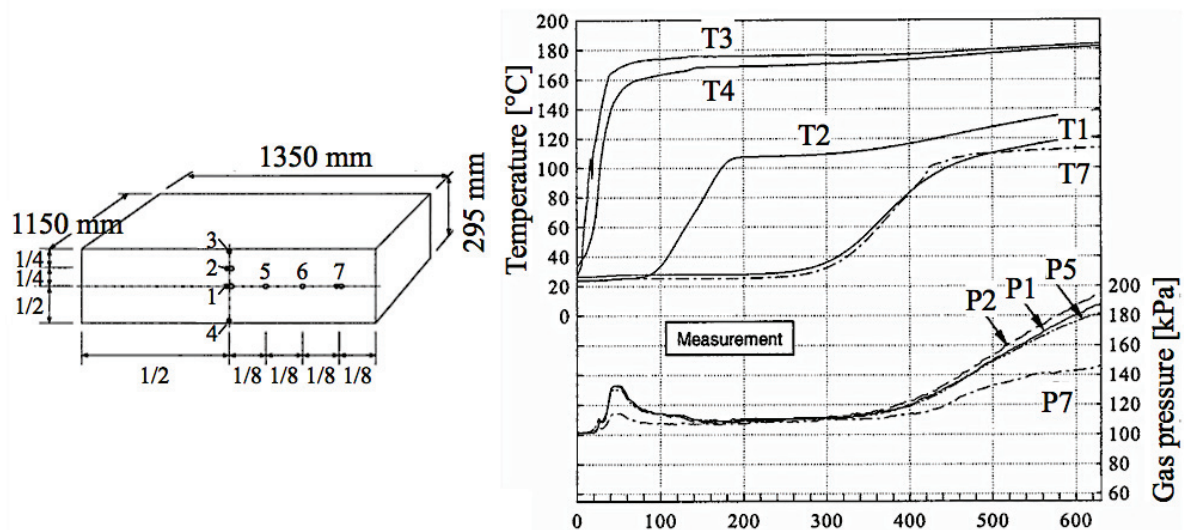
Figure 2.7 Dimensions and positions of sensors in a medium-density fiberboard mat and variation of temperature and gas pressure as a function of press time [56].

According to Equation 2.11, the heat from the hot press platens initially causes evaporation of water from the wood particles, so that the core layer T remains at 100 °C, but subsequently accumulates in the fiberboard, raising its T to greater than 100 °C. This hypothesis was evaluated experimentally, and, as shown in Figure 2.7, the core temperature was confirmed to remain at about 100 °C (the platen T was set to 190 °C in the example shown) until the water in the wood particle formulation had evaporated, as reflected by an increase in gas pressure, and then gradually increased.

Commercial adhesive systems for wood composite panel process have generally been developed to be compatible with the above conditions. However, if specific types of foam precursors are employed, the optimum conditions for initiation and stabilization of foaming do not necessarily correspond to a core temperature of 100 °C. Determination of processing windows that allow synchronization of adhesive cure and foaming is therefore of particular importance for any prospective foam core particleboard process. For example, if the foaming system requires a lower processing temperature than 100 °C because of a low softening temperature or a need to limit loss of the blowing agent through diffusion, reduced platen temperatures and low temperature curable adhesive systems and might be envisaged, e.g. a modified tannin-hexamine binder cured at 70 °C or a urea-formaldehyde resin with ammonium peroxodisulfate as a catalyst, which has a gelation temperature of 80 °C [57].

2.2.3   Mechanics of sandwich structures and particleboard

Mechanics of sandwich structures

Sandwich structures are used for a variety of structural applications, providing excellent specific properties. As shown in Figure 2.8, typical sandwich structure consists of two stiff, but thin face skins separated by a light-weight core such as wood, foam or honeycomb [58].

Figure 2.8 Schematic of typical sandwich structures with various core materials [58].

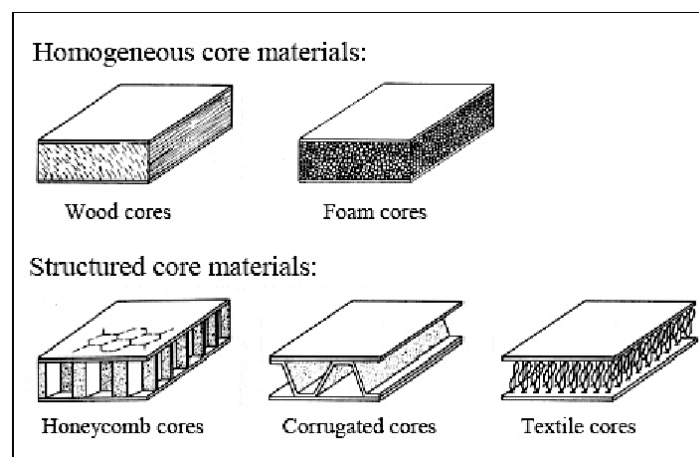The relationship between the external load and the stress in the face and the core of an ideal sandwich panel is [59]

$$\sigma = \frac{PL_S}{2t_f(t_S + t_C)b} \qquad (2.12)$$

$$\tau = \frac{P}{(t_S + t_C)b} \qquad (2.13)$$

where σ and τ are the bending stress of the face and the shear stress of core, respectively, P is the peak load, L_S is the span length, b is the width of the sandwich and t denotes thickness with subscript S for the sandwich, C for the core and f for the face. Equations 2.12 and 2.13 show that the thicknesses of the skin and the core layer are of particular importance for mechanical property optimization. Once the target mechanical property is defined, e.g. a bending load requirement for a furniture application as shown in Figure 2.5, and the mechanical behavior of the skin and core layer is known, the thickness profile may be optimized. However, it should be born in mind that modifying the relative thicknesses of these layers will also alter the overall density [17].

In practice the load bearing mechanisms of the sandwich structure play an important role in its mechanical response. Kumar S. A. *et al*. investigated the flexural behavior of a sandwich with a phenolic foam core and glass fiber reinforced plastic faces and identified different load bearing mechanisms according to loading conditions, i.e. bending of the face material for high span to depth ratios and shear of the core material for low spans [60].

Particleboard mechanics

It follows from the previous section that it is important to understand the relationship between the processing parameters, microstructure and properties of the particleboard faces and foam core if the desired properties are to be obtained. In the foam core particleboard of interest in the present work, relatively thin particleboard layers will serve as the skins of the sandwich structure. There have been substantial efforts to investigate the structure of wood based composites at the micro and sub-micrometer level [61,62]. The correlation between the microstructure and macroscopic properties of wood-based panels may then be analyzed using numerical models. Figure 2.9 shows the X-ray micro-computed tomography (CT) images of particleboard, showing void distributions

and local accumulation of the adhesive, which are assumed to be important for mechanical properties, and are controlled by processing parameters such as the amount of resin and/or the applied pressure.
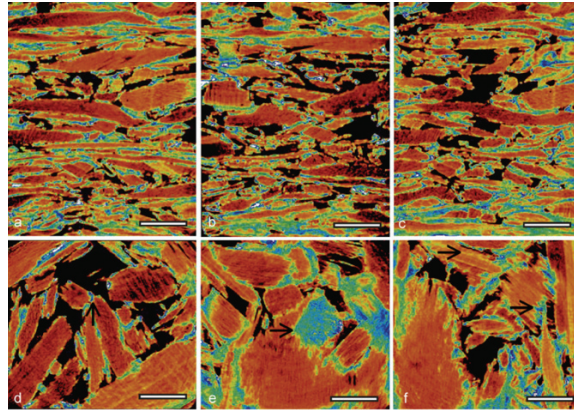
Figure 2.9 X-ray µ-CT images of particleboard prepared from a commercial adhesive and wood particles. The wood particles, adhesive and voids are shown in red, blue and black, respectively [61].

An example of multi-scale modeling of wood-based panels was given by Stuerzenbecher R. *et al*. [63]. The representative volume element (RVE) technique was employed to predict mechanical characteristics of strand board, as shown schematically in Figure 2.10. Although numerous factors are known to influence the mechanical properties in strand-based wood composites, e.g. the density profile, the orientation and quality of the strands and the distribution of the adhesive, this approach led to acceptable agreement between the predicted behavior and experimental data from bending tests on 30 mm thick strand boards.
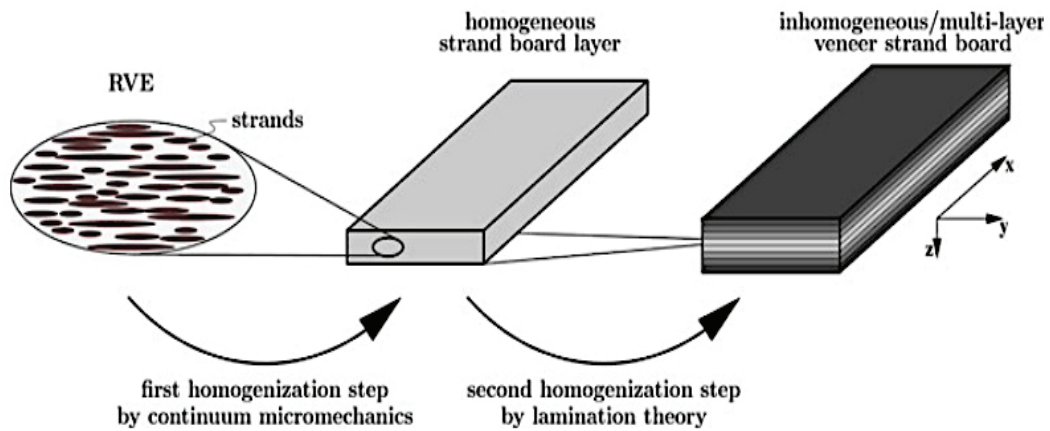
Figure 2.10 The concept of multiscale modeling based on laminate theory using RVE [63].

Foam mechanics

The Ashby model [64] is widely used to predict mechanical properties of cellular solids. The basic idea is that the mechanical behavior of foams is related to the cell wall materials and cell structural parameters such as relative density, open cell content and the anisotropy of the foam.

The 3-dimensional cube model with cell edges and faces is shown in Figure 2.10.

(a) (b)
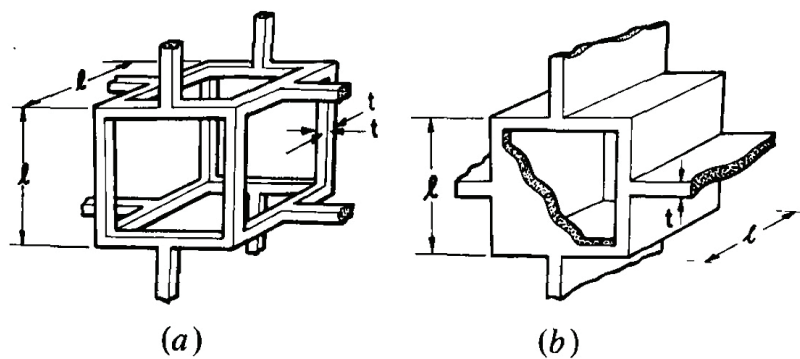
Figure 2.11 3-dimensional models for (a) an open cell and (b) a closed cell foam [64]. *l* and *t* denote the cell wall length and the thickness of the cell edges, respectively.

Four deformation modes, linear elasticity, nonlinear elasticity, plastic collapse and fracture, are shown in Figure 2.11 based on a 2-dimensional hexagonal model and Table 2.2 gives expressions

for different foam properties based on bulk foam parameters. It is seen that the density ratio between foam and unfoamed solid material, ρ_f/ρ_s, is a dominant factor for overall performance.
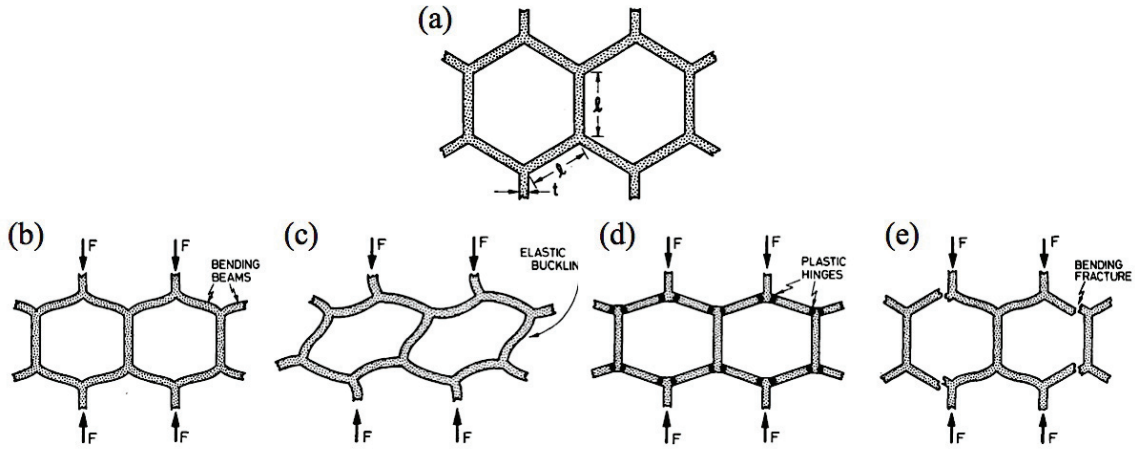
Figure 2.12 2-D hexagonal model for different cell wall deformation modes: (a) linear elastic deformation: cell wall bending, (b) nonlinear deformation: cell wall buckling, (c) plastic yielding and (d) fracture. *l, t* and *F* are the cell wall length, the cell edge thickness and the applied force, respectively.

Table 2.2 Expressions for the mechanical properties of foams [64]. *E* and *ρ* are the modulus and density respectively, K_{IC} is the fracture toughness of foam with units of MPa m$^{1/2}$, C_1 to C_2 and B_1 to B_2 are dimensionless constants, *l* is the cell size and the subscripts "solid" and "foam" denote the properties of the solid and the foam.

Property	Open cell foam	Closed cell foam
Linear elasticity	$\dfrac{E_{foam}}{E_{solid}} = C_1 \left(\dfrac{\rho_{foam}}{\rho_{foam}}\right)^2$	$\dfrac{E_{foam}}{E_{solid}} = B_1 \left(\dfrac{\rho_{foam}}{\rho_{foam}}\right)^3$
Fracture toughness	$K_{IC} = C_2 \left(\dfrac{\rho_{foam}}{\rho_{solid}}\right)^{3/2} \sigma_{foam}\sqrt{\pi l}$	$K_{IC} = C_2 \left(\dfrac{\rho_{foam}}{\rho_{solid}}\right)^2 \sigma_{foam}\sqrt{\pi l}$

Although the unit cell based Ashby model provides insight into cellular solid mechanics, it is of limited relevance to real foam materials, whose geometry is typically irregular and disordered. To solve the non-repeating cell problem, considerable use of statistical and/or numerical techniques has been made [65–68]. Numerous studies have identified negative contributions to mechanical properties from irregular cell structures, e.g. non hexagonal or defective cell wall structures show decreased compressive elastic modulus at a given density [65], and curved or corrugated cell walls result in reduced stiffness in metallic foams [66]. However, numerical models, illustrated in Figure 2.12, incorporating various degrees of non-uniformity, have also shown that limited non-uniformity may improve stiffness in an open cell foam [67]. Such models may well be applicable to the mechanical behavior of the foams to be described in this thesis, but they require detailed structural information that is difficult to obtain systematically, and are unwieldy compared with the Ashby approach, which is generally sufficient for order-of-magnitude correlations.
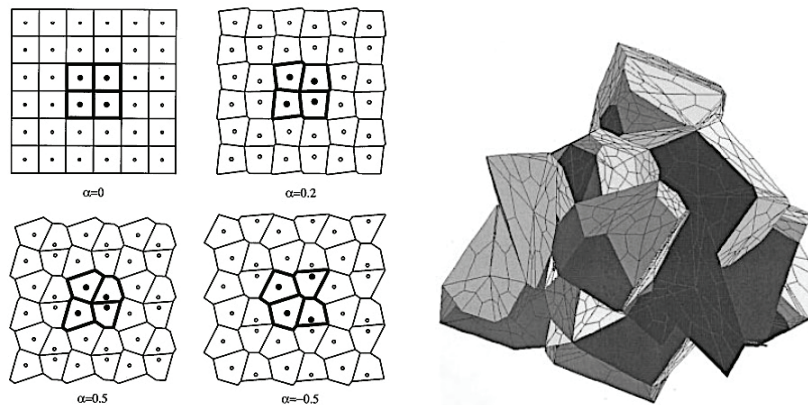
Figure 2.13 2D and 3D cellular model with irregularity represented by α [67].

If the matrix materials are compounded with fillers or reinforcements, the calculation of the modulus may incorporate predictions for the cell wall modulus based on standard expressions for particle or fiber reinforcement. The Halpin-Tsai equations, for example, are widely used to describe the elastic modulus, E, in a composite material containing randomly distributed geometrically anisotropic fillers [69,70]:

$$E = \frac{3}{8}E_L + \frac{5}{8}E_T \qquad (2.14)$$

$$E_L = E_m \left[\frac{1 + (\frac{2l}{d})\eta_L V_f}{1 - \eta_L V_f} \right] \; and \; E_T = E_m \left[\frac{1 + 2\eta_T V_f}{1 - \eta_L V_f} \right] \qquad (2.15)$$

$$\eta_L = \frac{(E_f/E_m) - 1}{(E_f/E_m) + (2l/d)} \; and \; \eta_T = \frac{(E_f/E_m) - 1}{(E_f/E_m) + 2} \qquad (2.16)$$

where E_L and E_T are longitudinal and transverse modulus of the composite, E_f and E_m are Young's modulus of the reinforcement and matrix, η_T and η_L constants given by equation 2.16, V_f is volume fraction of reinforcement and l/d is aspect ratio of the reinforcement. The Halpin-Tsai equation is considered to be one of most accurate models for the prediction of the elastic behavior of natural fiber based composites from the geometry and orientation of the fibers and the elastic properties of the fibers and matrix [71,72].

2.3 PLA foaming

PLA

Poly(lactide) (PLA) is an aliphatic polyester considered to be a competitive "green" alternative to polystyrene (PS) [73]. Although it is a synthetic polymer, it is derived from yearly renewable resources such as corn sugar, and is biodegradable, which has attracted considerable interest. As shown in Figure 2.13, PLA is polymerized by direct condensation of lactic acid or ring-opening polymerization of cyclic lactide [74].
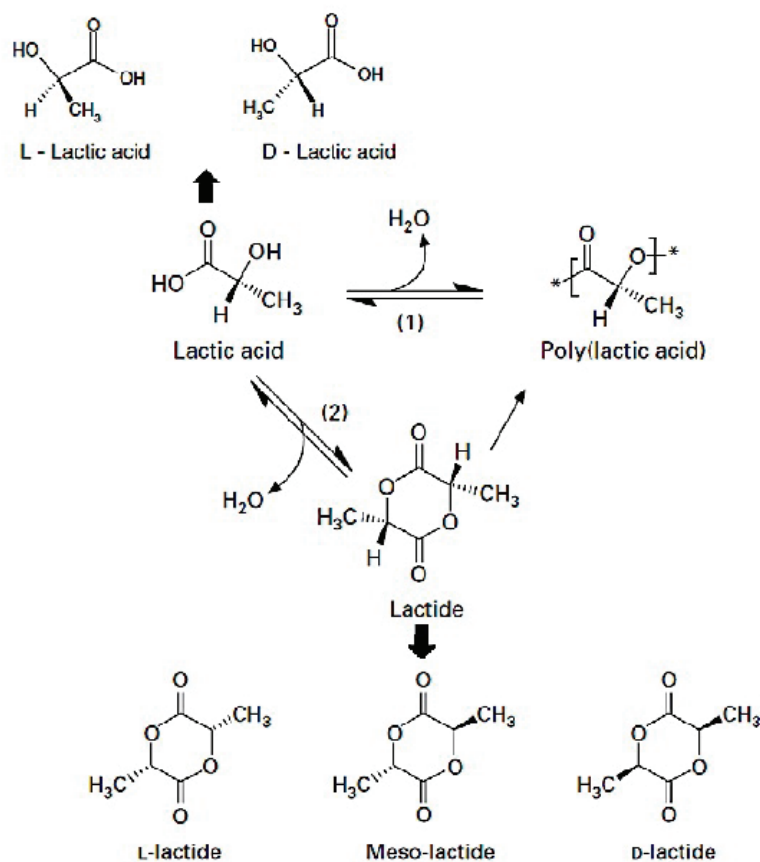
Figure 2.14 PLA polymerization by (1) condensation and (2) ring-opening polymerization. Lactic acid is a chiral molecule with two L- and D-enantiomers. [75,76].

The ring-opening process is known to be capable of not only producing high molecular weight polymers but also facilitating control of the molecular architecture through control of the enantiomer ratio. The D- to L-lactide ratio is important for the crystallization behavior and related characteristics such as the thermal, mechanical and rheological behavior. PLA is usually amorphous at high D-isomer contents (>10%), but semi-crystalline at low D-isomer contents (<2%). Semicrystalline PLA crystallizes between 110 and 130 °C, and the crystallization rate is slower than those of typical commodity thermoplastics. Table 2.3 summarizes some important physical properties of PLA [74,77,78].

Table 2.3 Typical properties of PLA.

	Semi-crystalline PLA	Amorphous PLA
Glass transition temperature [°C]	55-65	55-65
Melting temperature [°C]	150-170	-
Tensile strength [MPa]	59	44
Elastic modulus [GPa]	4	3.5
Elongation at break [%]	5.5	7
Yield strength [MPa]	70	50

PLA degradation may occur by hydrolysis or reaction with enzymes. In general, high molecular weight polymer chains are hydrolyzed to lower molecular weight oligomers and enzymatic degradation then follows. CO_2, H_2O and humus are the end products. Amorphous regions absorb moisture easily and degrade faster than crystalline regions, and process may be accelerated by high temperature and high moisture content. Possible depolymerization in the presence of water means that a thorough drying step is needed prior to the use of melt processes such as extrusion and injection molding [79].

Unmodified PLA shows a low melt viscosity and poor melt strength due to its linear chain structure and relatively low molecular weight. These characteristics make thermoforming difficult, but the poor melting strength can be overcome to a certain extent by introducing chain extender during melt processing [80–82].

2.3.1 PLA foaming technology

D-isomer content and crystallization

As briefly mentioned in Section 2.3, it is known that the D-isomer content significantly influences the crystallization behavior of PLA, and low D-isomer content PLA may be beneficial for foaming because of the higher melt strength engendered by the formation of a network of nucleated crystals during foaming, and the consequent improvement cell stability. The effect of D-isomer content on PLA foaming has been widely investigated using batch processing and foam extrusion [11,44,83]. Initially amorphous PLA with 1.4 to 11.8 % of D-isomer content was

foamed by subcritical CO_2 treatment, followed by immersion in water at 80 °C [11]. It was reported that high D-isomer contents resulted in smaller cell sizes and a lower open cell content (Figure 2.14), which are believed to be favorable for the mechanical properties of foams. On the other hand, while a fine cell structure was obtained with 1~4 % D-isomer PLA and batch processing using supercritical CO_2, D-isomer contents of 10 and 28.5 % gave unsatisfactory foam microstructures under these conditions because of extensive cell coalescence and cell rupture during cell growth [83]. Moreover, cell rupture due to low melt strength may cause premature gas loss during foam expansion and hence severe shrinkage [84].
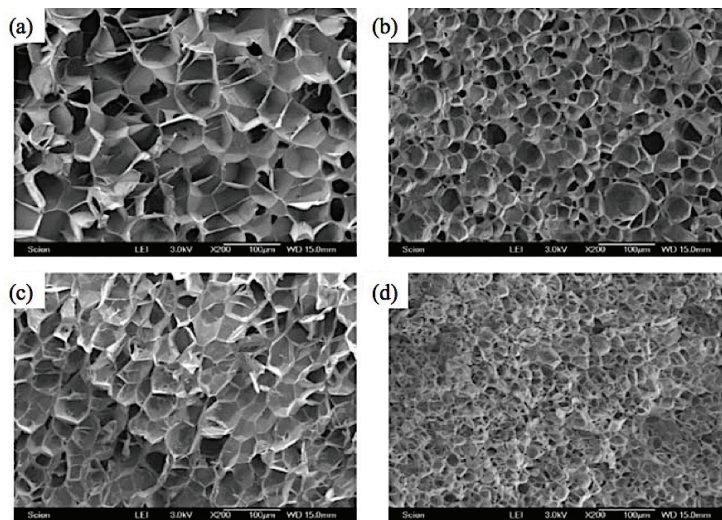
Figure 2.15 The foam morphology of (a) 1.4, (b) 4.3, (c) 7.7 and (d) 11.8 % D-isomer content PLA foams treated with supercritical CO_2 and foamed at 80 °C [11].

Crystallization can also promote cell nucleation [44,85]. Heterogeneous nucleation at the surface of a spherulite in low D-isomer PLA with supercritical CO_2 as the blowing agent is shown in Figure 2.15 [86]. The nucleation density was found to be significantly increased as the spherulite density increased. This was explained by expulsion of the CO_2 from the crystalline phase, which resulted in a locally increased CO_2 concentration in the amorphous phase.

(a) 0 sec (11 MPa) (b) 5.1 sec (7.2 MPa)

(c) 6.1 sec (6.8 MPa) (d) 7.1 sec (6.5 MPa)
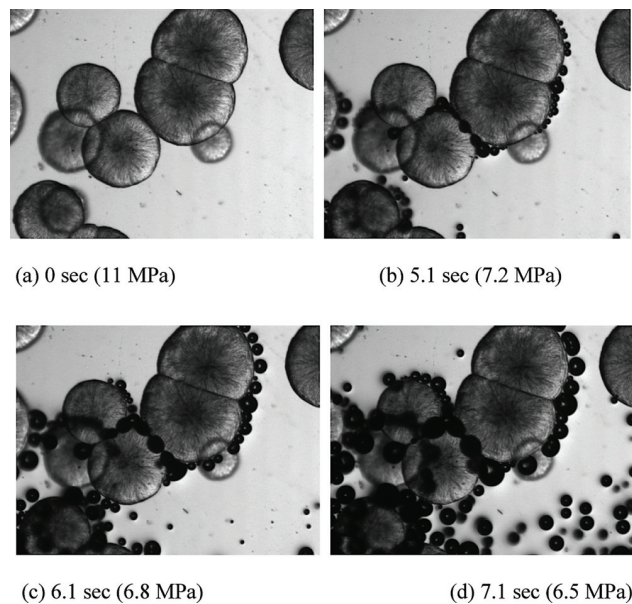
Figure 2.16 Optical microscopy of foam cell nucleation in PLA with 1 % D-isomer in the presence of supercritical CO_2. The saturation pressure and temperature were 11 MPa and 180 °C, respectively [86].

Recent studies have focused on CO_2 foaming of PLA beads that show a double crystal melting peak [87,88]. This novel approach is claimed to be cost effective and suitable for sintering in steam chest molding. Long chain branched PLA with 4.6 % D-isomer contents was treated by sub- or supercritical CO_2 at 140 to 150 °C. After the desired saturation time had elapsed, PLA was foamed by pressure release and cooling to ambient conditions. High melting temperature, T_m, crystals are formed by CO_2 saturation at relatively high temperatures and pressures, and low T_m crystals are formed during foaming and degassing. The crystallinity permits handling of the partially foamed beads, but when the subsequent steam chest molding temperature is chosen to be between the upper T_m and lower T_m, the beads partially melt, allowing further expansion and bonding. The crystalline structure in foams prepared by this technique may be advantageous in terms both of foam stability and microstructure, and the mechanical and thermal behavior in the target application. However, the required processing temperature, > 140 °C, is too high for this approach to be of direct interest for the particleboard process.
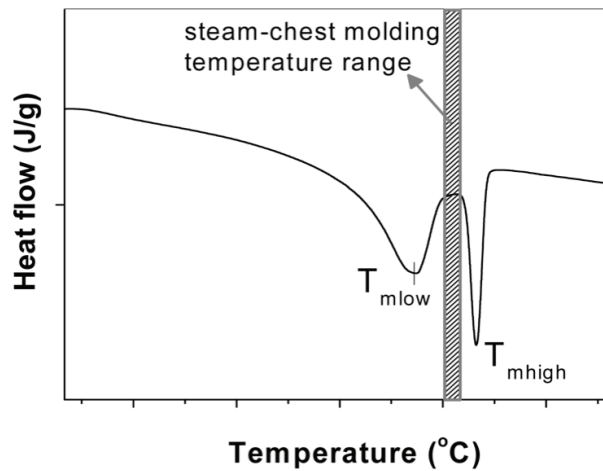
Figure 2.17 Schematic of double crystal melting behavior in a DSC scan and the temperature range for steam chest molding [87].

PLA composite foam products

A wide range natural or synthetic additives have been employed to promote cell nucleation in foams and/or obtain the desired final properties [89–93]. For example, micron and sub-micron sized additives such as cellulose fibers, talc or nanoclays are widely used to increase the cell nucleation rate by providing heterogeneous nucleation sites.

In the case of PLA, there has been particular interest in the use of bio-sourced fillers to give fully biodegradable composite foams with improved mechanical properties. These include flax fiber [91], silk fibroin powder [92], wood flour [93] and microfibrillated cellulose (MFC) [40]. Flax fiber was compounded with low D-isomer PLA and an epoxy functional silane as a coupling agent using a twin screw extruder [91]. Supercritical N_2 assisted injection molded 1, 10 and 20 wt% flax-PLA composite foams showed a higher cell density, higher crystallinity and improved specific modulus with respect to unmodified PLA foams. Up to 7 wt% of silk fibroin powder was mixed with PLA by solvent processing using CH_2Cl_2 and foamed by a supercritical CO_2 batch process [92]. A decrease in cell size from 52 μm in neat PLA foams to 15 μm at 7 wt% filler, and an increased cell density was reported, but no mechanical test data. Batch foaming behavior of PLA-10, 20, 30, and 40 wt% wood flour composites was observed by Matuana *et al*. [93]. A

decreased cell size was observed with increasing filler content but also a reduced expansion ratio, which was attributed to increased matrix stiffness.

Nano sized additives such as nanofibrillar cellulose (NFC) or carbon nanotubes (CNT), have been employed to produce microcellular or nanocellular foams (the cell density of a microcellular foam is defined as 109 to 1012 cells/cm^3, and that of a nanocellular foam is >1012 cells/cm^3 [94]). Compared with conventional foams, micro- or nanocellular foams have been reported to show superior impact strength [95], higher fracture strength [96], longer fatigue life [97] and superior heat insulation properties [98]. The primary processing requirement for these additives is the achievement of a homogeneous dispersion and/or exfoliation in the matrix. If this can be achieved, the addition of nano fillers may not only promote cell nucleation but also improve the melt strength of the polymer, resulting in reduced cell coalescence [99]. Thus, PLA-nanoclay foams produced by a batch foaming technique showed sub-micron sized cells, and the high aspect ratio and platelet-shaped structure of the nanoclay resulted in superior viscoelastic properties in the polymer melt [100,101].

2.3.2 PLA foam processing

PLA foam extrusion

Considerable effort has been devoted to developing PLA foam processing techniques. Three main processing methods have been adopted, namely foam extrusion, injection and batch foaming. In the foam extrusion process, the polymer is fed into the extruder and then the blowing agent gas is introduced into the extruder barrel to dissolve or mechanically mix the gas with the polymer melt under high pressure. The pressure drop at the extrusion die induces thermodynamic instability and phase separation, resulting in cell nucleation and cell growth. Finally, the foam product is stabilized by cooling [26,84].
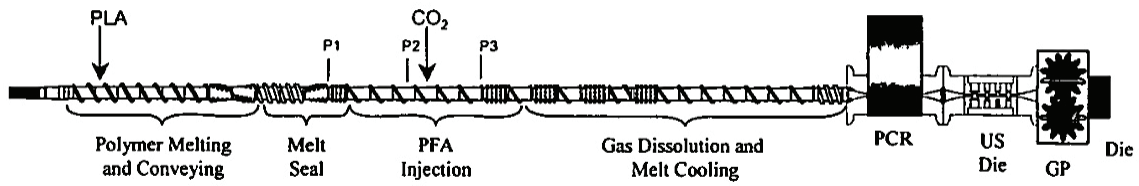
Figure 2.18 Schematic of the foam extrusion process [102].

PLA/sub- or super-critical CO_2 foam extrusion has been widely investigated for applications such as food packaging [103]. Reignier *et al.* obtained low density foams using amorphous PLA/9 wt% CO_2 (Figure 2.17) with a foam expansion ratio of up to 25, although the foam morphology was non-uniform and the cells coalesced and shrunk [102]. Cell coalescence and shrinkage could nevertheless be minimized by improving the melt strength via chain branching and/or compounding PLAs with different D-isomer contents [44,104]. Finally, Figure 2.18 shows a tandem extrusion set-up that has been shown to provide a more homogeneous polymer/blowing agent mixture and more precise temperature control with help of additional mixing in a second extruder [85].
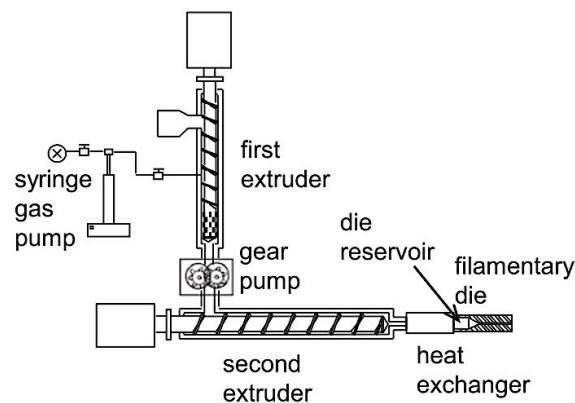
Figure 2.19 An example of a tandem foam extrusion set-up for foam extrusion of PLA.

PLA foam injection molding

Injection molding technique is generally advantageous over other melt processing techniques in terms of dimensional stability and cycle time. In the foam injection technique, a mold cavity is fully filled with the polymer/blowing agent mixture under high pressure. Supercritical N_2 is the usual blowing agent, as in the MuCell® injection molding technology, but has a lower solubility in PLA than CO_2 [34]. Investigations have focused on microcellular foaming with/without nano sized additives [105,106]. The enhanced melt strength obtained by reactive compounding with a chain extender results in a uniform foam morphology with cell sizes of 3-40 μm. Further developments include mold opening as an additional process step and low pressure foam injection [107]. These allow higher foam expansion ratios with larger average cell sizes than conventional techniques.

PLA batch foaming

Batch foaming has typically done in a high pressure chamber and been widely used to investigate the influence of parameters such as composition [108–110], the type of blowing agent and content, and the use of additives on the foaming behavior [10,43,111–115]. A matrix polymer sample is placed in a temperature controlled high pressure chamber and impregnated with the blowing agent under the desired conditions. A decrease in pressure and/or an increase in temperature lowers the solubility of the gas and softens the polymer matrix. This results in nucleation and growth of foam cells. A disadvantage of this type of foaming process is its low productivity rate. In general, a considerable time is required to produce the desired polymer/gas mixture because of the need to establish a high pressure and high temperature environment, and the low gas diffusion rate into the polymer matrix, especially at a low temperatures. Moreover, the production capacity per batch is typically small owing to the limited space inside the pressure chamber.

Even so, foam products aimed at biomedical applications have been demonstrated with considerable success using this approach [112,114], thanks to the well controlled foam structures, due in turn to the precisely determined process conditions. A bioresorbable PLA grade was compounded with a ceramic filler and foamed under supercritical CO_2 conditions at 100 to 250 bar and 195 °C using a batch foaming process. The correlation between the processing parameters

and cell morphology was investigated, higher cell densities being observed at higher pressures, and as the depressurization rate increased from 2.3 to 8.0 bar/s, with an increase in cell coalescence as the cooling rate decreased from 4.5 to 3.4 °C/s. [43,111].

Plasticized PLA foams have also been investigated for bioresorbable tissue replacement scaffolds. A biomedical grade polyethylene glycol (PEG) was compounded with amorphous and crystalline PLA. Samples with compositions were saturated with CO_2 at pressures of 150 to 280 bar, and temperatures of 150 to 180 °C, with degassing and cooling rates of 1.6 to 17 bar/s and 0.6 to 7 °C/s, respectively. Foams produced from PLA-20% PEG showed rubber like properties at 37 °C and larger cell sizes than unmodified PLA foams [108–110].

PLA/NFC and PLA/WF composite foams were prepared by a wet process and processed with supercritical CO_2. The resulting foams showed good mechanical properties in compressive tests. However, because of PLA degradation by water contained in the cellulose, reinforcement in certain foams was offset by a loss in matrix properties. The use of NFC and WF reinforcement therefore offers potential for mechanical property improvement but also potential drawbacks in the context of the particleboard process, in which the presence of water is unavoidable [10].

PLA bead foaming

Another important PLA foam production technique is bead foaming, which may be used to mold foam products with a three dimensional geometry, and has been widely employed for expandable polystyrene (EPS) foam products [46]. As mentioned in Section 2.1, this technique comprises three main steps: (a) a physical blowing agent (PBA) is introduced into a polymer matrix; (b) the impregnated foam beads are pre-expanded and the PBA content stabilized; (c) the mold cavity is partially filled with the foam beads and hot air or steam is used to provoke further expansion and fusion. In commercial PLA bead foaming, typically a high D-isomer content PLA in pellet form is impregnated by CO_2 under sub- or super-critical conditions and pre-expanded and conditioned at a relatively low T. The pre-expanded beads are then molded using high T steam [7,116,117]. Figure 2.20 shows one example of the transformation of PLA pellets into a final foam product. (Low D-isomer content PLA bead foaming technology has also recently been investigated [11,87], but is not yet available on the market to the best of our knowledge.) Moderate impregnation

conditions, e.g. impregnation with liquid CO_2 at 6 MPa and 10 °C, and low depressurization rates are known to be employed in the industrial process, and up to about 40 % of CO_2 by weight is initially absorbed by the PLA. More than 11 % of CO_2 is retained in 11.6 % D-isomer content PLA after pre-expansion at low T, followed by 42 hr storage at -18 °C and ambient pressure. Chest molding using steam 110 °C steam results in acceptable fusion between the beads and low foam densities. The overall properties of final foams are shown in Table 2.4.
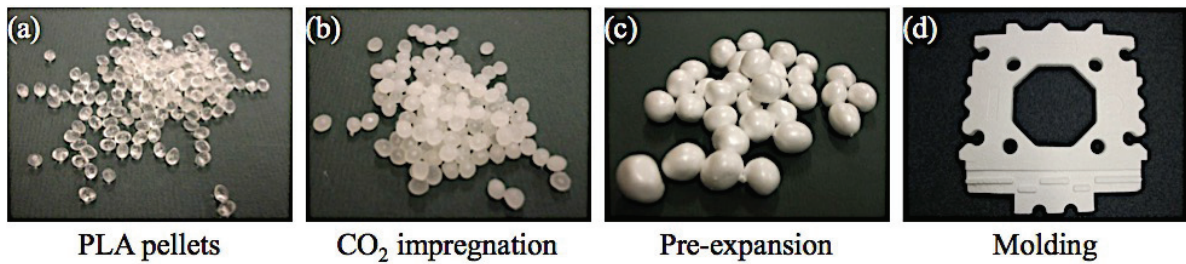
Figure 2.20 PLA bead foam process [7,116]

Table 2.4 Properties of chest molded PLA foam in comparison with EPS foam [116].

	PLA bead foam	EPS foam
Density [kg/m^3]	25	25
Thermal resistance [m^{2}K/W]	~0.69	~0.68
Thermal conductivity [W/mK]	~0.035	~0.035
Compressive modulus [MPa]	2.9	5.3
Compressive stress [MPa]	0.07	0.12
Shear modulus [MPa]	3.0	3.2
Shear strength [MPa]	0.11	0.12

Chapter 3

Experimental

This chapter presents the main experimental approaches used in this thesis and other specific techniques will be introduced in subsequent chapters. First, foam core materials and skin materials of the foam core sandwich panels are described. Sample preparation methods, i.e. hot press molding, extrusion and injection molding, are then introduced, along with the impregnation and foaming procedures. Finally, the characterization techniques are briefly described.

3.1 Materials

3.1.1 Foam precursor: polymers and additives

Two different grades of PLA were obtained from NatureWorks LLC in pellet form, and are referred to as PLA1 and PLA2 in what follows. PLA1 contained 1.4 % D-isomer and was nominally semicrystalline, while PLA2 contained 11.6 % D-isomer and was nominally amorphous. PLA must be dried before use and the producer recommends moisture levels below 250 parts per million (ppm). Unless mentioned otherwise, all PLA materials were dried at 40 °C under vacuum for at least 18 hr prior to use, following the standard procedure.

An injection grade poly(methyl methacrylate) (PMMA) was provided from Evonik Industries AG in pellet form. The PMMA pellets were dried at 90 °C for at least 1 hr in a convection oven prior to use.

A general purpose grade of talc from Fisher Scientific was used as a foam nucleating agent and 99.9 % pure CO_2 from Carbagas AG was used as a blowing agent.

To produce biocomposite matrices, bleached birch wood fiber (WF) (Innventia AB) and commercial microcrystalline cellulose (MCC) (Sigma-Aldrich) were used as additives. The WF and MCC were dried in a convection oven at ambient pressure for 24 hr at 80 °C and 100 °C, respectively.

3.1.2 Surface layer materials: wood particles and adhesive system

Conventional fine wood particles, mainly spruce and pine, with an average particle size of less than 2 mm, were supplied from a particleboard mill. The particles was mixed with 12 wt% urea formaldehyde (UF) resin (Kaurit 350, BASF, Germany) based on dry mass of the wood particles. 3 wt% ammonium persulfate was added to the resin as hardener. The adhesive was then sprayed onto the particles in a rotating drum-type blender using a compressed air spray head. The target density and thickness for the surface layers were 750 kg/m^3 and 3 mm, respectively.

3.2 Specimen preparation

3.2.1 Molding and compounding

Hot press molding

The as-received or compounded pellets were hot-pressed to fabricate 1 mm thick discs with the diameter of 25 mm by using a hot press (Fontijne TP 50 with 255×255 mm^2 heating platens) after drying as described in Section 3.1.1. The pellets were placed between polyimide release films in a stainless steel mold and melted without any force at 200 °C for 5 min. A nominal hydraulic force of 6 kN, which was 0.25 MPa to the mold, was then applied at the same temperature for a further 5 min, after which the platens were cooled under pressure to below 40 °C over approximately 10 min using the integrated water cooling system. 0.2 to 0.5 mm thick films for dynamic mechanical analysis (DMA) were also produced following same hot pressing procedures but without the disc shape mold.

Extrusion

A twin-screw extruder equipped with a pelletizer (Prism TSE 16, Thermo Electron Corporation, 16 mm barrel diameter, L/D ratio of 15:1) was used to prepare compounds of polymers with/without nucleating agent. The temperatures at the feeding, melting and metering zone of the extruder barrel were set to 190, 220 and 210 °C, respectively. The drive motor speed was set to 20 rpm and the internal pressure of the barrel was 30 to 40 bar. The resulting filaments of 1 to 1.5 mm in diameter were cooled in air at ambient temperature and pelletized into 2 to 3 mm long granules.

Micro extrusion and injection molding

A tabletop twin conical co-rotating micro extruder shown in Figure 3.1 (DSM Micro 5 compounder and Microinjection molder 5.5, Netherlands) was chosen to compound polymers and/or additives in a small quantity, less than 5 cc. The temperature of the extrusion barrel was set to 200 °C, the screw rotation speed was 100 rpm and the residence time was kept constant at 120 s. After the dwell time elapsed, the nozzle was opened and the polymer melt was either extruded into air and cooled down or molded using an injection unit supplied with the extruder, consisting of a cylindrical reservoir and a pneumatic piston, to produce dog-bone shaped specimens with an overall length of 75 mm, a thickness of 2 mm, an overall width of 12.5 mm and a gage width of 4 mm. The temperatures of the reservoir and the mold were 200 °C and 40 °C, respectively.
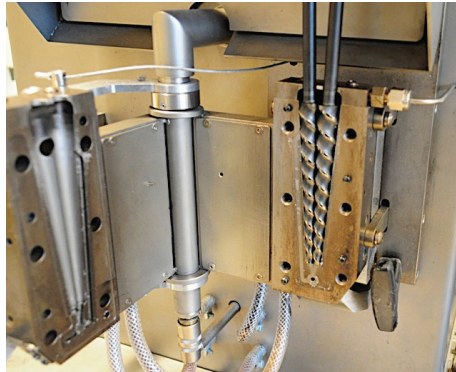
Figure 3.1 Conical screw configuration in the barrel of the micro extruder. In order to achieve homogeneous mixing the residence time could be varied by circulating the melt in the extruder via a back-flow channel visible to the left of the screws.

3.2.2   Impregnation and desorption of CO_2

Impregnation of the 1 mm thick discs with CO_2 was carried out at approximately 5 MPa and 10 °C using a high pressure chamber (Autoclave France), shown in Figure 3.2, equipped with a cooling system. Samples were placed in the chamber and CO_2 was then introduced until the desired pressure was reached. After the designated impregnation time had elapsed, depressurization was carried out at 0.01 MPa/sec. A 3 hr impregnation time was chosen to prepare CO_2 saturated specimens because longer impregnation times of up to 7 hr did not significantly increase CO_2 uptake in the specimens. Shorter treatments were also used to prepare specimens containing different amount of CO_2. This will be discussed in more detail in Section 4.3.

The desorption behavior of the 1 mm thick discs was investigated by gravimetry [8]. After impregnation and depressurization, the specimens were immediately transferred to a high precision balance and CO_2 loss was then monitored as a function of time. CO_2 contents were expressed as the weight of CO_2 per weight of the unimpregnated specimen.
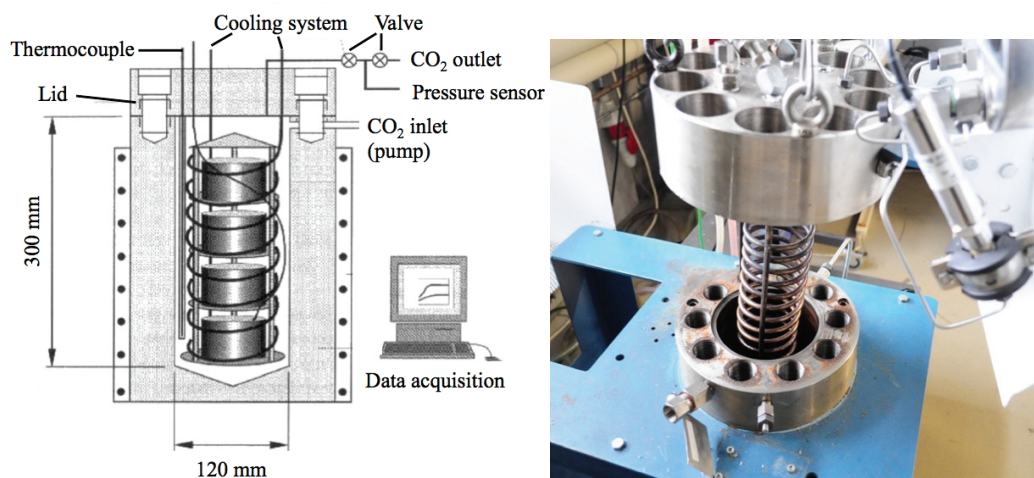
Figure 3.2 Schematic [70] and image of the high pressure chamber used in the thesis.

3.2.3 Foaming

Free foaming was carried out by immersing impregnated discs into a thermostatic bath filled with water or silicon oil at different temperatures. After 1 min foaming in the bath, the specimens were cooled down in a water bath at 20 °C. The *in situ* foaming behavior during the foam core particleboard production process, described in Section 2.2.1, was also investigated. The hot press temperature, pressure or closing gap, press open time and cooling time were the principle process parameters.

3.3 Characterization

3.3.1 Density measurements

The foam density was determined by measuring the weight per unit volume. Rectangular shaped specimens were cut out from the disc-shaped foams obtained as described in 3.2.3 and the weight and dimensions were measured. A skin-core morphology was often observed so that the reported values are averages for the whole specimen thickness.

The relative density between a solid and a foam, ρ_{solid}/ρ_{foam}, was used as a measure of the degree of expansion of the foams. A nominal density of 1.24 g/cm^3 was assumed throughout for unmodified PLA and the densities of the composites, ρ_{comp}, were calculated by

$$\rho_{comp} = V_f\rho_f + V_m\rho_m \qquad (3.1)$$

where V and ρ are the volume fraction and density and the subscripts f and m denote the filler and matrix respectively.

3.3.2 Differential scanning calorimetry (DSC)

The glass transition temperature (T_g), cold crystallization temperature (T_c), melting temperature (T_m) and crystallinity (X_c) were determined by DSC (TA Instruments Q100), which measures the difference in the amount of heat required to increase the temperature of a 5-6 mg specimen and an empty reference capsule. In this work, the thermal behaviour was generally determined with heating scans at 10 K/min in the temperature range 20-230 °C. T_g was taken from the mid-point of the corresponding step-like increase in heat flow rate. The degree of crystallinity (X_c) was calculated using the following equation

$$X_c = 100\,\frac{(\Delta H_m - \Delta H_c)}{\Delta H_{100\%}(1 - W_f)} \qquad (3.2)$$

where ΔH_m and ΔH_c are the measured melting and fusion enthalpies, $\Delta H_{100\%}$ is the melt enthalpy of 100 % crystalline PLA, taken to be 91 J/g [74], and W_f is the weight fraction of any additives present.

Both PLA grades showed T_g of ~60 °C as-received, and the melting temperature, T_m, of the as-received PLA1 was 170 °C. Specimens produced by extrusion, hot press molding and injection molding were generally amorphous in which case PLA1 showed a cold crystallization endotherm at about 100 °C. Details of the DSC investigations of the influence of blending, impregnation and foaming and will be provided in Section 5.

3.3.3 Dynamic mechanical analysis (DMA)

DMA provides information on the viscoelastic behavior of a material by applying small sinusoidal deformations to a suitable specimen. When a sinusoidal strain, ε, is applied to a viscoelastic specimen the corresponding stress, σ, shows with a phase lag, δ, such that

$$\varepsilon = \varepsilon_0 \sin(t\omega) \qquad (3.3)$$

$$\sigma = \sigma_0 \sin(t\omega + \delta) \qquad (3.4)$$

where ε_0 and σ_0 are the amplitude of strain and stress respectively, t is time and ω is the frequency of the solicitation. The storage modulus, E', and loss modulus, E'', represent the elastic response and viscous response of the specimen respectively and are defined by

$$E' = \frac{\sigma_0}{\varepsilon_0} \cos \delta \qquad (3.5)$$

$$E'' = \frac{\sigma_0}{\varepsilon_0} \sin \delta \qquad (3.6)$$

The ratio between these two moduli provides the phase lag,

$$\tan \delta = \frac{E''}{E'} \qquad (3.7)$$

Tensile mode DMA measurements (DMA Q800, TA instrument) were carried out on the hot pressed films, described in 3.2.1, using a 3 °C/min ramp rate from 20 to 150 °C and a 0.05% sinusoidal deformation at 1 Hz. The compressive behavior of foams was investigated using the same apparatus. Cuboid foam specimens with a cross-sectional area greater of at least 3×3 mm^2, were cut from the foamed discs using a razor blade in each case.

3.3.4 Mechanical properties

A screw driven universal testing machine (Series LFM-125 kN, Walter+Bai AG) was used to perform tensile tests on the injection molded dog-bone shaped specimens with the crosshead speed set to 5 mm/min. In each case, the elastic modulus was determined from the slope of the stress-strain curve in the elastic domain between 0 and 0.05 % strain.

3.3.5 Morphological characterization

The morphologies of the foams, i.e. open cell content, cell size & distribution and cell density, were investigated by scanning electron microscopy (SEM, Philips XLF30-FEG). Specimens were cut with razor blade and coated with a 15-20 nm thick layer of carbon using a carbon coater. Secondary electrons at a relatively low accelerating voltage (usually below 5 kV) were used for imaging.

An optical microscope (Olympus OM2) was chosen to investigate the fiber distribution and breakage in biocomposites and CO_2 induced crystallization behavior in PLA1. For the biocomposites, 0.2 to 0.5 mm thick hot pressed films were observed in transmitted light. Cross-sections of about 2 μm in thickness of PLA1 before and after treatment with CO_2 were observed in transmitted light using crossed polarizers. Thin sections were prepared at room temperature using a Reichert-Jung Ultracut-E ultramicrotome equipped with a diamond knife (Diatome).

Ultrathin sections of about 50 nm in thickness were prepared for transmission electron microscopy (TEM, Tecnai Spirit BioTWIN) in the same way from specimens stained by overnight exposure to RuO_4 vapor, and were observed in bright field with an accelerating voltage of 80 kV.

Chapter 4

CO$_2$ absorption, desorption and diffusion in PLA

As discussed in Section 2.2, the one step foam core particleboard process is one of the most promising production methods for achieving a lightweight structure without compromising mechanical properties and at an acceptable production cost. For the required sequence of process steps, i.e. 3-layered mat formation, surface layer consolidation, core layer expansion and stabilization, to be feasible, the foam precursor materials should be stable with respect to foaming at room temperature, allowing straightforward handling during the mat preparation step, but show adequate foaming behaviour at high temperature, T, and pressure, P. As set out in Section 2.1, the foaming behaviour and resulting foam structures are strongly dependent on the diffusion behaviour of the blowing agent in PBA assisted foaming. It follows that an investigation of the diffusion of the blowing agent in the polymer matrix, i.e. in this case, CO$_2$ in PLA, should be the first step for the development of a suitable foam precursor.

It is known from the literature that it is possible to produce expandable PLA by impregnation with CO$_2$ under supercritical conditions. However, the minimum CO$_2$ concentrations of around 10 wt%, widely considered to be necessary for the production of low density foams, are sufficient to reduce the matrix glass transition temperature, T_g, to temperatures well below those corresponding to the critical point of CO$_2$ (31.1 °C and 7.39 MPa). This makes it difficult to avoid foaming during the depressurization step and tends to result in agglomeration of the PLA granules, particularly when nominally amorphous grades of PLA are employed [73]. Moreover, the maximum CO$_2$ contents attainable at a given pressure are limited by the reduced slopes of the sorption isotherms for CO$_2$ in PLA at elevated T [34,36]. These drawbacks may at least to some

extent be overcome by processing with liquid CO_2 in the range of T immediately above the triple point (-56.6 °C and 518 kPa), where PLA remains in the glassy state up to relatively high CO_2 contents [7]. Even so, too high a CO_2 content will reduce T_g to well below room temperature, resulting in foaming and rapid desorption of the CO_2 subsequent to impregnation, again particularly when nominally amorphous grades are employed [73].

It has been demonstrated that the dependence of T_g on CO_2 content may be adequately described using the free volume model of Chow [45] with the lattice coordinate number, z, set to 2 [118]. However, only limited data for diffusion of CO_2 in PLA are available in the open literature, and, to our knowledge, there is little detailed indication of how diffusion rates vary with CO_2 content, although the plasticizing effect of CO_2 is expected to become critical at T in the vicinity of T_g. The overall aim of this section is: (i) to use simple gravimetric measurements of desorption rates of CO_2 from different grades of PLA in order to obtain a semi-quantitative description of dependence of the effective diffusion coefficient on temperature and CO_2 content in regimes of direct relevance to practical processing windows; (ii) to use this understanding to determine process parameters likely to satisfy basic performance requirements, namely adequate stability of foam precursors during handling at room temperature prior to thermally induced forming at elevated T; (iii) and to investigate morphological development during sorption of liquid CO_2 by a PLA with a low D-isomer content that crystallizes readily on annealing above T_g or during slow cooling from the melt.

4.1 Diffusion of CO_2 in semicrystalline PLA

4.1.1 Desorption measurements

Systematic measurements, described in Section 3.2.2, of the CO_2 desorption rates were carried out using PLA1 as a model system, because its tendency to undergo cold crystallization during impregnation inhibited foaming over a relatively wide range of T and CO_2 contents in the vicinity of T_g. It could therefore be assumed that the matrix of the test specimens formed a continuum under these conditions, as confirmed by visual inspection. Figure 4.1 shows desorption data at different T and ambient pressure for the disc-shaped specimens impregnated by immersion in

liquid CO_2 for 3 hr at approximately 10 °C and 5 MPa. This resulted in an initial overall CO_2 content of about 0.29 g/g, which was assumed to be saturated as introduced in Section 3.2.2. 60 °C was in this case the upper limit of the range of T in which no foaming was observed during desorption from specimens impregnated under these conditions. Above 60 °C significant whitening was observed, but only limited expansion as long as T remained well below T_m, as will be discussed later.
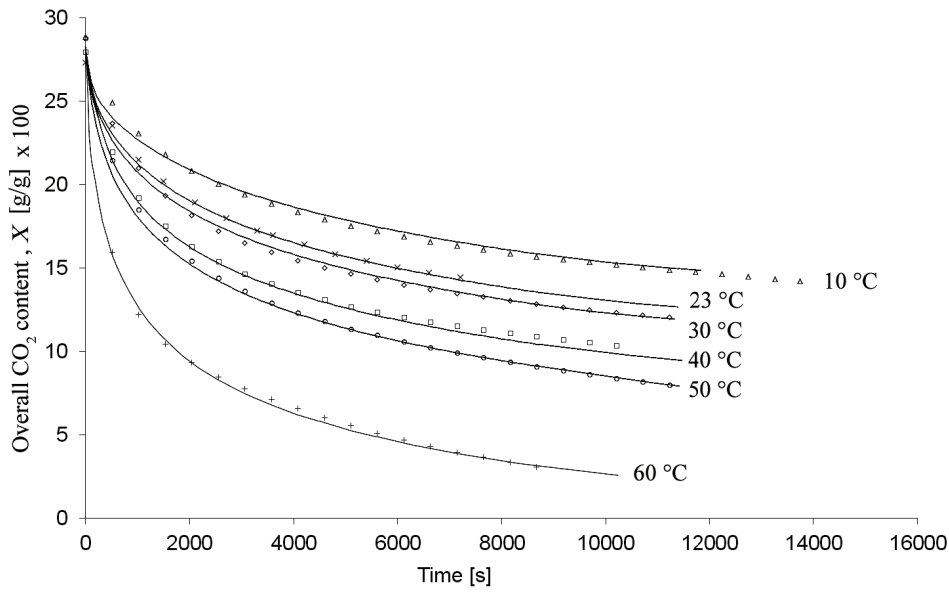
Figure 4.1 Experimental data for CO_2 desorption at the temperatures indicated from saturated discs of PLA1 with a thickness of 1 mm prior to impregnation, along with numerical fits to the data (continuous curves) using Equations 4.1 to 4.3 to describe 1-dimensional desorption of a non-swelling solute from an infinitely wide 1 mm thick sheet.

The data in Figure 4.1 were inconsistent with a constant diffusion coefficient, D, their implying D to decrease steeply with CO_2 content, c, as reflected by the tendency of the curves to flatten off at intermediate c after long times, t. It was assumed that desorption in the present case could be approximated to by Fick's second law in one dimension, i.e.

$$\frac{\partial c(x,t)}{\partial t} = \frac{\partial}{\partial x}\left(D[c(x,t)]\frac{\partial c(x,t)}{\partial x}\right) \qquad (4.1)$$

49

where x is normal to plane of the discs, $c[0 \leq x \leq l,0] = 0.29$ g/g and $c[0,t] = c[l,t] = 0$ g/g, where l is the plate thickness [119]. The dependence of D on c was modelled over the whole range of c using the empirical, but widely used expression for soluble penetrants

$$D[c(x,t)] = D[0] \exp[Ac(x,t)] \qquad (4.2)$$

where $D[0]$ and A are empirical fitting constants and $D[0]$ may be interpreted as the limiting value of D at zero CO_2 concentration [120–123]. The overall CO_2 content in g/g at time t was then given by

$$X[t] = \int_0^l \frac{c(x,t)}{l} dx \qquad (4.3)$$

$X[t]$ was determined numerically using the method of lines with second-order finite difference discretization incorporated in Mathematica 9™ (Wolfram Research). Approximate fits to the data were obtained by adjusting $D[0]$ and A, as shown in Figure 4.1. To maintain simplicity, no attempt was made to account explicitly for changes in the specimen dimensions due to swelling of the PLA by the CO_2, implying a systematic error in the absolute values of D of up to 10 % for the largest c considered here (assuming volume swelling to be approximately commensurate with the CO_2 content) [124,125]. There was also significant experimental uncertainty at short times, mainly owing to loss of CO_2 during transfer and temperature equilibration), resulting in an experimental error of about 2 % in the initial CO_2 content, although the numerical simulations indicated this to have little influence on $X(t)$ for t greater than a few minutes under the present conditions.

Figure 4.2 shows the values of $D[0]$ and A used to fit the data in Figure 4.1, plotted as a function of $1/T$. At T well below the nominal T_g of approximately 60 °C for PLA, A was estimated to be between 23 and 24 (the relative insensitivity of $X[t]$ to A in this range of T made precise determination difficult). A nevertheless decreased significantly as T approached T_g, indicating D to become less dependent on CO_2 concentration in this regime. The trends in $D[0]$ were consistent with an Arrhenius expression of the form

$$D[0.T] = D_0 \exp\left(-\frac{E_a}{RT}\right) \qquad (4.4)$$

for $T << T_g$, where E_a is an activation energy [J/(mol·K)], whereas above and immediately below T_g, $D[0]$ could be fitted with the Williams-Landel-Ferry (WLF) equation [126]

$$D[0.T] = D[0,T_r]exp\left(\frac{C_1(T - T_r)}{C_2 + T - T_r}\right) \qquad (4.5)$$
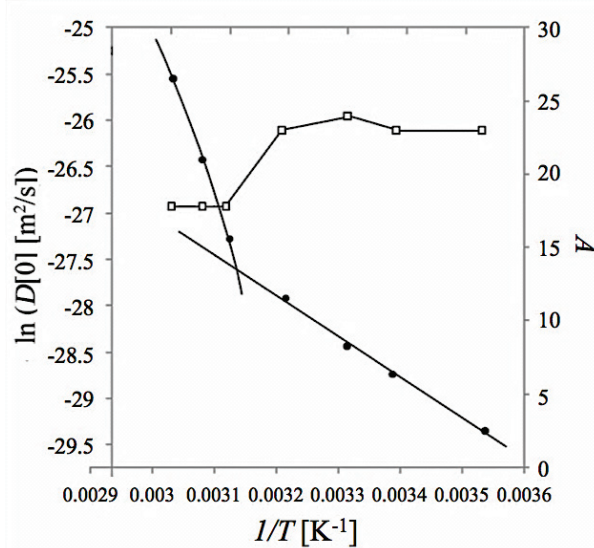
Figure 4.2 Fitting parameters used to obtain the numerical fits in Figure 4.1 as a function of $1/T$, along with fit of Equation 4.4 to the data for $D[0]$ for $T \leq 40$ °C (D_0=4.6 × 10^{-7}m^2/s and E_a/R = 4178 K) and a fit of Equation 4.5 to the data $D[0]$ for T ≥ 50 °C (T_r = 323 K, C_1 = 12.5 and C_2 = 60 K with $D[0,T_r]$ = 1.4 × 10^{-12} m^2/s).

as shown in Figure 4.2. Similar trends in the limit of zero concentration have been reported for measurements e.g. by forced Rayleigh scattering on other systems in the equivalent range of T [127], and the absolute values of both $D[0]$ and E_a were consistent with correlations established by Koros for a broad range of polymers and penetrants in the glassy state [128], bearing in mind that the degree of crystallinity of PLA1 was estimated from DSC to be approximately 34 wt% after saturation with CO_2 under the present conditions, and that experimental values of D are known to be reduced in semicrystalline polymers [120] (if the densities of amorphous and crystalline PLA are taken to be 1.25 g/cm^3 and about 1.4 g/cm^3 respectively [74], 34 wt% crystallinity implies an amorphous content of about 68 vol%).

4.1.2 Numerical modelling of the sorption process

The dependence of D on c determined empirically from the desorption data for PLA1 was also used to model the initial time dependence of sorption at 10 °C in liquid CO_2. This was problematical from a computational point of view owing to the relatively large values of A inferred from Figure 4.1. A strong dependence of D on c implies very steep concentration gradients during sorption, leading to numerical instabilities for any reasonable choice of time-step. These could be reduced by truncating D given by Equation 4.2 at c beyond the range of immediate interest, leading to results such as shown in Figure 4.3, where the boundary conditions were modified to simulate sorption into a semi-infinite plate with a surface CO_2 concentration of 0.29 g/g, using $A = 23$ and $D[0] = 1.8 \times 10^{-13}$ m^2/s. Consistent with previous observations on similar systems, e.g. PS/n-pentane [124], the diffusion profile showed some of the qualitative features associated with "case II" diffusion, i.e. steady advance of a well-defined step-like diffusion front [129–132]. However, the solute uptake predicted for a semi-infinite plate was not proportional to t, but rather increased as $t^{1/2}$. As shown in Appendix 1, where an analytical expression (Equation A5) for the CO_2 uptake by a plate of finite thickness l has been derived following Huang *et al.* [122], this is a direct consequence of the use of Equation 4.2 to describe $D[0]$.
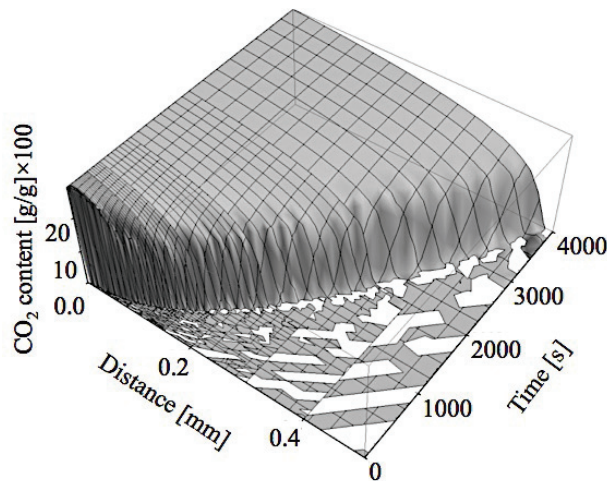
Figure 4.3 Sorption profile as a function of time predicted for 1-dimensional diffusion into a semi-infinite sheet of PLA1 at 10 °C assuming $c(x \leq 0,t)$=0.29 g/g, A=23 and $D[0]$=1.8 x 10^{-13} m^2/s.

Figure 4.4 shows the observed degree of sorption in as-molded and hence initially amorphous PLA1 discs immersed in liquid CO_2 at 10 °C and 5 MPa, normalized with respect to the concentration at saturation and plotted as a function of $t^{1/2}$, along with data for PLA2 obtained under the same conditions. As seen from Figure 4.4, the use of Equation A5 with fitting parameters derived from desorption experiments at 10 °C (cf. Figure 4.3) underestimated the sorption rate in the initially amorphous PLA1 discs. Indeed, it may be inferred from Equation A5 that the effective value $D[0]$ in the early stages of sorption into these latter was about twice that derived from the desorption data, assuming the effective value of Ac_o, where c_o is the saturation concentration, to remain constant (see Appendix 1).
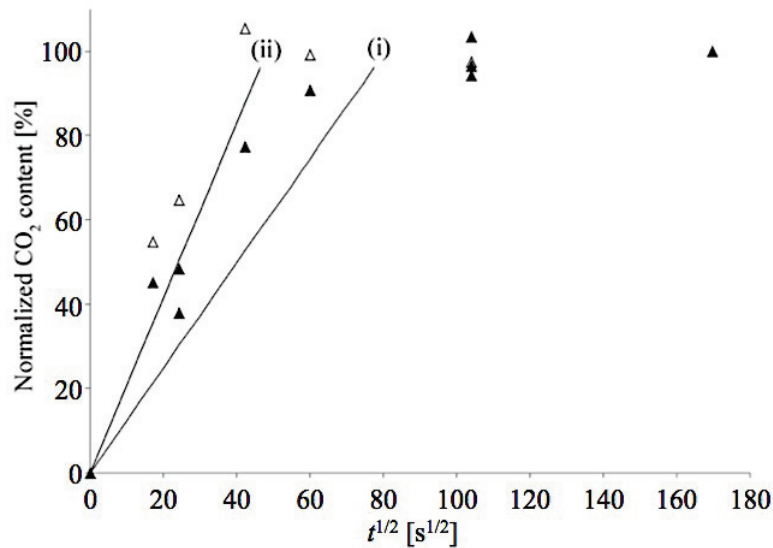
Figure 4.4 Normalized sorption as a function of $t^{1/2}$ for as-molded PLA1 (filled triangles) and PLA2 (open triangles) discs with an initial thickness of 1 mm, immersed in liquid CO_2 at 10 °C and 5 MPa, along with sorption profiles predicted from Equation A5 (solid curves) for $Ac_o = 6.67$ and (i) $D[0] = 1.8$ x 10^{-13} m^2/s and (ii) $D[0] = 3.6$ x 10^{-13} m^2/s.

The sorption data for PLA2, which remained essentially amorphous throughout impregnation, suggested the CO_2 content to reach saturation at about 0.43 g/g after roughly 2000 s immersion. For comparison, CO_2 contents of up to 0.55 g/g have been observed in PLDA under supercritical conditions [125], and the CO_2 content of about 0.29 g/g at saturation in PLA1 under the present conditions also implies a CO_2 content of 0.43 g per g of the amorphous phase. Moreover, while

the sorption rates for the initially amorphous PLA1 and PLA2 discs were similar at short times, those for PLA1 slowed significantly with respect to those of PLA2 after relatively long times, an effect that may be attributed to cold crystallization in regions of the discs behind the diffusion front. In cases where crystalline lamellae act essentially as a physical barrier to diffusion, i.e. diffusion of small molecules in polymers with relatively low degrees of crystallinity, D is often assumed to be equal to its value in the corresponding amorphous polymer, D_a divided by a tortuosity factor, $t \approx f_a^{-n}$. f_a is the amorphous volume fraction, i.e. about 0.68 in PLA1 after prolonged immersion in liquid CO_2, and n is an empirical constant between 1 and 2 depending on the polymer [133]. It follows from the results in Figure 4.4 that n was about 2 for PLA1.

These conclusions are nevertheless highly conditional on the underlying assumptions and approximations, e.g. the possible limitations of Equation 4.2 as an accurate description of $D[c]$, particularly at relatively large values of c, the experimental uncertainty in the transient CO_2 contents and the CO_2 content at saturation, and the lack of geometrical corrections for swelling. More importantly, any comprehensive description of the diffusion process may also need to take into account the non-Fickian processes (linked to time dependent swelling, multiple sorption mechanisms, physical aging etc.), that are widely assumed to be characteristic of the glassy state and the transition zone of polymeric materials [120,121,123,129–138]. The use of a single valued function $D[c]$ within a Fickian framework to describe both sorption and desorption may therefore be questionable. However, regardless of such detailed considerations, which are beyond the scope of the present work given the limited quality of the sorption data, an immediate practical consequence of the case II-type diffusion inferred from the simulations is that partial impregnation under these conditions will result in near-saturation of the outer regions of the specimens, while the inner regions remain substantially free of CO_2.

4.1.3   Desorption from partially impregnated specimens

Figure 4.5 shows simulated CO_2 concentration profiles for 1-dimensional desorption from 1 mm thick PLA1 sheets as a function of time at 10 °C, assuming a step-like initial CO_2 concentration profile, with a maximum CO_2 concentration of 0.29 g/g and two different overall CO_2 contents, assuming $A = 23$ and $D[0] = 1.8 \times 10^{-13}\,m^2/s$, as previously (an hence implicitly that the specimens had undergone cold crystallization).
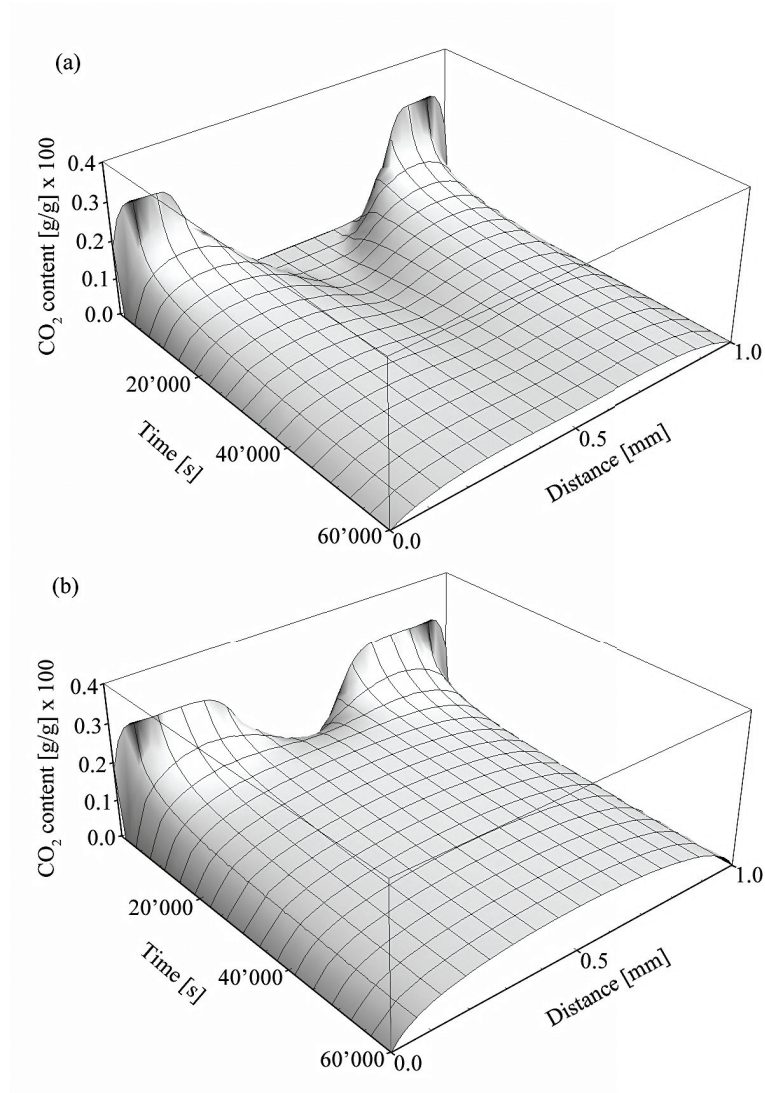
Figure 4.5 Desorption profile as a function of time predicted for an infinitely wide 1 mm thick sheet of PLA1 at 10 °C assuming a step-like initial CO_2 concentration profile (t=0) corresponding to overall CO_2 contents of (a) 0.10 and (b) 0.20 g/g, A=23 and $D[0] = 1.8 \times 10^{-13} \, m^2$/s.

The concentration profile rapidly became relatively uniform across most of the sheet thickness at the timescale shown, and the long term behaviour was insensitive to the exact form of the initial concentration profile and any transient sorption, a case II-type diffusion front advancing rapidly to

the mid-point of the sheet during the early stages of desorption (moreover, in the light of the previous discussion it is reasonable to assume the rate of diffusion into the core of initially amorphous specimens of PLA1 to be underestimated in these simulations, because the core is not expected to show significant cold crystallization).
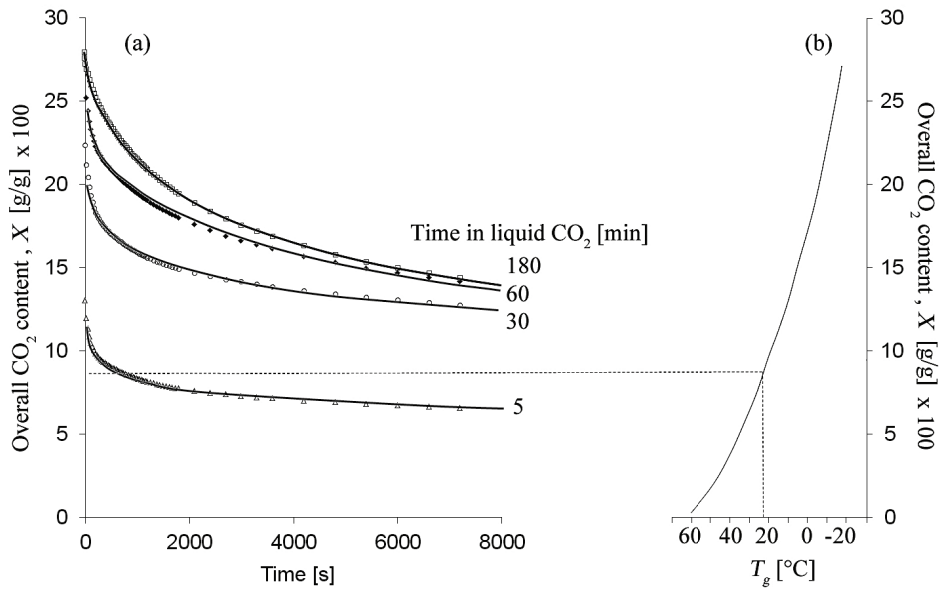
Figure 4.6 . (a) Experimental data for CO_2 desorption at 23 °C from partly saturated discs of PLA1 with a thickness of approximately 1 mm prior to impregnation and numerical fits to the data assuming an infinitely wide 1 mm thick sheet (continuous curves) and initial concentration profiles adjusted to match the initial overall level of sorption as described in the text with $A=23$ and $D[0]=3.3$ x 10^{-13} m^2/s; (b) dependence of T_g on CO_2 concentration in amorphous PLA following Chow, taking $z=2$.

The relevance of the model predictions to the experimental data is borne out by Figure 4.6 (a), in which experimental data for CO_2 desorption at 23 °C from partly saturated discs of PLA1 with a thickness of approximately 1 mm prior to impregnation and different overall CO_2 contents, is seen to be well described by: (i) assuming an initial step-like CO_2 concentration profile (slightly smoothed to avoid numerical instabilities) and adjusting this latter to match the initial overall CO_2 contents measured experimentally and (ii) taking $A = 23$ and $D[0] = 3.3$ x 10^{-13} m^2/s throughout. It was inferred from these results that it should be possible to stabilize the room temperature CO_2

56

content at around 0.1 g/g (assumed to be adequate for foaming) throughout the interior of the discs, by partial impregnation in liquid CO_2 followed by partial desorption. Indeed, existing protocols for the production of expandable PLA using liquid CO_2 emphasize the need for a low temperature conditioning step at ambient pressure in order to reduce the CO_2 content in saturated specimens to manageable levels [7]. On the other hand, Figures 4.5 and 4.6 (a) suggest that it should be possible to achieve close to ideal CO_2 dispersions using relatively short impregnation times. That a CO_2 content of 0.1 g/g should be stable under these conditions may be inferred from Figure 4.6 (b), where T_g has been plotted as a function of c, using a fit of Chow's equation [45] to experimental data from the literature [118], indicating T_g of amorphous PLA to fall below room temperature at close to 0.1 g/g. It follows that amorphous PLA containing a uniform dispersion of 0.1 g/g of CO_2 should not show premature foaming during handling at room temperature.

An alternative means of obtaining a relatively flat CO_2 profile at a relatively low overall CO_2 contents is to saturate the discs at higher temperatures, i.e. under supercritical conditions, where the equilibrium sorption is lower. Figure 4.7 shows experimental desorption data for CO_2 desorption at 23 °C from PLA1 impregnated at 40 °C and 8 MPa along with a fit of Equations 4.1 to 4.3 obtained by assuming $A = 23$ and adjusting the initial CO_2 content and $D[0]$. Because depressurization was carried out over a period of around 1000 s in order to restrict foaming, it was assumed somewhat arbitrarily that $t = 0$ in Figure 4.7 corresponded to $t = 1000$ s in the simulation, so that the initial transients seen e.g. in the data in Figure 4.1 were absent. The value of $D[0]$ of 2 x 10^{-13} m^2/s obtained by this fitting procedure was nevertheless significantly lower than the value of 3.3 x 10^{-13} m^2/s inferred from the fits to the desorption data for specimens impregnated with liquid CO_2. It was beyond the scope of the present work to examine these effects systematically, so that the precise reasons for the reduced desorption rate in this case remain open to question. However, it appears that the effective diffusion constant during desorption may be sensitive to the sorption conditions, even where the final degree of crystallinity is insensitive to the method of impregnation. Indeed no significant differences were observed between DSC heating scans obtained after impregnation under supercritical conditions and in liquid CO_2.
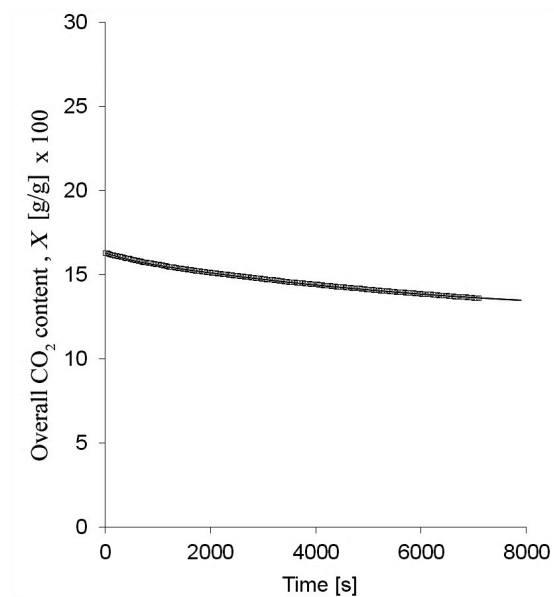
Figure 4.7 Experimental data for CO_2 desorption at 23 °C from a disc of PLA1 saturated under supercritical conditions (40 °C and 8 MPa for 3 hr) with a thickness of approximately 1 mm prior to impregnation and numerical simulation assuming an infinitely wide 1 mm thick sheet (continuous curves) and initial CO_2 content of 0.18 g/g, $D[0]$=2 x 10^{-13} m²/s and A=23 with a time delay of 1000 s (see the main text).

4.2 Desorption from PLA2

At 0.43 g/g of CO_2, the T_g of PLA may be assumed to be well below room temperature (more than 40 °C below room temperature according to Chow's equation [45]). Indeed when room temperature desorption measurements were attempted on specimens of PLA2 saturated with liquid CO_2 at 10 °C, not only did the specimens foam, but the foam structures were unstable, leading to rapid desorption of the CO_2 via rupture of the cell walls. This is reflected by Figure 4.8, which shows data for desorption at 23 °C from 1 mm thick discs of PLA2 fully and partly impregnated with liquid CO_2, along with data for a PLA2 disc impregnated under supercritical conditions, as described for PLA1 in the previous section. The specimen temperatures decreased to about -30 °C immediately after depressurization, (indeed the depressurization rates used here were sufficient to produce dry-ice in the autoclave chamber). However, as T approached room temperature after 100 to 200 s, the CO_2 content of the saturated specimens not only diminished

rapidly to much lower levels than for PLA1 for a given t (cf. Figure 4.1) but also fell to levels below those observed for partially saturated PLA2. On the other hand, while specimens of PLA2 impregnated under supercritical conditions showed some degree of foaming during depressurization, as evidenced by their opacity after removal from the autoclave, their final CO_2 content was about 0.18 g/g, implying T_g to be close to 0 °C (cf. Figure 4.6 (b)). There was no further significant expansion at 23 °C, and subsequent desorption was relatively slow, as seen from Figure 4.8, suggesting stability to be maintained up to T somewhat greater than T_g.
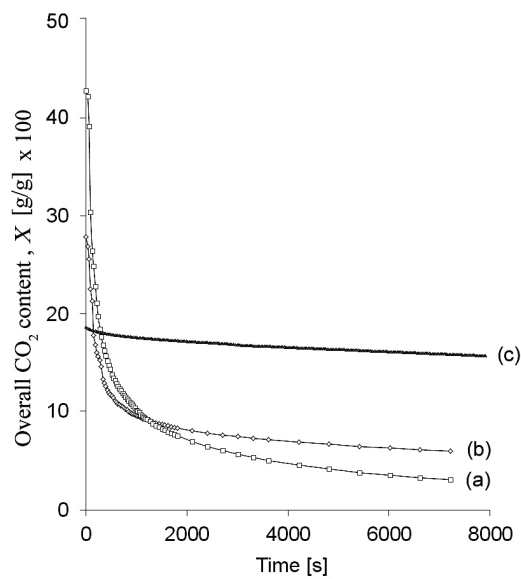
Figure 4.8 Experimental data for CO_2 desorption at 23 °C from discs of PLA2 with a thickness of approximately 1 mm prior to impregnation for (a) 3 hr and (b) 10 minutes in liquid CO_2 at 10 °C and 5 MPa, and (c) under supercritical conditions (40 °C and 8 MPa for 3 hr).

4.3 Consequences for foaming

It was inferred from the results described in the preceding sections that it should be possible to produce an acceptable solid amorphous PLA2 precursor by partial impregnation in liquid CO_2 at 10 °C and 5 MPa followed by conditioning at ambient pressure at a sufficiently low temperature to prevent foaming. Conditioning was carried out by rapidly transferring the specimens to a freezer maintained at 10 °C, i.e. more than 30 °C above the estimated T_g for the highest CO_2

contents. There was nevertheless little sign of foaming owing to the reduction in T due to depressurization, which was presumably sufficient to prevent foaming during transfer and the initial stages of conditioning. However, for any reasonable choice of $D[0]$, the step-like CO_2 concentration profiles assumed for partially impregnated specimens were predicted to flatten after relatively short times, as discussed previously for PLA1 (cf. Figure 4.5). Thus, a PLA2 disc partially impregnated by immersion in liquid CO_2 for 10 minutes to give an initial overall CO_2 content of about 0.25 g/g was estimated to contain between 0.1 and 0.2 g/g of CO_2 over most of its width after conditioning for 2 hr at 10 °C, assuming $D[0] = 5 \times 10^{-13}$ m^2/s and $A = 23$ (values consistent with the observed sorption rates in PLA2).

Figure 4.9 SEM micrograph of a diametric cross-section through a PLA2/10 wt% talc disc with an initial thickness of 1 mm, after immersion in liquid CO_2 for 10 minutes, conditioning at 10 °C for 2 hr and immersion in boiling water.

Figure 4.9 shows an SEM micrograph from the central part of a diametric cross-section through a specimen of PLA2/10 wt% talc held in liquid CO_2 at 10 °C for 10 min, conditioned for a further 2 hr at 10 °C after depressurization and then foamed by immersion in boiling water. The presence of the talc made little difference to the sorption and desorption behaviour, although the CO_2 content at saturation decreased in proportion to the amount of talc. However, the nucleating effect of the talc during foaming generally led to relatively fine, closed-cell foam microstructures that

were more straightforward to interpret in terms of the impregnation conditions that the coarser, irregular structures obtained without addition of talc. As seen from Figure 4.9, foaming of PLA2 under these conditions led to a relatively homogeneous morphology across the specimen cross-section, roughly spherical cells, consistent with the observation of uniform macroscopic expansion, and a final foam density of around 30 kg/m^3. This was in marked contrast to specimens removed from the autoclave immediately after impregnation, which showed little lateral expansion owing the constraining effect of the specimen core, which was substantially free of CO_2, and very limited expansion in the thickness direction, any cellular structure formed in the outer regions of the discs tending to collapse, even during the spontaneous foaming observed at room temperature.

The situation was more complex in the case of the as-molded PLA1 discs owing to cold crystallization during impregnation. Figure 4.10 shows SEM micrographs from the central part of diametric cross-sections of as-molded PLA1 discs foamed by immersion in boiling water after various impregnation treatments, along with numerical predictions of the through-thickness concentration profiles expected for cold-crystallized discs subjected to the same impregnation treatments. These predicted concentration profiles were assumed to provide at least a rough indication of the distribution of the CO_2 prior to foaming. Specimens held in liquid CO_2 at 10 °C for three hours, i.e. sufficient for the CO_2 content to approach saturation, showed limited expansion on immersion in boiling water and a final density of about 500 kg/m^3. On the other hand, specimens partially impregnated in liquid CO_2 at 10 °C for 10 minutes to give an overall CO_2 content of about 0.15 g/g, underwent significantly greater expansion, leading to a density of about 350 kg/m^3. It is seen from Figure 4.10a that the internal morphology consisted in this case of unexpanded skin and core regions separated by relatively large cells elongated in the thickness direction. The assumption of a case II-type diffusion profile during sorption implies regions within about 0.25 mm of the surface to have CO_2 contents close to saturation under the corresponding impregnation conditions, from which it is inferred that they undergo cold crystallization, preventing subsequent expansion in any direction. On the other hand, cells nucleated at the edge of the skin are able to expand into the amorphous interior of the specimen, although their lateral expansion is constrained by both the skin and the CO_2-free core, as was apparent from the observed cell morphology.

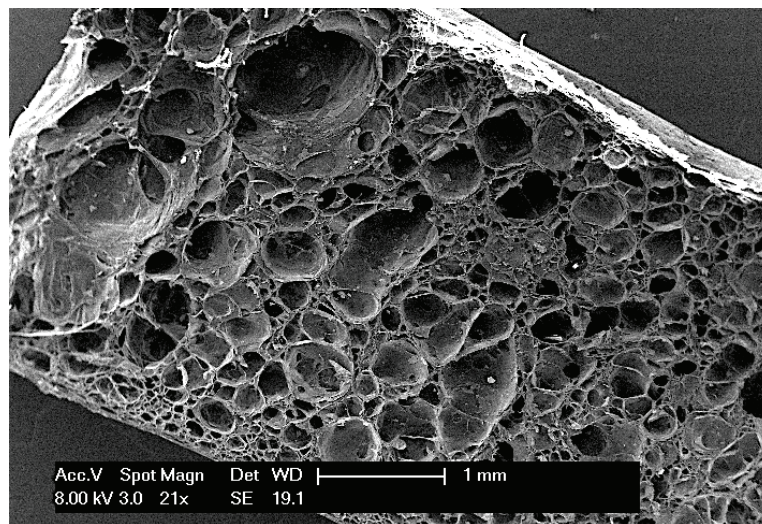Figure 4.10 SEM micrograph of a diametric cross-section through a PLA1 disc with an initial thickness of 1 mm, immersed in boiling water after: (a) immersion in liquid CO_2 for 10 minutes; (b) immersion in liquid CO_2 for 10 minutes followed by conditioning at 10 °C for 2 hr; (c) immersion in liquid CO_2 for 10 minutes followed by conditioning at 10 °C for 4 hr. Numerical estimates of the through-thickness CO_2 concentration profiles prior to foaming are also shown in each case.

The specimens in Figure 4.10b and 4.10c were impregnated for in liquid CO_2 for 10 minutes and then held at ambient pressure after depressurization at a nominal temperature of 10 °C for 2 and 4 hr, respectively. After conditioning for 2 hr, the numerical simulations suggested the CO_2

concentration in the core to remain relatively low, and the microstructure was similar to that in Figure 4.10a, in that unexpanded skin and core regions were still present. However, the extent of expansion of the intermediate layers in the thickness direction was substantially greater than in the unconditioned discs, resulting in a density of about 280 kg/m^3. As suggested by the simulations, conditioning for 4 hr resulted in a more uniform CO_2 concentration throughout the interior of the specimens so that in this case, with the exception of the skin regions, expansion was uniform in the thickness direction, and the final density was about 200 kg/m^3 in spite of the lack of lateral expansion and the relatively low overall CO_2 content after conditioning.

Figure 4.11 shows the internal morphology of as-molded PLA1 discs impregnated for 30 minutes in liquid CO_2 to give an overall CO_2 content of about 0.23 g/g, and conditioned for various times. Only limited expansion was visible in the outer regions of the specimens foamed without conditioning, but in contrast with saturated specimens, the core regions, assumed to remain amorphous immediately after impregnation, broke down, resulting in pronounced blistering (Figure 4.11a). In specimens foamed after conditioning for 30 minutes at 10 °C, the skin regions were no longer cavitated, presumably owing to their lower CO_2 content, and as seen from Figure 4.11 (b), they were about 0.4 mm in thickness, i.e. significantly thicker than for the shorter impregnation times in Figure 4.10. Hence, while the remainder of the specimen showed a cellular structure, consistent with the predicted CO_2 profile, i.e. a relatively high CO_2 content throughout the thickness after conditioning, there was again no lateral expansion and the density was relatively high at 480 kg/m^3. The morphology of specimens foamed after conditioning for 1 hr was similar (Figure 4.11 (c)), but the core showed less expansion and the final density of 570 kg/m^3 did not represent a significant improvement over the densities achieved with saturated specimens, suggesting significant further cold crystallization to have taken place during the condition step.
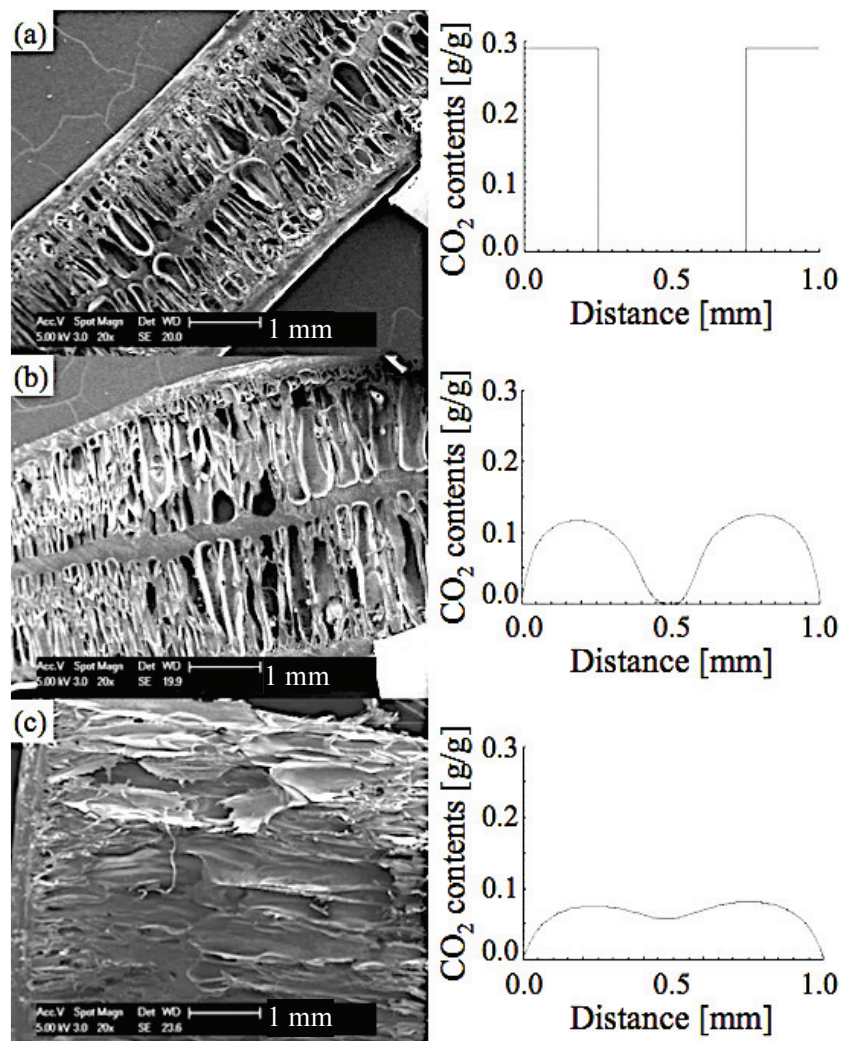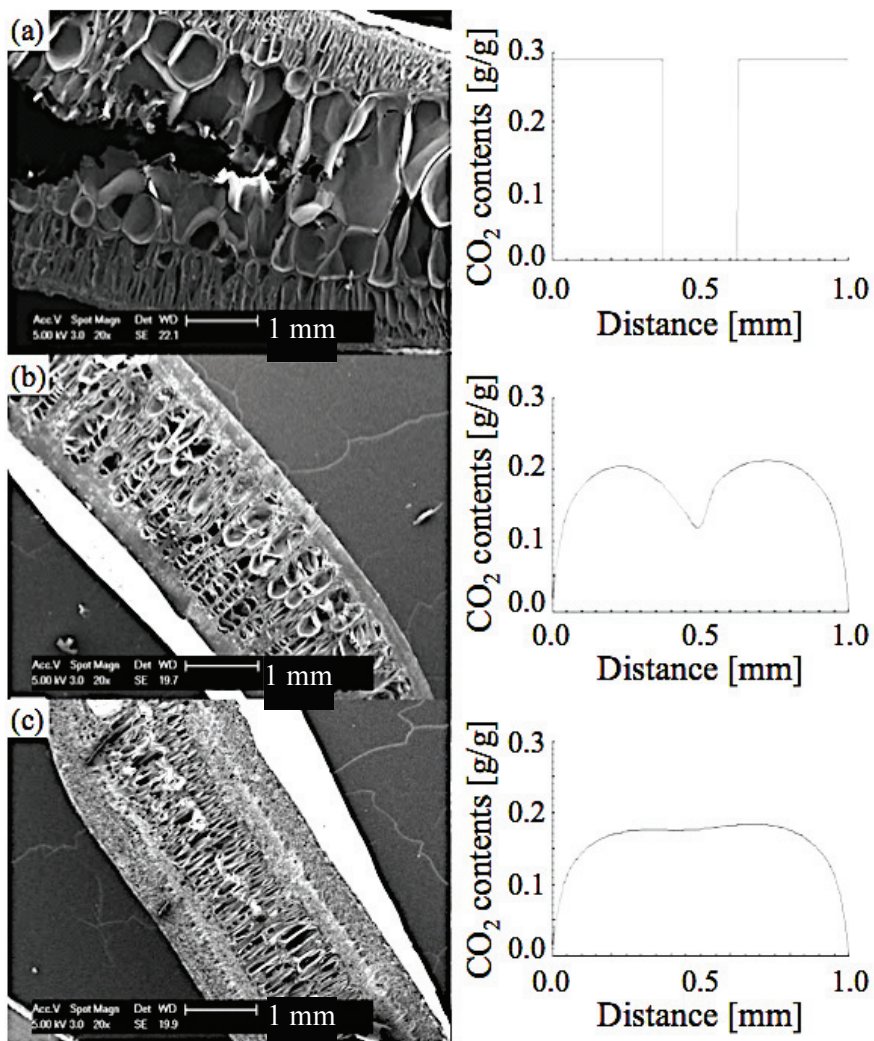
Figure 4.11 SEM micrograph of a diametric cross-section through a PLA1 disc with an initial thickness of 1 mm, immersed in boiling water after: (a) immersion in liquid CO_2 for 30 minutes; (b) immersion in liquid CO_2 for 30 minutes followed by conditioning at 10 °C for 30 minutes; (c) immersion in liquid CO_2 for 30 minutes followed by conditioning at 10 °C for 1 hr. Numerical estimates of the through-thickness CO_2 concentration profiles prior to foaming are also shown in each case.

4.4 Crystallization of PLA during impregnation with liquid CO_2

The distinct foam structures obtained for PLA1 after different immersion times in CO_2 at 5 MPa and 10 °C followed by low T conditioning (cf. Figures 4.10 and 4.11), were attributed in the previous section to CO_2 induced crystallization. To investigate this phenomenon further, the internal morphology of initially amorphous hot pressed PLA1 discs after various CO_2 treatments was characterized using a combination of microscopy techniques.

As shown in Figure 4.12, PLA1 specimens impregnated for relatively short times, t_{imp}, in liquid CO_2 at 10 °C showed a well-defined, uniform, but weakly birefringent layer, extending to a constant depth from both surfaces, with no clear fine structure when observed in the optical microscope. The core regions of these specimens showed little birefringence.
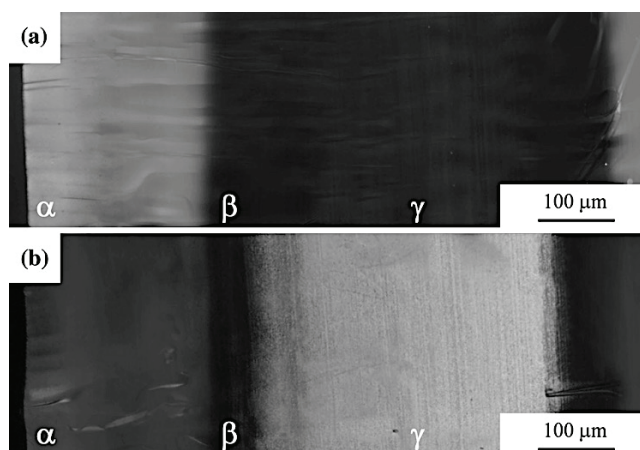
Figure 4.12 Optical micrographs between crossed polarizers of (a) a semi-thin cross-section taken from a specimen held in liquid CO_2 at 10 °C for 10 min, after desorption of the CO_2, (b) a semi-thin cross-section from the same specimen and subsequently heated to 130 °C at 20 K/min using a hot stage. α, β and γ indicate the approximate positions of the specimen surface, the limit of the birefringent surface layer and the midpoint of the specimen respectively.

In Figure 4.13, estimates of the volume fraction corresponding to the birefringent layers from optical microscopy are compared with $X(t)$, the measured mass uptake of CO_2 expressed in g of CO_2 per g of PLA, normalized with respect to the mass uptake of CO_2 at saturation, c_o (estimated

to be 0.29 g/g), which was reached for t_{imp} greater than about 3 hr. While there was considerable experimental scatter for short t_{imp}, and t_{imp} itself was associated with an uncertainty of the order of 1 min (the time necessary to reach steady-state conditions in the autoclave), the results shown in Figure 4.13 suggested the thickness of the birefringent layer to be approximately proportional to the CO_2 uptake throughout the impregnation process.
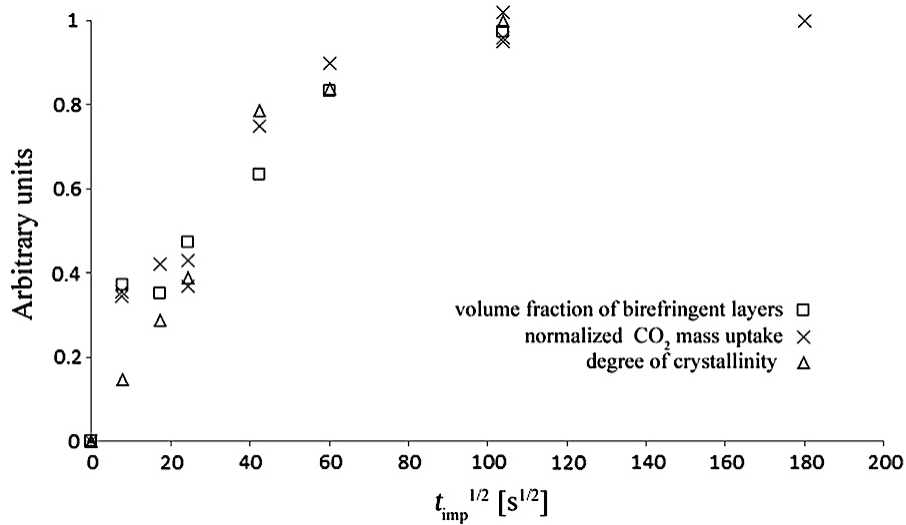
Figure 4.13 The influence of impregnation time, t_{imp}, on: the estimated volume fraction of the birefringent layers observed by optical microscopy; the mass uptake of CO_2 normalized with respect to its value at saturation (0.29 g/g); the relative degree of crystallinity after desorption of the CO_2, defined as the overall melting enthalpy (in J/g) determined from DSC heating scans, normalized with respect to its limiting value after long t_{imp} (estimated to be 32 J/g).

Figure 4.14 shows TEM micrographs of the morphology of specimens crystallized in CO_2. Although RuO_4 is known to be effective as a stain for semicrystalline PLA [139], the morphology corresponding to the birefringent regions of the specimens was poorly defined, consistent with the lack of structure in the optical images. There was nevertheless some suggestion from the TEM micrographs that a lamellar texture with a lamellar thickness of roughly 10 nm was already established locally after short t_{imp}.
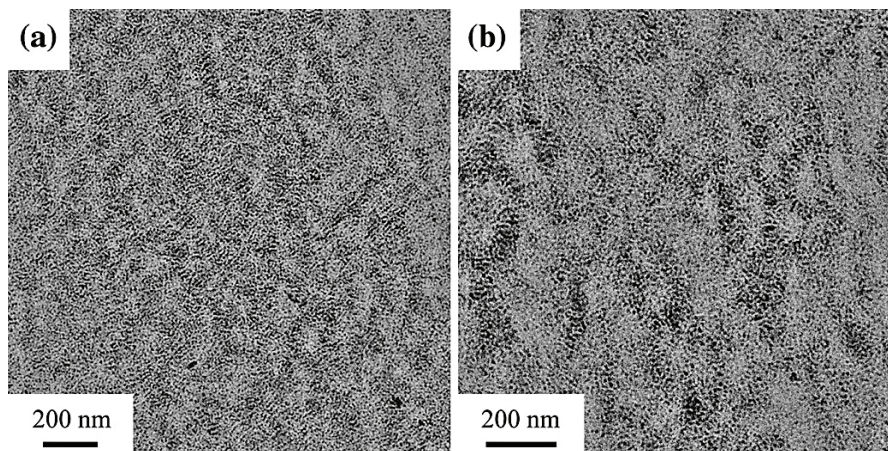
Figure 4.14 TEM micrographs of RuO_4 stained sections taken from the birefringent layers in specimens exposed to liquid CO_2 at 10 °C for (a) 5 min and (b) 3 hr, after desorption of the CO_2.

Figure 4.15 and Table 4.1 give results from DSC heating scans at 20 K/min on samples of about 5 mg in mass taken through the whole thickness of the impregnated specimens after desorption of the CO_2. T_g showed little systematic variation for long t_{imp}, remaining at about 62 °C under these measurement conditions, but for relatively short t_{imp}, T_g increased somewhat to about 65 °C, and was associated with a marked endothermic peak, effects that were attributed to physical ageing. The as-molded PLA specimens did not show an exothermic peak at T_g, indicating the physical ageing to have taken place during impregnation and/or desorption. The as-molded specimens were also initially highly amorphous and crystallization during DSC heating and cooling cycles was suppressed at scanning rates of 20 K/min. However, significant crystallinity was observed in the impregnated specimens for all the t_{imp} considered. The qualitative behavior was similar in each case: a broad exothermic peak appeared as T increased above T_g, followed by a marked endotherm, with a peak temperature of between 168 and 173 °C, depending on t_{imp}. A heating rate of 20 K/min ensured the onset of the exotherm to be sufficiently well separated from the glass transition and the associated endotherm to allow unambiguous definition of a linear baseline from which the overall enthalpy change during the scans could be determined, regardless of t_{imp} (this was not true of lower heating rates, but results obtained at 10 K/min were generally consistent with those shown here).

67
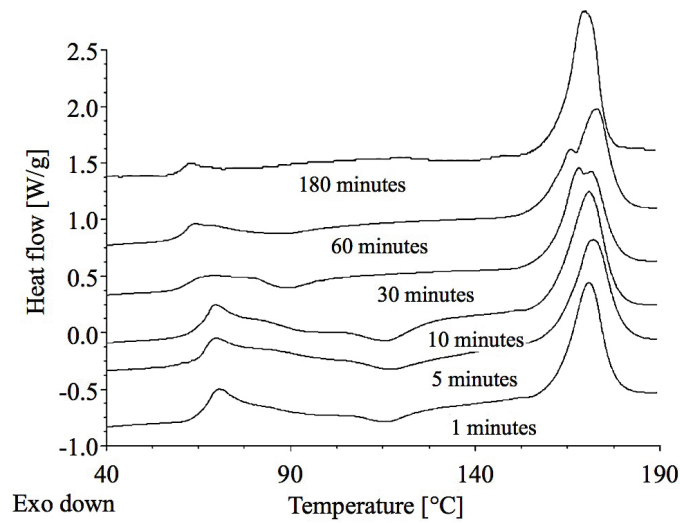
Figure 4.15 DSC first heating scans at 20 K/min for the different t_{imp} indicated.

Table 4.1 Summary of data from DSC first heating scans at 20 K/min.

t_{imp} [min]	T_g [°C]	Exotherm peak [°C]	Upper melting peak [°C]	Lower melting peak [°C]	Melting enthalpy [J/g]
1	65	116	170	-	4.69
5	65	117	171	-	9.24
10	65	116	171	-	12.5
30	63	90	171	168	25.2
60	62	87	172	166	26.9
180	62	-	169	-	32.0

The melting enthalpy tended to about 32 J/g after long t_{imp} (3 hr or more), and, as seen from Figure 4.13, the enthalpy change obtained at intermediate t_{imp} (t_{imp}>5 min) normalized with respect to this limiting value were broadly similar to the normalized degree of CO_2 uptake at the same t_{imp}. On the other hand, for shorter t_{imp} , the normalized melting enthalpies were relatively low, suggesting a few minutes to be necessary for the degree of crystallinity to reach its limiting value in regions of high CO_2 content.

The peak temperature of the main exotherm in the DSC heating scans was close to 116 °C for low t_{imp}, which is in the same temperature range as the peak spherulite growth rates determined from hot-stage microscopy of specimens crystallized from the melt, and the maximum crystallization rates in isothermal DSC measurements. It may be inferred, therefore, that these exotherms corresponded mainly to crystallization of regions of the specimens that remained substantially amorphous during impregnation, although the nucleation rate was presumably higher than in the as-molded specimens. Corroborating evidence for this was provided by hot-stage optical microscopy of sections from partially impregnated specimens (Figure 4.12 (b)), which showed the core to develop a fine spherulitic texture during heating. As the original CO_2 content approached saturation, the DSC exotherm weakened, and its peak shifted to lower temperatures, e.g. about 87 °C for t_{imp}=1 hr. Moreover, the form of the onset of the exotherm appeared similar in all the specimens, possibly reflecting the existence of a "transition zone" of enhanced nucleation between the birefringent layers and the amorphous core. The peak temperature of the main melting endotherm initially changed little with increasing t_{imp}, remaining at between 170 and 171 °C. For longer t_{imp}, however, two melting peaks were observed; the upper peak temperature increasing to about 172 °C as t_{imp} increased to 1 hr, while the temperature of the lower melting peak decreased from 168 to 166 °C as t_{imp} increased from 0.5 to 1 hr. Finally, in saturated specimens (t_{imp} of 3 hr or more), a single melting peak was observed at about 169 °C. The main DSC melting peak at comparable scanning rates for PLA crystallized by heating from the glassy state or for specimens crystallized isothermally at temperatures below about 125 °C generally results from reorganization during the scan. Even so, the relatively low final melting temperature of these latter was assumed to reflect an initial state of reduced crystalline order.

The results presented this section are consistent with the existence of a step-like diffusion front during diffusion of liquid CO_2 into PLA at 10 °C as argued in Section 4.1.2. For initially amorphous low D-lactide PLA specimens, the position of the diffusion front after a given impregnation time was shown to be associated with a step-like increase in birefringence, which was associated with CO_2 induced crystallization above a certain critical concentration of CO_2. The most obvious consequence of this crystallization was a significant decrease in the rate of CO_2 uptake and overall CO_2 content at saturation compared with that observed for PLA with a relatively high D-lactide content that showed little tendency to crystallize. This may be seen as a consequence of the establishment of physical barrier to diffusion at the specimen surface that

shields the interior from the high CO_2 concentrations associated with the immersion of fully amorphous PLA in liquid CO_2. Even so, the qualitative insight into the diffusion process provided by the present work is expected to contribute to efforts to optimize precursor geometries (effective specimen thickness) and impregnation conditions (time, temperature) for the CO_2 foaming of low D-isomer PLA at the particleboard processing temperatures, i.e. above the nominal T_g, but below the melting T.

4.5 Conclusions

The results described in the present chapter have confirmed the usefulness of approximate numerical models for the diffusion of CO_2 in PLA over a wide range of concentrations as a guide to optimizing impregnation and conditioning treatments for the in situ foaming of amorphous PLA at the foam core particleboard process. In the case of semicrystalline PLA, cold crystallization played an important role in both the diffusion and foaming behaviour of initially amorphous specimens. For example, saturation of such specimens by holding them for 3 hr at 10 °C in liquid CO_2 led to relatively high degrees of crystallinity and little expansion on immersion in 100 °C water. Thus, the skin regions of partially impregnated specimens, which were predicted from the diffusion model to contain CO_2 concentrations close to the saturation concentration, showed little or no expansion, depending on their CO_2 content after conditioning. On the other hand, regions of the specimens that were initially free from CO_2 (as a consequence of the step-like concentration profiles predicted from the diffusion model) and in which the CO_2 content rose to more modest levels during conditioning, foamed readily, in spite of the low CO_2 content and the lateral constraints imposed by the relatively rigid skin in the present disc geometry. This follows from the assumption that T_g should be close to 10 °C in the range 0.1 to 0.15 g/g CO_2 (Figure 4.6b), so that cold crystallization should be minimal at this temperature, even after very long times, provided the CO_2 content never greatly exceeds these levels. A possible future direction might therefore be to use impregnation/conditioning at lower temperatures to obtain roughly uniform dispersions of around 0.1 g/g CO_2 or less in the as-molded PLA1 discs, and hence suppress cold crystallization both during impregnation and on raising T to room temperature, or alternatively to control the tendency to crystallize, so that crystallization is

suppressed under the present impregnation conditions, but is able to take place during foaming. This latter possibility will be explored further in Chapter 7.

With regard to foaming, no attempt has been made to investigate factors such as the role of heat transfer during foaming, nor to optimize the foaming process with respect to the precursor geometry, although this is important for controlling the final foam morphology, as will be discussed in Chapter 8. The numerical models presented in this section are nevertheless useful for optimizing processing parameters such as the impregnation and conditioning times, which should ideally be as short as possible in an industrial process, and retention time for the CO_2 at high temperatures, which should be as long as possible in order to provide adequate flexibility in terms of processing windows.

Chapter 5

Solid state PLA-PMMA foam precursors

Poor thermal stability and long-term durability are well known to limit the applications of PLA. T_g and heat deflection temperature in the amorphous state are about 60 and 50 °C respectively, i.e. far lower than those of PS, for example, whose T_g is about 100 °C. This is potentially problematic for the one step particleboard process given that stable foaming should take place at temperatures compatible with skin layer consolidation. Preliminary trials using EPS showed that relatively high platen T of about 160 °C (the core layer T was not measured but was assumed to be close to 100 °C given the high water content of the skin layer formulation) resulted in both stable foaming and significantly better dimensional stability of the surface layer than for a platen T of 130 °C [23], whereas use of amorphous PLA led to unstable foaming and foam collapse even at the lower platen T. As set out in the previous Section 4.3, semicrystalline PLA, which has a T_m of about 170 °C, showed only limited expansion in this temperature range. The possibility of improving the thermal properties of the amorphous PLA grade were therefore considered.

Various means of improving the thermal properties of PLA exist, including stereo complexation [140], filler addition, copolymerization and blending [141]. Blending with one or more relatively high T_g polymers is potentially a particularly straightforward and effective way to tailor the glass transition, provided that the different blend components show adequate compatibility and physical characteristics [142,143]. One promising candidate is atactic PMMA which is an inexpensive amorphous thermoplastic with T_g typically around 110 °C, depending on its comonomer content and tacticity. While the behavior of PLA-PMMA blends may vary significantly with molar mass, the degree of crystallinity and the processing conditions, they have been demonstrated from calorimetric data to show at least partial miscibility and composition dependent T_g [9,143–152].

Moreover, the solubility of CO_2 in PMMA-PLA blends under both sub-critical and super-critical conditions has been found to be sufficient to permit its use as a physical blowing agent for the preparation of low density foams [148,153].

In this thesis, we are specifically interested in the use of liquid CO_2 to prepare PLA-PMMA foam precursors for the one step particleboard process. The CO_2 impregnated PLA-PMMA precursors should meet the requirements, i.e. in the form of pellets or granules that are sufficiently stable under ambient conditions to allow straightforward handling, but expand on heating to form low density foams with significantly higher T_g than that of unmodified PLA foams [8,73]. In what follows, we describe: (i) the preparation of model PLA-PMMA foam precursors by melt blending and impregnation with liquid CO_2; (ii) preliminary studies of the thermally induced foaming behavior of these precursors and the characteristics of the resulting foams.

5.1 Thermal and mechanical properties of the PLA-PMMA blends

All the compression molded, extruded and injected specimens were suggested by DSC heating scans from 20 to 230 °C and 10 K/min to be substantially amorphous in so far as the net enthalpy changes during the scans were very much less than the heat of fusion of fully crystalline poly-L-lactide of 93 J/g [154]. Semicrystalline PLA1 nevertheless showed a cold crystallization exotherm with a peak at about 112.5 °C, followed by a melting endotherm with a peak at about 170 °C, and approximately the same area as the crystallization peak. As seen from Figure 5.1(a), the as-compounded PLA1-20 wt% PMMA pellets also showed a clear cold crystallization endotherm with a peak as about 150 °C and a melting peak at 170 °C. However, while a slight endotherm persisted in PLA1-40 wt% PMMA, there was no evidence of cold crystallization under these at higher PMMA contents.
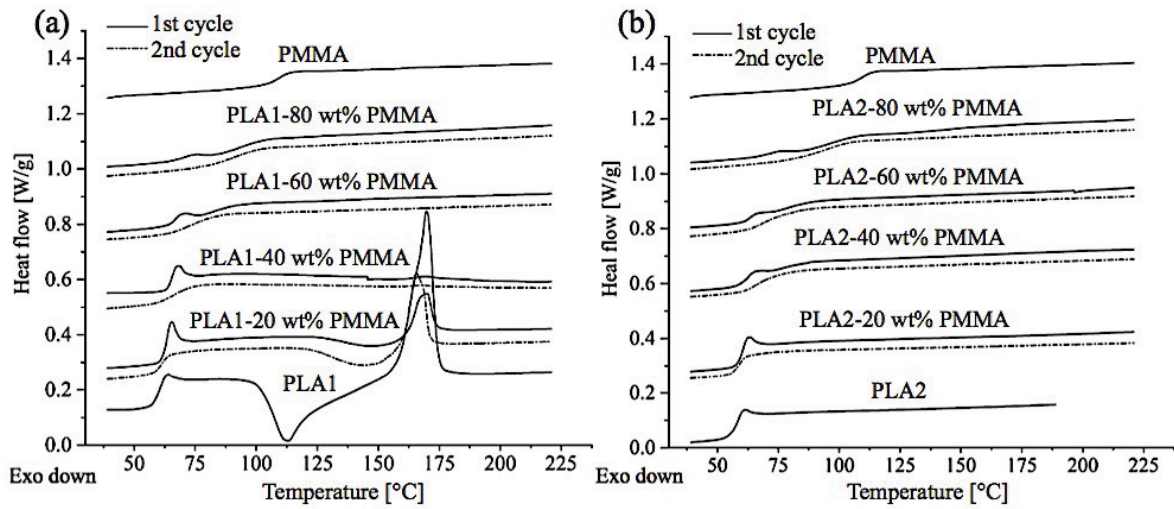
Figure 5.1 Thermal behaviors of (a) PLA1-PMMA blends and (b) PLA2-PMMA blends. In both PLAs, T_g was increased according to PMMA content.

The data in Figure 5.1 also suggested the presence of two glass transitions during the first DSC heating scan of the as-extruded blends, whose estimated mid-point temperatures are given in Table 5.1 as T_{g1} and T_{g2}, with the subscript 2 denoting the higher transition temperature. The blends with the lowest PLA2 contents showed an endothermic peak immediately above T_{g1}, which was attributed to physical aging, and may have masked a second glass transition in certain cases. However, a single, albeit relatively broad glass transition was observed in all the blends during subsequent cooling at 10 K/min from 230 to 20 °C, as well as in the following second heating scan. As seen from Figure 5.2, where the identifiable T_g have been plotted as a function of the PMMA content, the transition temperatures, T_{g12}, measured from the second heating scan were intermediate between T_{g1} and T_{g2}.

Table 5.1 Thermam transitions determined by DSC for the different PLA-PMMA blends

	wt% PMMA	T_{g1} [°C]	T_{g2} [°C]	T_{g12} [°C]	T_{ma} [°C]	T_{mb} [°C]	ΔH_a [J/g]
Extruded PLA1-PMMA	0	60.6			169.9		32.6
	20	61.0	-	61.0	170.1	166.2	8.0
	40	62.5	77.4	66.1	168.6	168.6	0.5
	60	68.0	83.7	73.3	-	-	-
	80	71.2	92.4	88.7	-	-	-
	100	110.0			-	-	-
Extruded PLA2-PMMA	0	58.4			-	-	-
	20	60.3	-	59.7	-	-	-
	40	60.9	78.1	63.3	-	-	-
	60	66.5	81.6	72.3	-	-	-
	80	71.5	95.7	93.1	-	-	-
	100	110.0			-	-	-
Compression molded PLA1-PMMA	0	60.6			169.4		29.0
	20	58.6	-	61.66	167.0	165.8	17.0
	40	62.8	82.7	65.2	167.2	-	1.7
	60	73.4	-	75.49	-	-	-
	80	-	95.16	87.97	-	-	-
	100	109.6			-	-	-
Compression molded PLA2-PMMA	0	57.5			-	-	-
	20	55.3	-	58.29	-	-	-
	40	61.0	84.5	63.3	-	-	-
	60	68.9	-	72.82	-	-	-
	80	-	88.3	92.68	-	-	-
	100	109.6			-	-	-
Compression molded PLA1-PMMA after impregnation	20	56.3	-	-	169.5		29.5
	40	55.6	103.6	-	165.9		20.9
	60	58.9	104.7	-	162.8		13.4
	80	60.5	105.9	-	159.6		4.9
Compression molded PLA2-PMMA after impregnation	20	57.9	89.8	-		-	-
	40	56.3	94.1	-		-	-
	60	59.2	103.6	-		-	-
	80	60.2	109.8	-		-	-

For both PLA1 and PLA2, T_{g1} showed a significant but relatively small increase over T_g of the pure PLA as the PMMA content increased, and T_{g2} increased by around 30 K as the PMMA content was increased from 40 to 100 wt%, indicating partial miscibility in the as-extruded specimens [155]. On the other hand, the observation of a single glass transition on cooling form 230 °C and during second heating cycle was clearly suggestive of miscibility, the evolution of T_{g12} with PMMA content indicating strong plasticization by PLA over the whole composition range. Following Herrera *et al.* [156], this plasticizing effect could be accounted for empirically using the Brekner equation for a two component blend [157]:

$$T_g(\phi) = T_{gA} + (T_{gB} - T_{gA})[(1 + k_1)\phi - (k_1 + k_2)\phi^2 + k_2\phi^3] \qquad (5.1)$$

where ϕ is the volume fraction of component B (the PLA in this case), with $k_1 = -0.9$ and $k_2 = 0.4$, as shown in Figure 5.2.
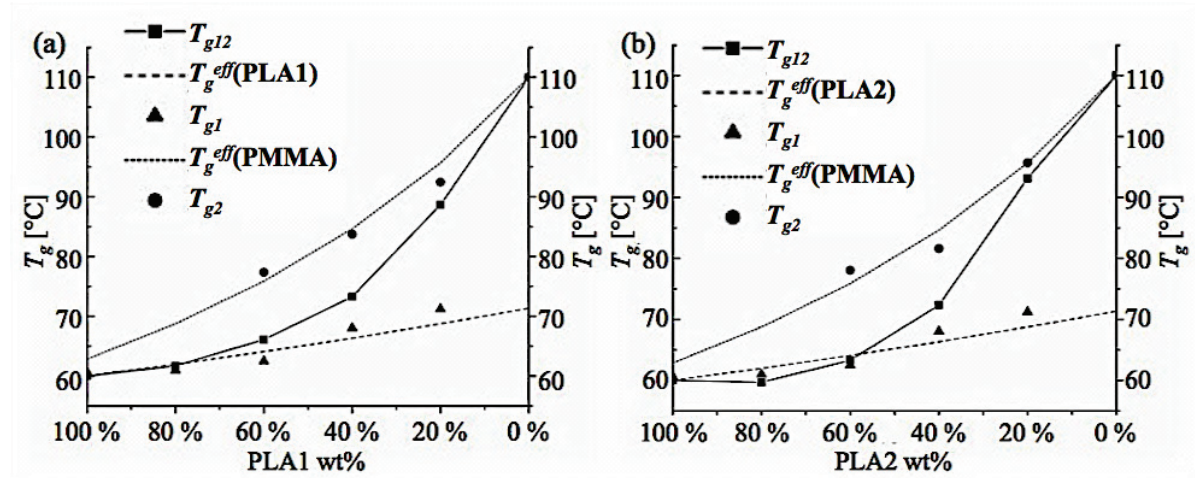
Figure 5.2 T_g of the blends estimated from Figure 1 as a function of PLA content. The solid curve is a fit to the data from the second DSC heating scans using Equation 1 and the hatched curves are corresponding estimates of the effective local T_g for the PLA- and PMMA- rich regions obtained as described in the main text.

These results are at least qualitatively consistent with literature results for PLA-PMMA with comparable M_w after thermal cycling [149,151,152], for which it has been suggested that there

exists an upper critical solution temperature (UCST) in excess of 200 °C, depending on the molar mass, composition and tacticity, such that initially phase-separated blends show a single, broad calorimetric T_g after heating to above the UCST [149,150]. A broad calorimetric glass transition may nevertheless correspond to distinct effective glass transitions associated with intrinsic variations in the local composition, as has been demonstrated for a range of miscible amorphous polymers by e.g. thermally stimulated depolarization current experiments [156,158]. Estimates of the effective local T_g for the PLA- and PMMA-rich regions of the specimens showing a single calorimetric T_g are also included in Figure 5.2, assuming the same mixing rule as for T_{g12} (equation 5.1) but by replacing the global concentration by the local "self-concentration", following [156] (the characteristic ratios, C_∞, were taken to be 11.7 and about 9 for PLA [159] and atactic PMMA [160] respectively). The T_{g1} and T_{g2} of the as-extruded blends were generally well outside this envelope at intermediate compositions.

It follows that the present melt blending procedure, for which the extrusion temperatures (maximum 220 °C) and drying conditions were chosen to limit degradation of the PLA, was inadequate to give homogeneous blends and, similarly, double glass transitions persisted in the molded specimens (Table 5.1). For comparison, Samuel *et al.* [152] have reported melt blending with an extrusion temperature of 210 °C to give homogeneous blends between PLA with $M_w =$ 218'000 g/mol and PMMA with M_w in the range 92'000 to 97'000 g/mol. However, they also found phase separation in solvent cast specimens to be irreversible even after heating to 250 °C, implying shear deformation during the extrusion process to be an important factor for the effective miscibility of PLA-PMMA blends. It would therefore be of interest to carry out more systematic studies of the influence of the initial processing conditions on phase separation in the present case. However, in view of the effect of the subsequent CO_2 impregnation step to be discussed below, this was not of immediate practical concern for the preparation of the foam precursors.

DMA results are shown in Figure 5.3 for compression molded films of the pure resins and PLA-50 wt% PMMA. The a transition temperatures, T_a, defined as the temperature of the main peak in tan δ were 86.9 and 85.8 °C for PLA1-50 wt% PMMA and PLA2-50 wt% PMMA, whereas the T_α were 69.4, 70.6 and 126.2 °C for PLA1, PLA2 and PMMA, respectively. PLA1 also showed a marked increase in storage modulus above about 90 °C owing to cold crystallization, but this

effect was absent for PLA1-50 wt% PMMA. Consistent with the observation of two glass transitions at 65.5 and 85.1 °C in DSC scans of the films, the DMA transitions for the PLA1-50 wt% PMMA and PLA2-50 wt% PMMA showed relatively small step-like drops in storage modulus at about 67 and 65 °C, respectively, followed by a more substantial decrease as the temperature increased further.
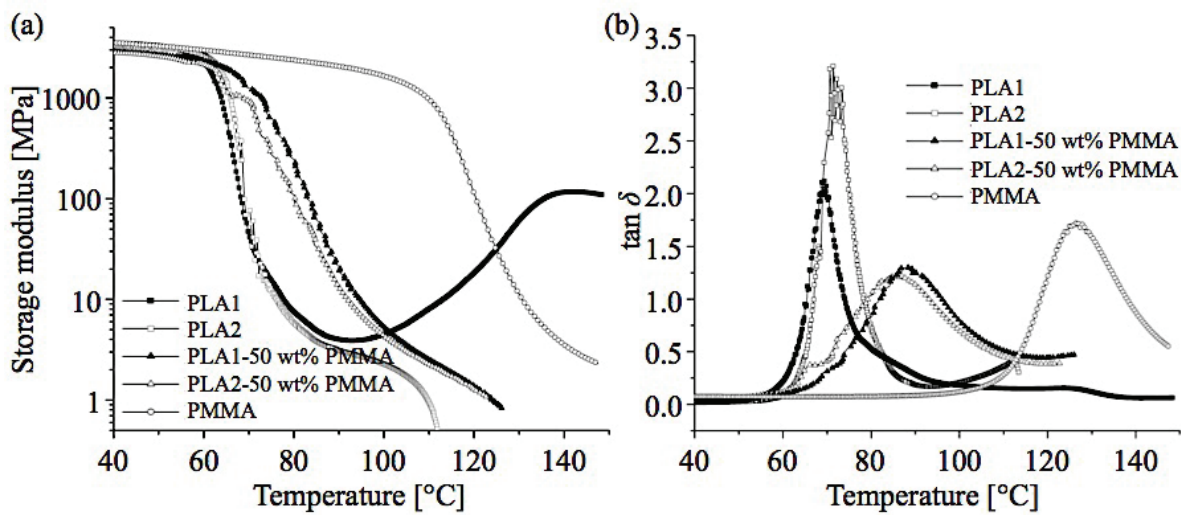
Figure 5.3 DMA results from compression molded films testes in tension: (a) storage moduli and (b) tan δ.

5.2 CO_2 impregnation and desorption behavior

Because the CO_2 content stabilized in all the materials for impregnation times in liquid CO_2 at 5 MPa and 10 °C longer than about 3 hr, it was assumed to have reached saturation under these conditions, implying equilibrium CO_2 contents of about 0.27 g/g, 0.42 g/g and 0.27 g/g for neat PLA1, PLA2 and PMMA, respectively. As set out in section 4, high CO_2 contents are predicted to reduce T_g of PLA to well below the impregnation temperature of 10 °C [8,45], facilitating crystallization, and the degree of crystallinity of initially amorphous specimens of PLA1 has been found to be about 34 wt% after impregnation [8,35]. The difference in the equilibrium CO_2 contents of PLA1 and PLA2 may therefore be accounted for by assuming the CO_2 to be insoluble in the crystalline phase and a simple rule of mixtures. Gas solubility in polymer blends is also expected to follow a simple rule of mixtures [161], as borne out in the present case by the data in

Figure 5.4. Indeed, the overall equilibrium CO_2 content was roughly independent of composition in the PLA1-PMMA blends, implying phase separation and crystallization of the PLA1 over the whole composition range (and a local CO_2 content in the amorphous regions of the PLA1 that significantly exceeded the global CO_2 content).
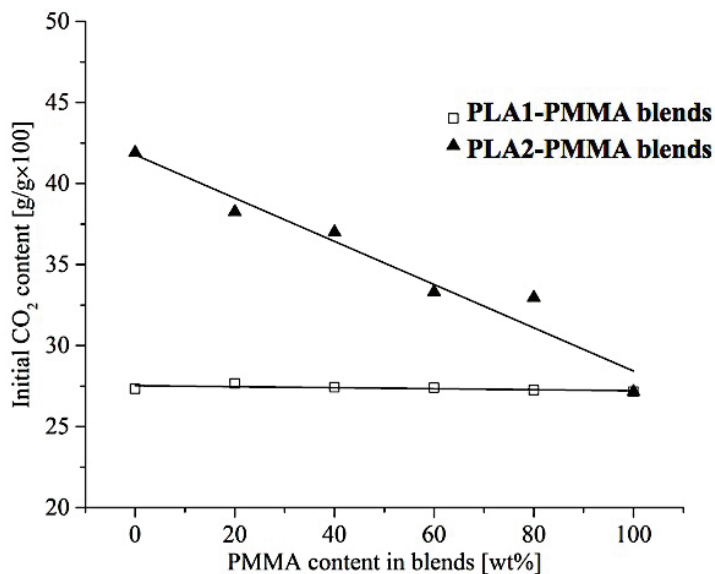
Figure 5.4 Initial CO_2 content versus PMMA content in the compression molded disc after impregnation for 3hr in liquid CO_2 at 5 MPa and 10 °C.

As shown in Figure 5.5, DSC heating scans of the blends after impregnation in liquid CO_2 for 3 hr, followed by complete CO_2 desorption (which could be achieved e.g. by storage under ambient conditions for a minimum of one week [8]), showed two well-separated glass transitions for all the compositions investigated, and T_{g1} and T_{g2} were relatively close to the T_g of the PDLLA and PMMA respectively (cf. Table 5.1), indicating significantly greater phase purity than prior to impregnation. Moreover, all the PLA1-PMMA blends showed a clear melting peak, with a single maximum that decreased from 169.5 to about 159.6 °C and whose area decreased from 32.0 to 5.0 J/g as the PMMA contents increased from 20 to 80 wt%. Thus, the presence of the CO_2 was confirmed to favor both phase separation and crystallization in the blends at 10 °C, consistent with the observed trends in the overall equilibrium CO_2 content in Figure 5.4.
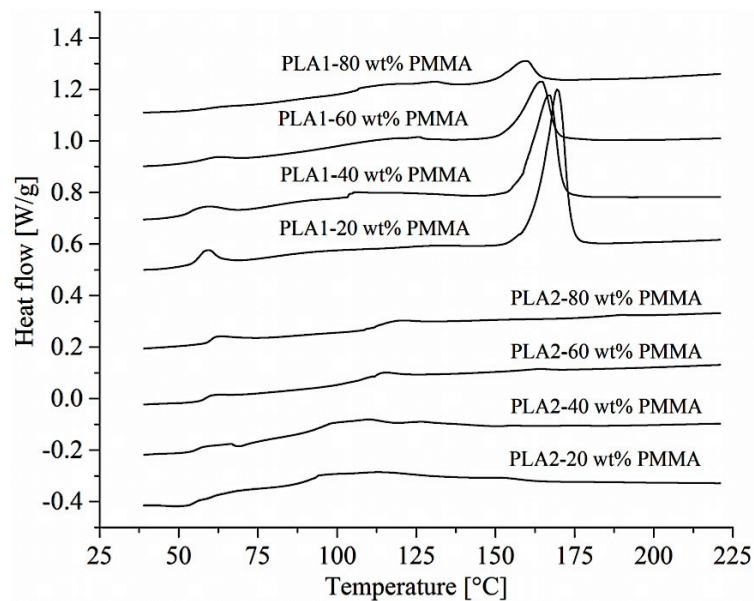
Figure 5.5 DSC heating scans from the impregnated compression molded discs after complete CO_2 desorption.

Figure 5.6 shows the CO_2 content of the compression molded discs, expressed as the overall mass of CO_2 per unit mass of the un-impregnated specimens, as a function of time at 21 °C after impregnation for 3 hr in liquid CO_2 at 5 MPa and 10 °C. The desorption rates from PLA1, PMMA and PLA1-PMMA at ambient temperature were comparable, and while the PMMA and the PMMA-rich blends showed somewhat greater mass loss after short times, the CO_2 content decreased to about 0.15 g/g in all the specimens after desorption for 1 hr and little or no foaming was observed during the measurements. As observed previously [17], crystallization induced by the CO_2 was therefore sufficient to stabilize the PLA1 with respect to foaming at temperatures well below its melting point, and estimates of T_g as a function of CO_2 content [25] suggested the glass transition of the PMMA not to decrease to substantially below room temperature, even at saturation. On the other hand the amorphous PLA2 and its blends with PMMA foamed spontaneously on heating to 21 °C after impregnation, resulting in relatively rapid desorption of the CO_2, particularly at high PLA2 contents, where PLA2-rich regions presumably formed a continuous phase. The blends with intermediate compositions showed the lowest CO_2 contents after desorption for 1 hr, owing to both their reduced overall CO_2 contents at saturation and the

effect of foaming. Indeed, even PLA2-80 wt% PMMA showed significantly faster CO_2 desorption than the pure PMMA under these conditions.
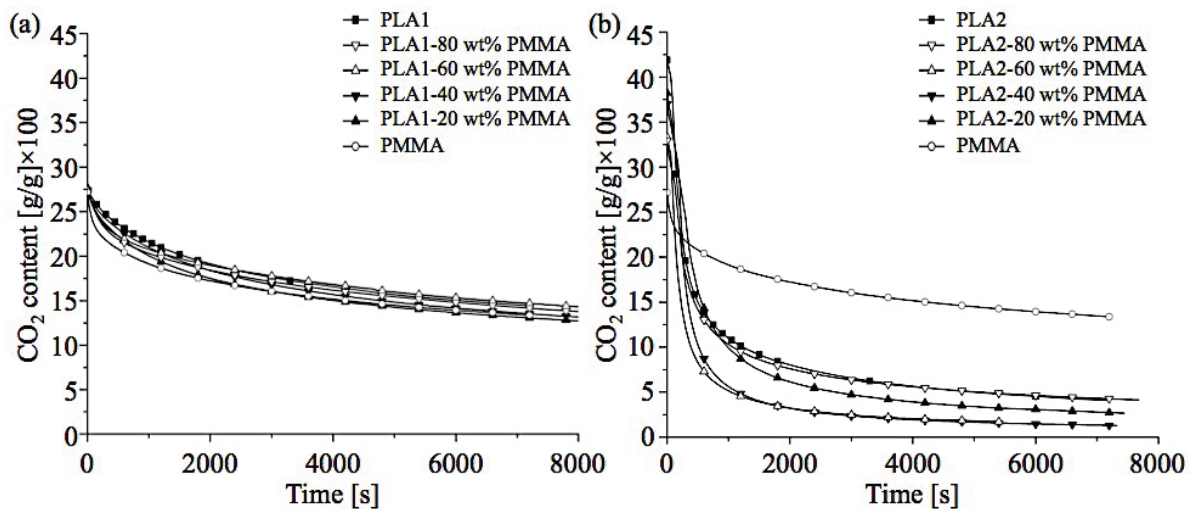
Figure 5.6 CO_2 desorption from compression molded discs of (a) PLA1-PMMA and (b) PLA2-PMMA and the corresponding homo polymers.

5.3 Foaming behavior

Only amorphous PLA2, PLA2-PMMA and PMMA were considered for foaming tests, because crystallization of PLA1 and PLA1-PMMA during impregnation tended to suppress foaming not only at ambient temperature, but also in temperature regimes of immediate interest for the direct replacement for EPS. In order to promote relatively homogeneous cellular structures at the scale of the specimen thicknesses, 1 wt% talc was included in the formulations as a nucleation agent. Mineral fillers have been reported to influence the mechanical properties of PLA [162,163], but this level of loading did not result in significant changes in either mechanical properties or CO_2 transport in the present case. As discussed in the previous section, the amorphous PLA2 and PLA2-PMMA precursors saturated with CO_2 at 5 MPa and 10 °C became unstable with respect to foaming on removal from the autoclave, because of the associated reduction in T_g. Following section 4, the CO_2 content was adjusted by partial impregnation in liquid CO_2 at 10 °C and 5 MPa, followed by conditioning in air at 10 °C and at ambient pressure, which served to homogenize the CO_2 concentration in the specimen interior [8]. As shown in Figure 5.7, impregnation for 30 min

and conditioning for 2 hr led to overall CO_2 contents of 0.17 g/g and 0.13 g/g in PLA2 and PLA2-50 wt% PMMA respectively, whereas impregnation for 2 hr and conditioning for 2 hr gave an overall CO_2 content of about 0.08 g/g CO_2 in the pure PMMA. For comparison, 0.1 g/g of CO_2 would ideally lead to a minimum bulk foam density close to 20 kg/m^3 assuming expansion of the CO_2 to take place entirely within the foam.
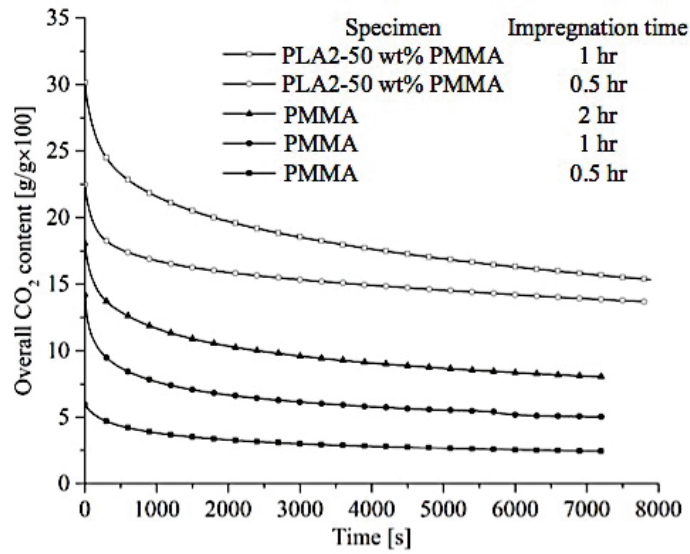
Figure 5.7 Desorption from compression molded discs of PMMA and PLA2-50 wt% PMMA blend for different impregnation times.

Figure 5.8 shows the expansion ratio, ρ/ρ^*, where ρ is the matrix density and ρ^* is the foam density, for the impregnation and conditioning treatments in Figure 5.7 as a function of the foaming temperature, along with SEM micrographs of the resulting cell morphology. Consistent with its relatively high initial CO_2 content, PLA2 generally showed the highest degree of expansion, with ρ/ρ^* reaching a maximum of 56.9 ($\rho^* = 22$ kg/m^3), at 80 °C, falling off as the temperature was increased further. Expansion was reduced for PLA2-50 wt% PMMA owing to its reduced overall CO_2 content, but the maximum in ρ/ρ^* of 18.8 ($\rho^* = 67$ kg/m^3), shifted to 100 °C. Similarly, PMMA showed a maximum in ρ/ρ^* of about 26.1 ($\rho^* = 46$ kg/m^3), at 130 °C.
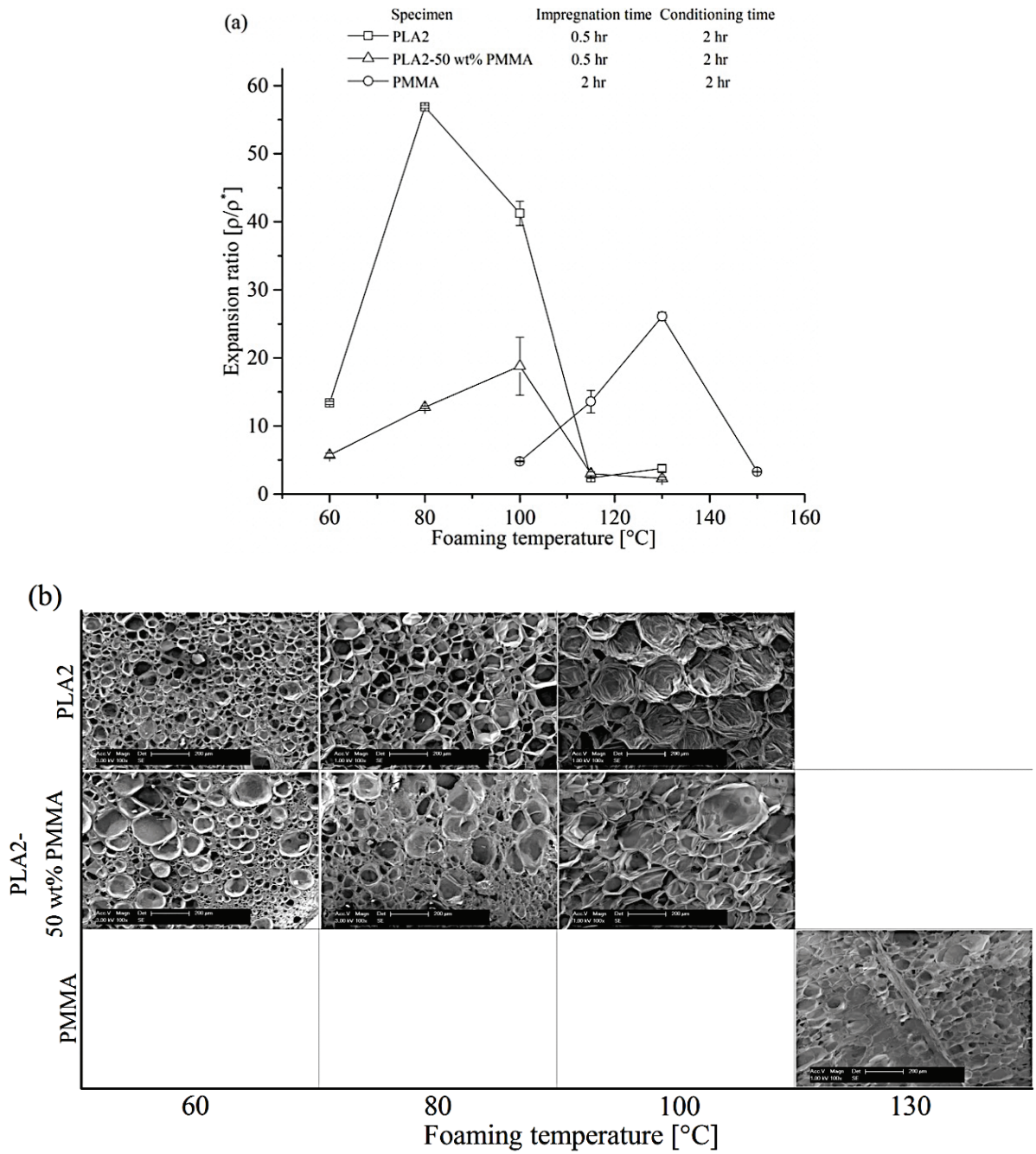
Figure 5.8 (a) Expansion ratio, ρ/ρ^*, after free expansion of PLA2, PMMA and PLA2- 50 wt% PMMA at various temperature and for the impregnation/conditioning conditions specified. (b) SEM micrographs of the corresponding cellular morphology of the foams.

For PLA2 and PMMA the maximum in ρ/ρ^* occurred at about $T_g + 20$ °C, where T_g is the glass transition temperature in the absence of CO_2 (Table 5.1). T_{g1} and T_{g2} were estimated from DSC heating scans (Figure 5.9) to be about 64 and 96 °C respectively in PLA2-50 wt% PMMA after impregnation and desorption of the CO_2, although the glass transitions were less well defined than for the fully impregnated specimens (cf. Figure 5.5). The weak endotherm visible at 123 °C was also present in DSC heating scans of pure PLA2 after partial impregnation in the presence of talc, and was attributed to residual crystallization (this effect was less evident in the unmodified PLA2 as seen from Figure 5.5). The glass transitions were even less well defined after foaming at 100 °C, as also shown in Figure 5.9. In this case, the heat capacity increased gradually over the whole of the temperature range between about 60 and 110 °C and the endotherm at 123 °C was absent. Finally, a second heating scan of the foams after cooling at 10 °C from 230 °C showed a single broad glass transition centered on about 70 °C. While the relatively complex thermomechanical history and non-uniform exposure to CO_2 of these specimens rendered detailed interpretation of these results difficult, it is speculated that the high strains associated with cell expansion may have promoted homogenization of the matrix microstructures during high temperature foaming, as has been suggested previously for extrusion blending [152]. Certainly, the observation of a maximum in ρ/ρ^* at about 100 °C for the blends implied an effective softening temperature intermediate between those of the pure PLA2 and PMMA.
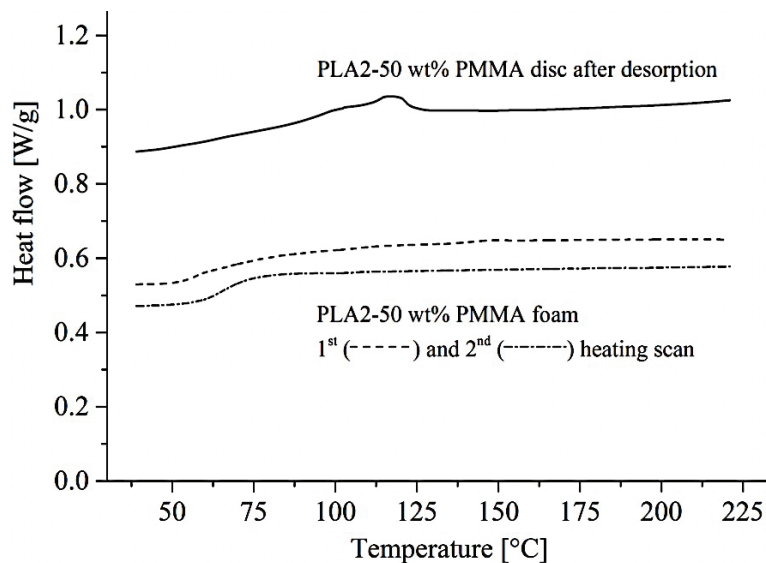
Figure 5.9 DSC heating scans from PLA2-50 wt% PMMA after impregnation for 30 min in liquid CO2 and conditioning for 2 hr, followed by complete desorption of the CO2, and after impregnation/conditioning under the same conditions followed by free expansion at 100 °C.

The SEM micrographs of the various PLA2, PLA2-50 wt% PMMA and PMMA foams in Figure 5.8(b) were generally suggestive of a mixed open and closed cell morphology. Although closed cells are found to be dominant, even so characteristics of open cells such as connected cells and holes on the cell walls are observed. The apparent maximum cell size increased as the foaming temperature increased in both PLA2 and PLA2-50 wt% PMMA, a trend that was attributed to increasing matrix softening and hence increasing competition between cell growth and/or coalescence, and cell nucleation, there being no simple correlation between the cell sizes and the overall expansion ratio. Moreover, at the highest foaming temperatures, significant shrinkage was observed in the outer regions of the foams subsequent to expansion, presumably because the cell walls were no longer sufficiently rigid to prevent strain recovery associated with the drop in CO_2 pressure towards the end of the expansion process. This led to both an increase in the overall density and inhomogeneous microstructures. The PMMA foams also showed a relatively dense core, implying incomplete penetration of the CO_2 during the impregnation step [8].

86
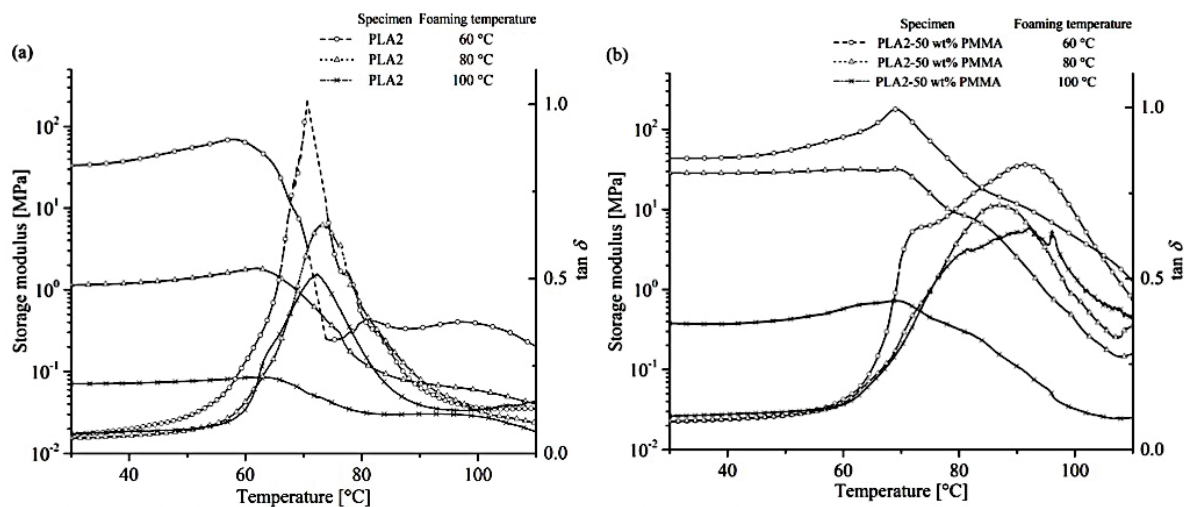
Figure 5.10 DMA results from various foams tested in compression: (a) PLA2 and (b) PLA2-50 wt% PMMA.

The room temperature storage moduli of the foams, $E^{*'}$, obtained from compressive DMA tests varied between 0.1 and 50 MPa depending on the foaming temperature and the matrix, while the a transition temperatures corresponding to the peak in tan δ (Figure 5.10) were broadly consistent with the thermal behavior inferred from the DSC measurements. Thus the PLA2-50 wt% PMMA foams showed broad α-transitions with an onset between 60 and 70 °C, but extending to well above 100 °C, such that tan δ reached a maximum at temperatures between 80 and 90 °C, i.e. significantly higher than for the PLA2 foams. Both the PLA2 and PLA2-50 wt% PMMA foams showed significant shrinkage during the measurements, particularly at the lowest foaming temperatures, 60 °C, which was reflected by an increase in $E^{*'}$ as the temperature approached the onset of the α-transition.
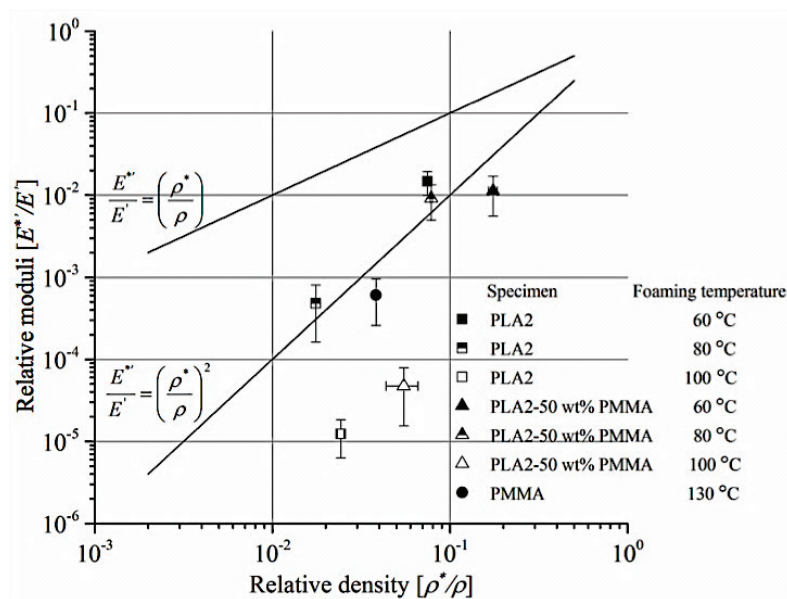
Figure 5.11 Relative storage moduli for the different foams as a function of their relative density.

Relative moduli, $E^*{}'/E'$, where E' is the room temperature storage modulus of the corresponding compression molded specimens, have been plotted against ρ^*/ρ in Figure 5.11. Also shown are simplified Ashby-type scaling laws for a closed-cell foam (linear dependence on ρ^*/ρ) and for an open-cell foam (quadratic dependence on ρ^*/ρ) [164]. The foam moduli appeared roughly consistent with quadratic scaling, with the exception of the foams produced at 100 °C, for which the moduli were more than an order of magnitude less than would be expected on this basis. However, as described above, relatively high foaming temperatures resulted in inhomogeneous internal morphologies, so that the overall foam densities were no longer necessarily determinant for the observed compression moduli.

5.4 Conclusion

It has been demonstrated that it is possible to produce solid-state foam precursors for one step particleboard process by melt blending of a commercial amorphous PLA and PMMA, followed by impregnation with liquid CO_2 and conditioning at ambient pressure in order to adjust the overall CO_2 content. These precursors were shown to be stable with respect to both foaming and

short-term CO_2 desorption at room temperature, but could be expanded to form foams with relative densities down to about 0.05 by immersion in a silicon oil bath at temperatures in the neighborhood of 100 °C. The maximum extrusion temperatures for the blends were limited to 220 °C in order to limit degradation of the PLA, under which conditions they tended to show two distinct T_g. Moreover, both DSC and DMA indicated impregnation with liquid CO_2 to result in marked phase separation, obviating any attempt to obtain homogeneous blends by prior heat treatment. Even so, the present results indicated that blending amorphous PLA2 with PMMA may provide a relatively straightforward means of not only tailoring the process window corresponding to foam expansion, but also increasing the effective softening temperature of the resulting foams. The use of a thermostatically controlled silicon oil bath to initiate expansion in the present case was chosen for convenience rather than to represent a practical processing route, and therefore no attempt was made to optimize the foam microstructures with respect to blend composition, molar mass, impregnation conditions, precursor geometry, additives and foaming temperature, for example. However, we have been able to demonstrate the suitability of granular amorphous PLA2-50 wt% PMMA precursors impregnated with liquid CO_2 for the production of low density foams using an open hydraulic press in which the foaming temperature is constrained to be close to 100 °C. This provided the focus for our efforts towards optimization of the foam core particleboard process, to be discussed in Chapter 8.

Chapter 6

Biocomposite foam precursors

It has been shown that a PLA foam precursor blended with a relatively high T_g polymer, PMMA, resulted in improved heat stability and a processing window potentially better suited to the particleboard process than pure amorphous PLA precursors [165]. However, ideally we would prefer to reproduce the advantages of blending with PMMA, while avoiding the use of non-sustainable additives. We have therefore investigated the effect of combining PLA with a range of natural fiber reinforcements, including microcrystalline cellulose (MCC) and wood fiber (WF). These cellulose reinforcements are known to be not only renewable, biodegradable and recyclable, but also potentially capable of effective reinforcement at low volume fractions, due to the high stiffness and high aspect ratios of the individual cellulose fibers [166–170].

Based on the successful approach of Boissard *et al.* [10] to obtaining improved elastic properties and heat stability during supercritical CO_2 foaming, PLA was extrusion compounded with WF or MCC. The resulting biocomposites were impregnated with liquid CO_2 following the procedures described in the Section 4.1 [8], and their foaming behaviour investigated under conditions representative of the particleboard process. The chapter begins with a discussion of the influence of the additives on the sorption and desorption behaviour of the CO_2 during impregnation and storage as determined using the experimental approach introduced in Section 4.2 [8], with emphasis on the importance of CO_2 transport along the matrix-fibre interfaces for diffusivity and the role of the filler network continuity. The influence of the fibres on the processing windows corresponding to foaming, and on foam expansion and the final morphology is then presented. Finally, the benefits of cellulose fibre reinforcement for the final foam stiffness are considered, based on results from compressive DMA tests.

6.1 Thermal and mechanical properties of biocomposites prepared by melt compounding

Figure 6.1 and Table 6.1 show the morphology and basic characteristics of the WF and MCC respectively employed in this work. These additives showed large differences in aspect ratio, i.e. ~ 81 for WF and ~ 3 for MCC.
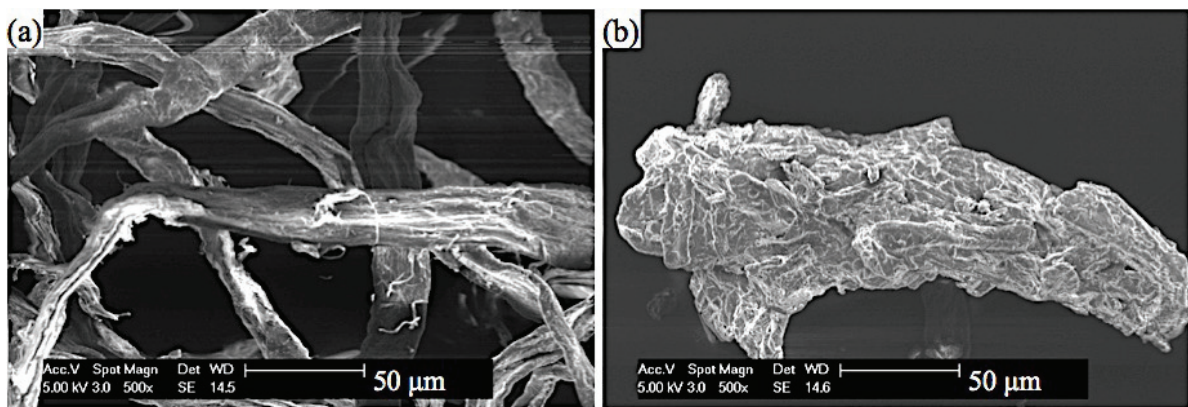
Figure 6.1 SEM micrographs of (a) WF and (b) MCC show contrasting dimensions and surface topography.

Table 6.1 Physical characteristics of the WF and MCC.

	WF [70,171]	MCC
Manufacturer	Innventia AB	Sigma-Aldrich
Dimensions [μm]	Length: 2.34×10^3 Width: 28.8	< 50
Density [cm^3]	1.2	1.46 [172]
Young's modulus [GPa]	39.9	25 [173]
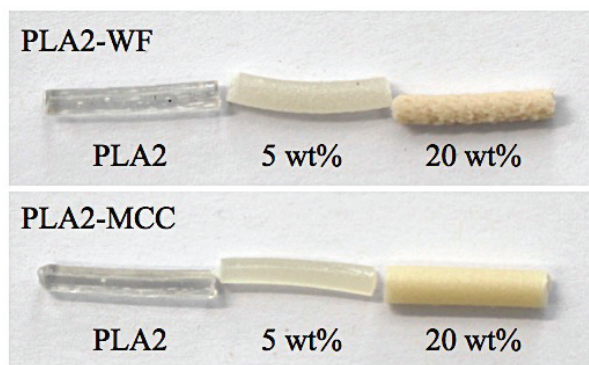
Figure 6.2 PLA2 composite extrudates processed by a laboratory scale twin screw extruder at 200 °C for 2 min.

Melt compounding was carried out for approximately 2 min at 200 °C using the laboratory scale microextruder described in Section 3.2.1. As shown in Figure 6.2, the extrudates containing WF and MCC were opaque and brownish, in spite of careful drying before every process step, whereas the PLA was colorless and transparent. This discoloration was particularly apparent at high WF contents. Although no quantitative measurements were carried out in the present work, discoloration is widely assumed to reflect hydrolysis of PLA [174], and the present high T process employed here was assumed *a priori* to favor degradation in the presence of any residual water associated with the additives. The high shear also caused severe breakdown of the WF into particles with aspect ratios <10 (Figure 6.3), while the original shape of the MCC was conserved (Figure 6.3). Varying the WF content did not substantially change the resultant fiber length in composites containing up to 20 wt% WF.

OM also suggested that addition of 3 or more wt% of WF might result in some degree of fiber networking, although in view of the thickness of the compression molded specimens shown in Figure 6.3, this remains to be confirmed. Fiber-to-fiber load transfer may therefore contribute to mechanical properties at high fiber contents, but it is also expected to hamper foam expansion, as will be discussed further in what follows. Indeed, Neagu *et al.* suggested the network formed by 10 wt% microfibrillar cellulose (MFC) with an aspect ratio of about 80 may represent a critical

threshold beyond which it is no longer possible to prepare low density foams by supercritical CO_2 processing [70]. The hydrophobic PLA matrix and hydrophilic WF and MCC are also thought to show relatively weak interfacial interactions, as suggested by the SEM micrographs of fracture surfaces shown in Figure 6.4.
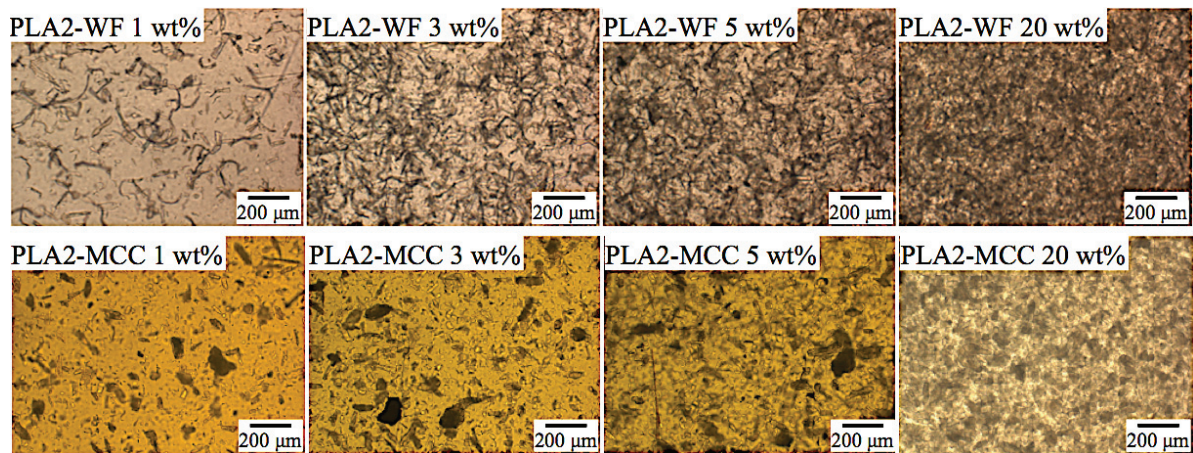
Figure 6.3 Optical micrographs of compression molded ~0.2 mm thick films of 1, 3, 5 and 20 wt% of WF and MCC extrusion compounded with PLA2.
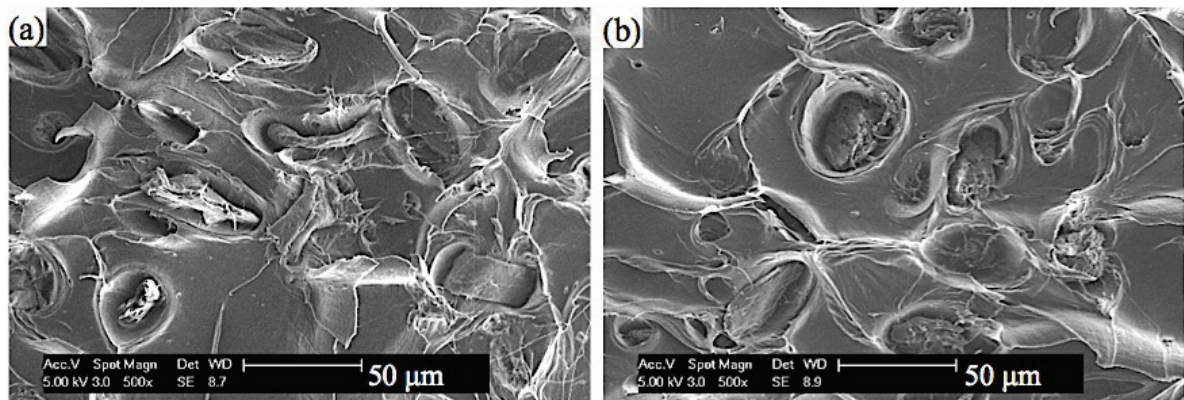
Figure 6.4 Representative SEM micrographs of fracture surfaces after static tensile tests on injection molded dog-bone shape specimens with 2×4 mm^2 cross sections in the gauge length; (a) 5 wt% WF- and (b) 5 wt% MCC-PLA1. Both additives were pulled out of the matrix during the fracture process. Typical features of a composite with weak fiber matrix interfacial interactions include large voids, and gaps between the filler and matrix.
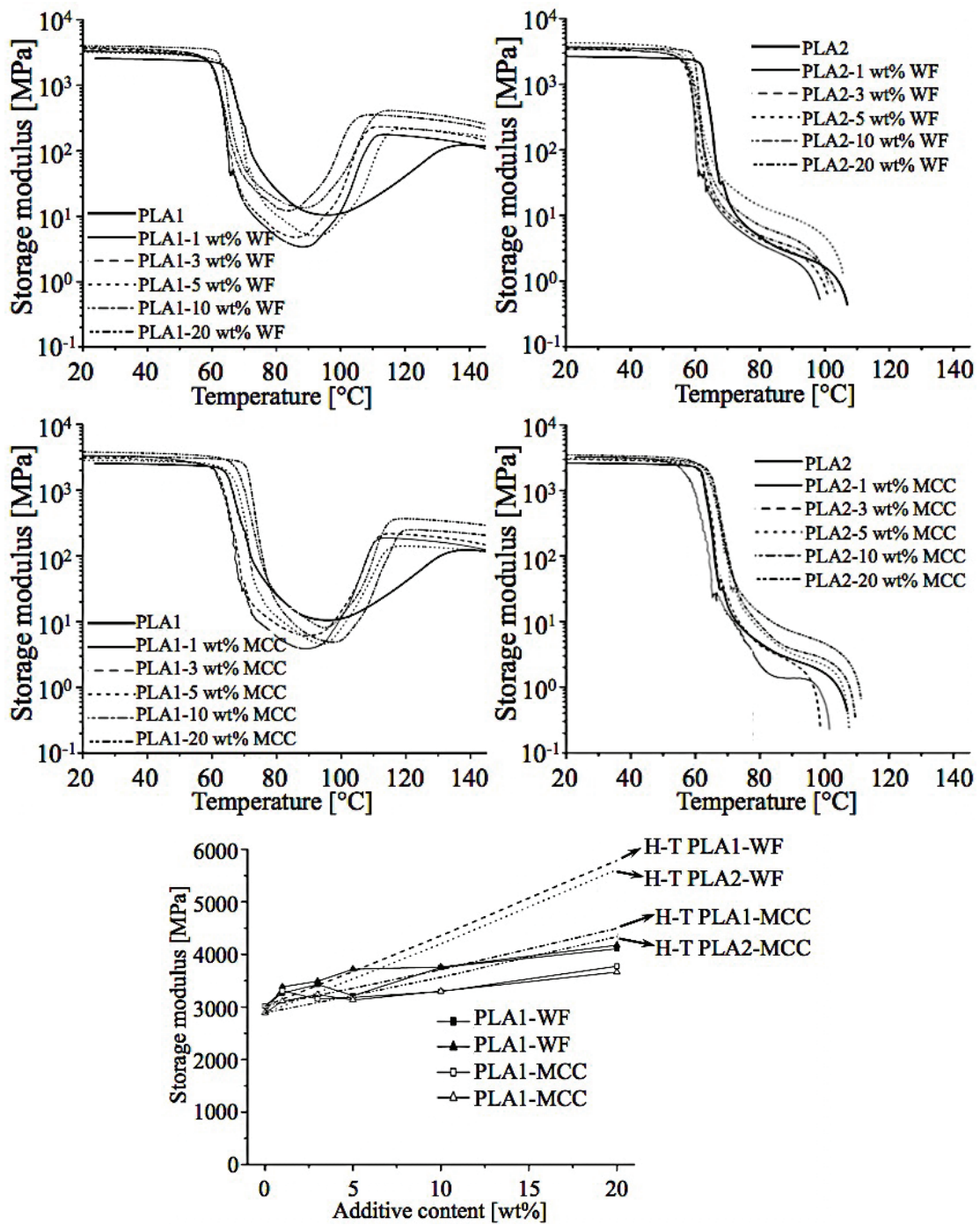
Figure 6.5 The storage moduli, *E'* in the *T* range from 20 to 150 °C from DMA measurements at 1 Hz with a 3 °C/min ramp rate, along with the dependence of *E'* at 20 °C on additive content, and the predictions of equation 2.14 for comparison.

Tensile mode DMA tests were performed on the 0.2 mm thick hot pressed films shown in Figure 6.3. The storage moduli, E', versus temperature are shown in Figure 6.5. In PLA1 the onset of cold crystallization was found to be shifted to lower T in both types of composite, starting in the range 83 - 92 °C as opposed to about 95 °C in the neat PLA1, and the crystallization peaks were significantly sharper. Decreased crystallization temperatures, T_c, were also seen in DSC heating scans, as summarized for PLA1-WF in Figure 6.6 and Table 6.3 respectively. However, the enthalpy of fusion also increased with WF content, a phenomenon that may be associated with a decrease in molecular weight of the PLA due to hydrolysis [174]. Any such decrease is also expected to reduce the melt strength of PLA and favor cell wall rupture during foaming. This would not only favor cell coalescence but may also contribute to foam shrinkage owing to accelerated loss of the CO_2 prior to stabilization of the foam structure, as will be discussed in Section 6.2 [84].
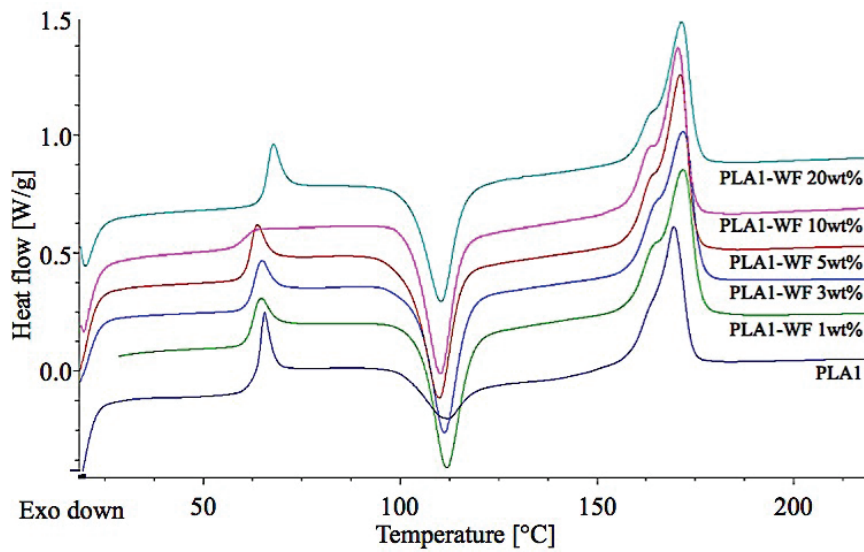
Figure 6.6 Results of DSC heating scans from PLA1 and PLA1-WF composites at a heating scan rate of 10 °C/min.

Table 6.2 Thermal properties of PLA1 and its composite products with different contents of WF.

Product	T_g [°C]	T_c [°C]	T_m [°C]	ΔH_m [W/g]
PLA1	61.92	112.36	169.36	29.64
PLA1-WF 1wt%	60.99	112.06	171.60	38.02
PLA1-WF 3wt%	61.16	111.49	171.57	37.70
PLA1-WF 5wt%	60.42	110.04	170.99	40.24
PLA1-WF 10wt%	60.54	110.31	170.55	36.34
PLA1-WF 20wt%	64.54	110.57	171.45	31.64

As shown in Figure 6.5, E' at 20 °C increased systematically as the additive content increased. The higher aspect ratio WF composites showed a somewhat greater increase in E' than the MCC for a given additive content. Theoretical values of the Young's modulus based on the empirical equation 2.14 developed by Halpin *et al.* [175] are also shown in Figure 6.5 (dashed lines). The predicted elastic moduli assuming l/d=10 for the WF and l/d=3 for the MCC did not account well for the data, particularly at high filler contents. This may be due to the following factors: (i) poor interfacial adhesion; (ii) a distributed l/d ratio; (iii) fiber curvature (particularly in the case of the WF) [90,169,171,176].

The high T plateau modulus of the PLA2-based composites, e.g. E' measured at 90 °C in a tensile DMA test, showed more marked increases at high WF and MCC contents (Table 6.3). The rubbery modulus is known to depend on relatively large scale chain motion [177]. Degraded polymer chain lengths may therefore explain the decreased E' at 90 °C at low additive contents, but reinforcement was nevertheless effective from 3 wt%. Because the interfacial adhesion in the composites was inferred to be poor, the primary contribution to the higher E' at 90 °C at WF was assumed to be the relatively high fiber aspect ratio and fiber networking.

Table 6.3 Storage modulus, E', at 90 C in PLA2 composites.

Additive content [%]		0	1	3	5	10	20
E'@90 °C [MPa]	PLA2-WF	2.64	2.14	2.76	3.32	4.48	9.18
	H-T PLA2-WF		2.91	3.46	4.04	5.59	9.28
	PLA2-MCC		1.37	2.32	3.21	3.77	6.97
	H-T PLA2-MCC		2.74	2.95	3.17	3.76	5.16

6.2 Impregnation with CO_2 and foaming behavior

Hot pressed composite discs with 1 mm thickness and 25 mm diameter were impregnated for 3 hr in liquid CO_2 at 5 MPa and 10 °C. Figure 6.7 shows the CO_2 desorption behavior at room temperature, i.e. the overall weight of CO_2 per unit weight of the un-impregnated specimen as a function of time [8]. The saturation CO_2 content was 0.27 g/g and 0.42 g/g for neat PLA1, PLA2 respectively. Because CO_2 is insoluble in WF and MCC [178], the overall solubility of CO_2 in the composites decreased as the additive content increased, as shown in Figure 6.7(e) .

The relatively rapid loss of CO_2 seen in Figure 6.7(b) and (d) was attributed to uncontrolled foaming at room temperature and overall diffusion rates were similar up to the highest additive contents. On the other hand, in PLA1, which was stable with respect to foaming at room temperature even when saturated with CO_2, an accelerating effect of the additives on the diffusion rate was clearly visible at 10 and 20 wt% WF, although it was far less marked for the MCC. This was accounted for by percolation of contacts between the relatively high aspect ratio WF, providing continuous paths for CO_2 to diffuse out of the composites via the additive-matrix interface. That the PLA2-MCC composites showed somewhat greater desorption rates than the PA2-WF composites therefore suggests that the additives may in this case contribute to desorption during foaming by promoting cell wall breakdown, as discussed above.
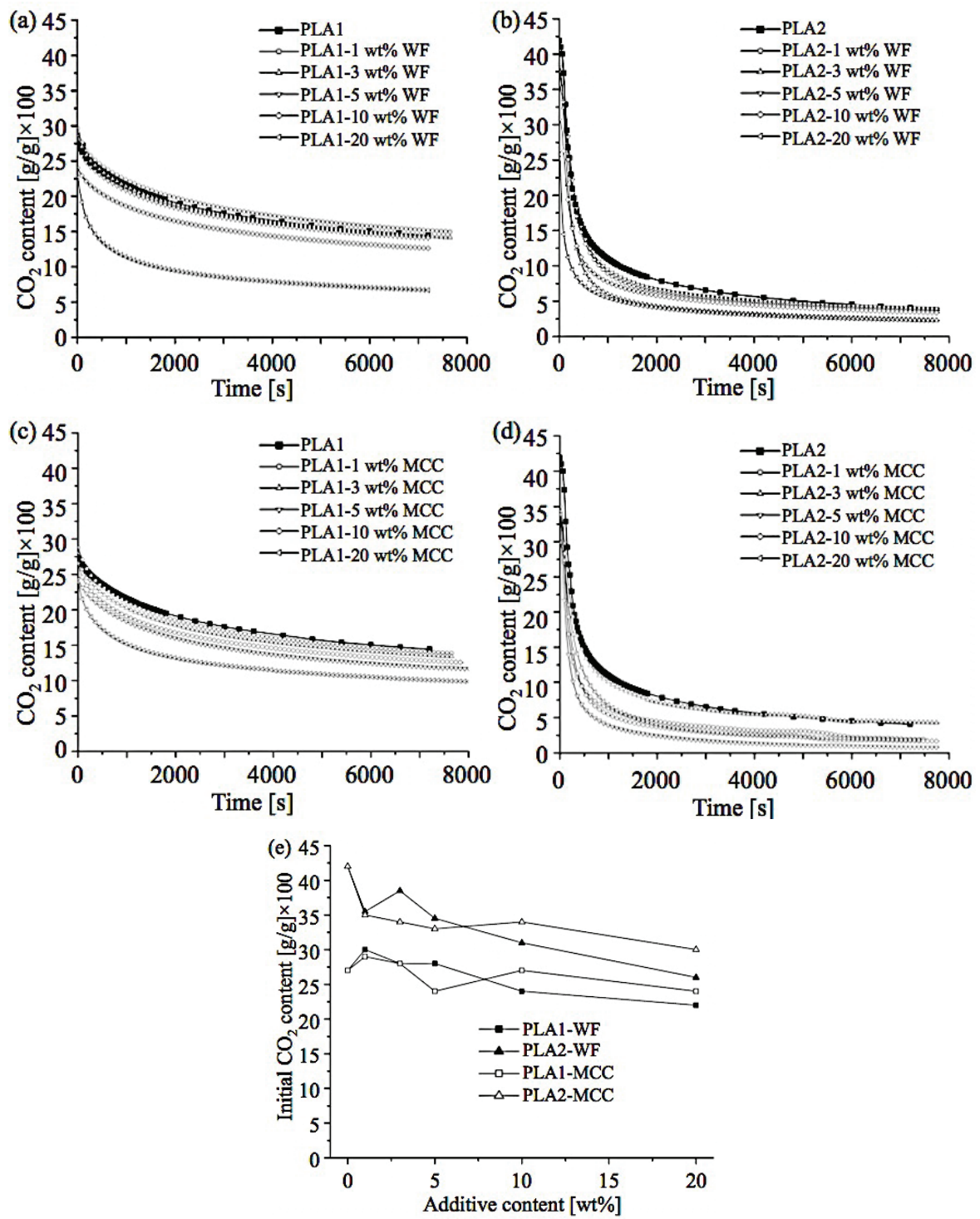
Figure 6.7 CO_2 desorption from composite discs as a function of time and the saturation CO_2 content as a function of additive content for the different types of composite.

It was nevertheless concluded from the results for PLA1, and those in Section 4.3 for pure PLA2, that it should be possible to prepare solid, stable PLA2 biocomposite foam precursors with adequate CO_2 contents (i.e. about 0.10 g/g) for additive contents up to at least 10 wt%. Indeed, a 10 min treatment in liquid CO_2 at 5 MPa and 10 °C, followed by 2 hr conditioning at 10 °C and ambient pressure led to CO_2 contents of 0.16 to 0.20 g/g in PLA2 composites containing up to 10 wt% WF or MCC, and 0.10 to 0.14 g/g in composites containing 20 wt% WF or MCC. Some limited expansion was observed after the conditioning of certain specimens, as evidenced by pores at the specimens surfaces and thickness changes, e.g. an increase from the initial thickness of 1 mm to about 3 mm in PLA2-5 wt% WF.
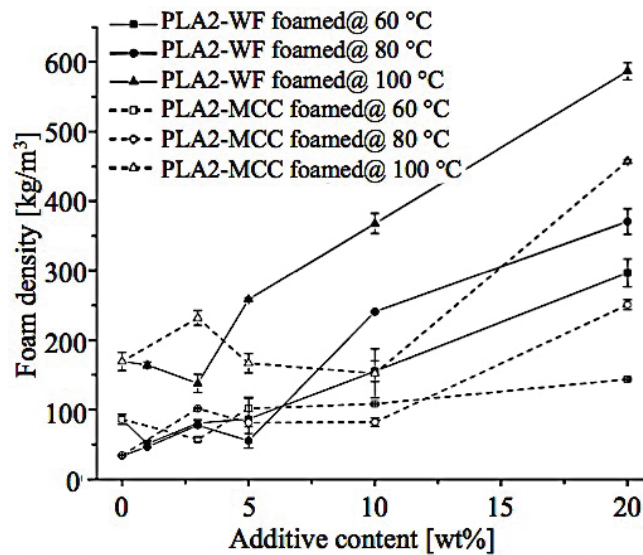
Figure 6.8 Foam densities for different formulations and foaming *T*.

The foam densities obtained by free foaming for 1 min in a thermostatic silicone oil bath at different foaming *T* and immediate cooling in water at 20 °C are shown in Figure 6.8. The overall trend was for the foam density to increase as the additive content increased at a given foaming *T*, and to increase as the foaming *T* increased from 60 °C. The increase in density was mainly due to shrinkage during foaming.

To highlight the role of shrinkage, a complementary foaming test was conducted at 80 °C for two different foaming times, i.e. 20 s and 120 s, using PLA2, PLA2-5 wt% WF and PLA2-20 wt%

WF discs. The results are shown in Figure 6.9. Severe shrinkage was seen in the foams subjected to 120 s immersion in the foaming bath, particularly for higher additive contents. During foaming at 80 °C, CO_2 bubbles were visible at the surface of the PLA2 discs for approximately 23 to 25 s, but they were no longer present after ~18 and ~17 s for additive contents of 5 and 20 wt% respectively. Moreover, vigorous effervescence was seen in PLA2 discs foamed at 100 °C as soon as they were introduced to the oil bath. In general, the foams began to shrink once as the CO_2 bubbles stopped forming. The driving force for cell expansion is known to be diffusion of the initially dissolved CO_2 into nucleated cells [26], and the duration of bubble formation was assumed to be closely associated with the length of time over which the cell expansion pressure was maintained, i.e. over which significant amounts of CO_2 remained within the discs.

T_f=80 °C, t_f=20 s, T_f=80 °C, t_f=120 s
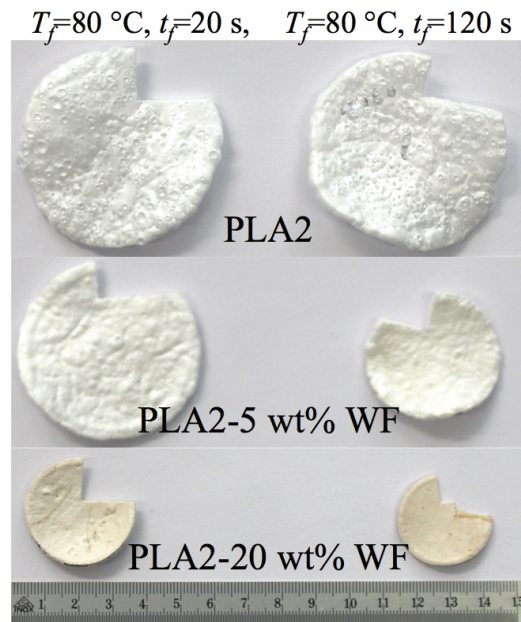
Figure 6.9 A representative example of the effect of foaming at 80 °C for the foaming times, t_f, indicated. The disc shaped foam precursor was prepared by immersion for 10 min in liquid CO_2 and conditioning at 10 °C for 2 hr.

The shrinkage itself is assumed to reflect viscoelastic recovery of the biaxially elongated polymer cell walls under conditions in which the polymer chains in the cell walls are not fully relaxed. It follows that two effects may promote foam expansion: (i) prolonged CO_2 retention times, giving

adequate time for cell growth and stress relaxation in the cell walls and/or (ii) rapid cooling so as to solidify the cell walls before the onset of shrinkage.

The potential effect of the duration of CO_2 retention on foam shrinkage was further investigated by carrying out relaxation tests and using the diffusion model introduced in section 4.2 to estimate CO_2 loss rates at the foaming T. The relaxation tests made use of the hot pressed specimens (~0.2 mm in thickness, ~0.5 mm in width and ~7 mm in gage length) and the DMA apparatus. Once the desired T was reached, a preset amount of tensile strain was applied to the sample and maintained for a time, t_{relax}. The applied stress was then reduced to zero and the specimen strain monitored for 30 min. Figure 6.10 shows the resulting changes in strain with time in PLA2 and PLA2-5 wt% WF at 80 °C and 100 °C. After 3 min isothermal conditioning at the test T, different strains, i.e. 100 % and 50 % at 80 °C and 100 °C respectively, were applied, which were the highest values attainable for a given specimen geometry and T. Strains greater than 100 % at 80 °C and 50 % at 100 °C exceeded the measurement limits and/or resulted in specimen breakage. This lower strain limit at 100 °C may imply cell wall rupture at lower expansion ratios, which may in turn contribute to CO_2 loss during foaming.

The recovered strain decreased strongly with t_{relax} (Figure 6.10 (a) and (b)). Thus, about 95 % of the strain was recovered in PLA2 after 0.5 min relaxation at 80 °C, while 45 % of the strain was recovered after 10 min. PLA2-5 wt% WF showed somewhat less recovery, e.g. 65 % for t_{relax} = 3 min and 40 % for t_{relax} = 7.5 min as compared with 75 % and 50 % in PLA2, but the overall behavior remained similar at 80 °C. Relaxation was more rapid in both materials at 100 °C and the differences between neat PLA2 and PLA2-5 wt% WF were more marked. Thus, no recovery was observed for t_{relax} = 3 min in PLA2 and t_{relax} = 10 min in PLA2-5 wt% WF. Indeed, the strain tended to increase at 100 °C owing to the effect of a minimum nominal force (0.1 N) that was applied during these measurements to prevent instabilities.
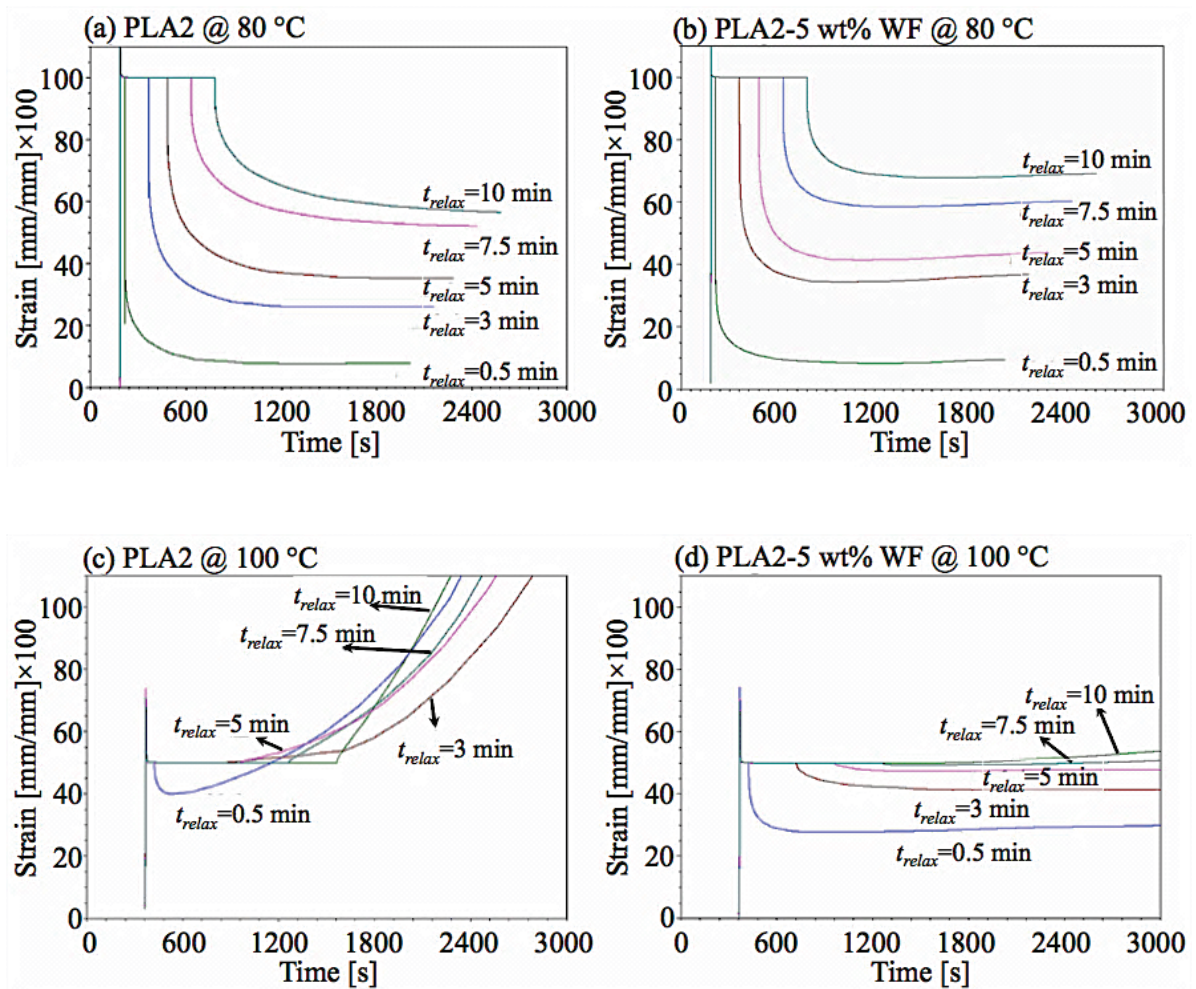
Figure 6.10 Strain-time plots from relaxation tests on (a) PLA2, (b) PLA2-5 wt% WF at 80 °C and (c) PLA2, (d) PLA2-5 wt% WF at 100 °C.

This behavior might at first sight appear to be in contradiction with the evolution of the foam densities in Figure 6.8. PLA2-5 wt% WF showed less recovery than neat PLA2 in the relaxation tests, but greater shrinkage during free foaming, leading to higher density foams. Moreover, on the basis of the relaxation measurements, one might expect a foaming temperature of 100 °C generally to result in lower density foams than 80 °C, again contrary to observation. However, if the parameters in the relaxation test, i.e. the applied strain, t_{relax} and the amount of strain recovery, are assumed to correspond to cell wall expansion, the time over which the CO_2 pressure is effectively maintained and shrinkage, respectively, it is seen that an increased CO_2 diffusion rate

due to e.g. addition of WF will reduce the effective value of t_{relax}, leading to increased shrinkage. Figure 6.11 shows predicted rates of CO_2 loss at different T, calculated for monolithic 1 mm thick specimens, assuming an initial CO_2 content of 0.1 g/g in pure PLA2 and a WLF dependence for $D[0]$ [8]. It is seen that not only is loss CO_2 more rapid as T increases, but also that the timescales are comparable with values of t_{relax} associated with high degrees of strain recovery. Bearing in mind that foaming itself, as well as addition of WF and MCC may also accelerate CO_2 loss, this strongly suggests that shrinkage, and the limited foam densities obtained at high T, are a consequence of inadequate retention of CO_2 during free expansion.
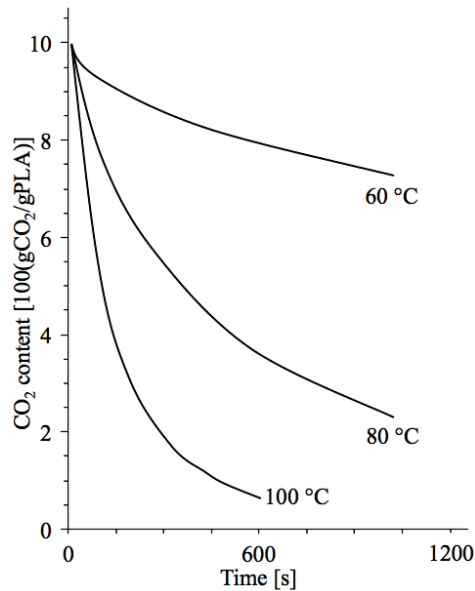
Figure 6.11 The predicted CO_2 loss as function of time from 1 mm thick PLA2 discs assuming an initial CO_2 content of 0.1 g/g.

6.3 Compressive stiffness of the composite foams

As described in section 3.3, compressive DMA tests were carried out from 20 to 150 °C with a3 °C/min ramp rate on > 3×3 mm^2 specimens cut from the foam discs. A sinusoidal 0.05 % strain was applied at 1 Hz in the thickness direction of the disc. A relatively dense skin was often observed in the foams and was retained in the test specimens.

Figure 6.12 shows the low T compressive moduli, $E^{*\prime}$, as a function of additive content. In the widely used Gibson-Ashby model for cell mechanics as shown in Chapter 2.2.3, foam properties are assumed to depend primarily on the matrix properties and cell structure, e.g. the foam density [164]. As discussed in Section 6.2, a significantly increased foam density was observed at 100 °C for additive contents greater than 10 % and the WF composite foams tended to show the highest density for a given set of conditions. Accordingly, $E^{*\prime}$ was increased at high foaming T and high additive contents, e.g. $E^{*\prime}$=2.09 MPa in PLA2-20 wt% WF foamed at 100 °C, as opposed to 0.49 MPa in neat PLA2 foamed at 100 °C. Similarly, low foam densities were obtained at 80 °C and $E^{*\prime}$ was correspondingly low.

Even so, particularly large values of $E^{*\prime}$ were observed in PLA2-5 wt% WF foams and indeed these foams showed outstanding values of the specific modulus, $E^{*\prime}/\rho^{*}$ (Figure 6.13). This tendency may be due to fiber orientation and/or network formation in the cell wall as a result of biaxial extension during expansion, although morphological investigation of the fiber network before and after foaming would need to be carried out to confirm this point. The effect of MCC on compressive stiffness in this regime was far less marked. The MCC composite foams showed low densities (around 100 kg/m^3) up to 10 wt% MCC (Figure 6.8), whereas at 10 wt% WF the density increased sharply, presumably owing to rapid CO_2 loss via the fiber network, and the values of $E^{*\prime}$ obtained at 10 wt% MCC were generally comparable with those obtained for neat PLA2.
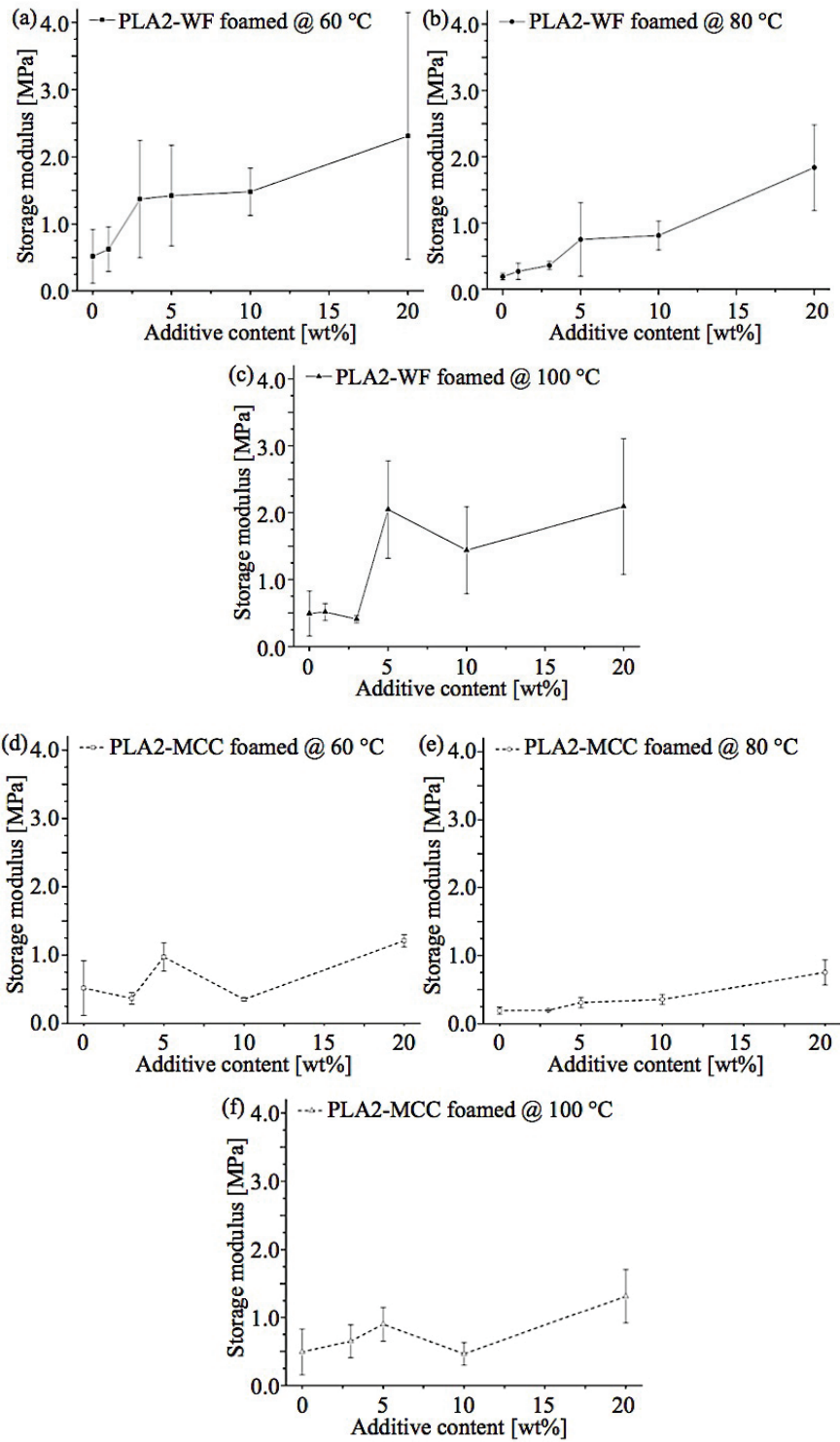
Figure 6.12 DMA results for the room temperature compressive storage modulus, $E^{*\prime}$, of the various foams at 1 Hz.
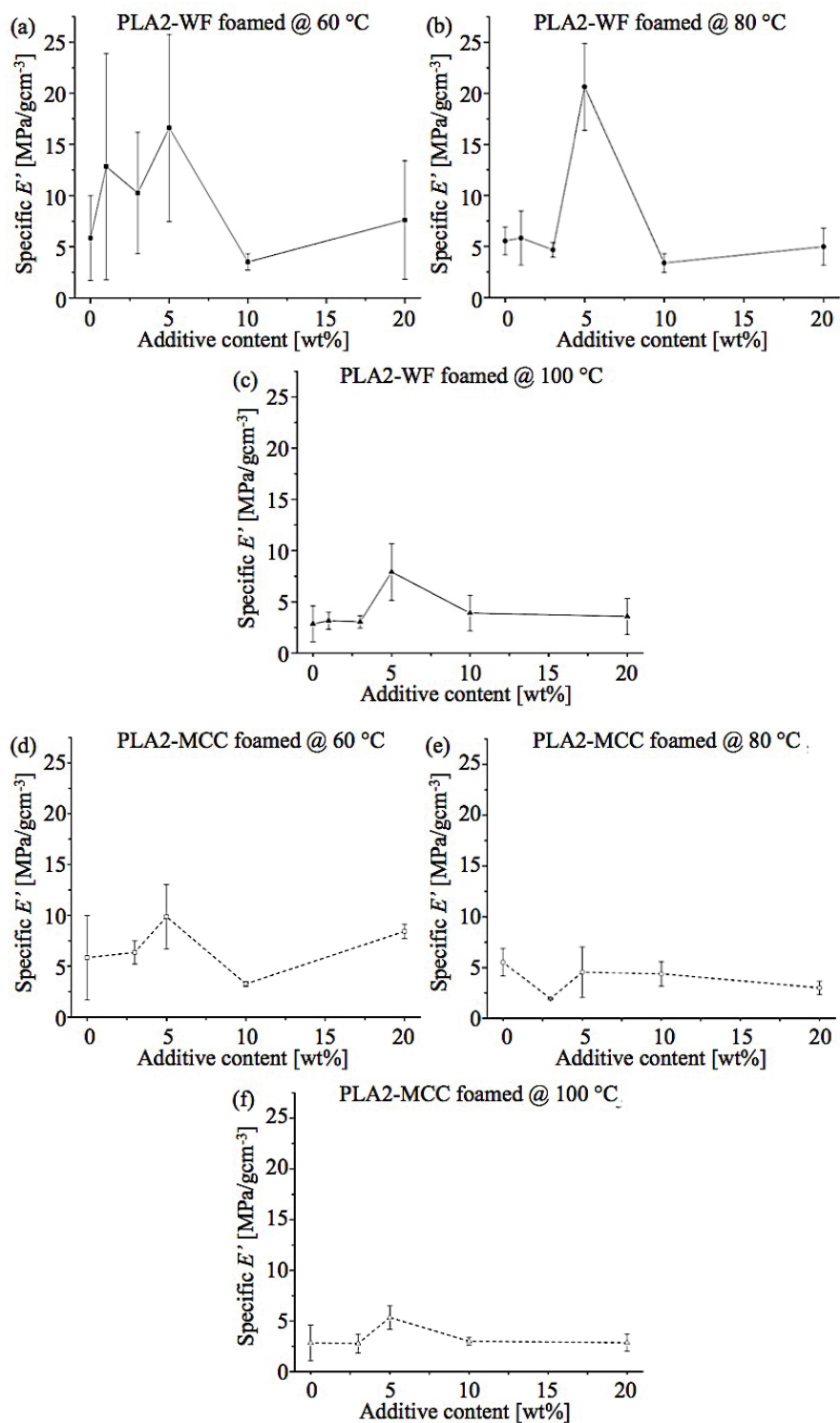
Figure 6.13 Specific modulus, $E^{*'}/\rho^{*}$, calculated from the ratio between the room T modulus and foam density for different formulations indicated.

6.4 Conclusions

Biocomposite foams were successfully produced by melt compounding of PLA and WF or MCC, and application of the liquid CO_2 process. Although the high shear melt compounding process reduced the WF fiber length, the aspect ratio of the WF remained greater than that of the MCC, and the WF consequently showed more efficient stiffness reinforcement in the solid composites and resultant foams. The PLA2-5 wt% WF composites showed promising specific properties, but it was difficult to achieve foam densities lower than 100 kg/m^3 at high WF contents. Severe thermal shrinkage was observed during free foaming in a hot oil bath and the primary cause for this was suggested to be increased rates of CO_2 loss. The increased CO_2 diffusion rates were attributed to a poor interface between the fillers and matrix, and a reduced melt strength of the PLA owing to hydrolysis, leading to a more open cell structure. The high foam densities observed under foaming conditions representative of the one step hot press process, i.e. around 1 min foaming at 100 °C, indicated that the primary goal of matching the processing characteristics of PLA-PMMA is unlikely to be achievable for the range of additive contents studied. It was nevertheless concluded that (i) if CO_2 can be retained for a sufficient amount of time and/or (ii) if it is possible to impose a sufficiently high cooling rate so as to freeze the stretched cell walls before recovery, it may be possible to produce lower density foams with improved stiffness using intermediate levels of WF addition.

Chapter 7

PLA foam precursors with different D-isomer content

As discussed in the previous Chapter, while PLA reinforced with cellulose additives show improved characteristics when processed with supercritical CO_2 [10], the corresponding solid biocomposite/CO_2 precursors showed excessive shrinkage during foaming for 1 min at 100 °C. This was attributed to enhanced CO_2 diffusion rates, loss of internal CO_2 pressure in the foams and subsequent elastic recovery. In an alternative approach to be discussed in the present chapter, a further effort was made to tailor the thermal response of the PLA without recourse to blending with a non-bio-sourced polymer such as PMMA. In this case, rather than attempt to control T_g or reinforce the matrix mechanically, the idea was to control the crystallization behavior such that the foam precursors develop only limited crystallinity during impregnation, but show strain induced crystallinity once adequate expansion has taken place to produce a low density foam. The strain induced crystallinity should then contribute both to the final foam properties and stabilize the cell walls with respect to shrinkage at the foaming temperature.

As discussed in Chapter 2, it is known that crystallinity and crystallization kinetics are sensitive to the ratio of D- and L-isomers, and PLA also undergoes strain-induced crystallization during thermoforming and foaming. In the present context, it should also be borne in mind that CO_2 is a strong plasticizer and increases the crystallization rate [11,35,179]. Hence, as shown in Chapter 4, PLA containing 1.4 % D-isomer (PLA1) crystallizes rapidly when exposed to liquid CO_2. In the work described in this chapter, PLA with a range of D-isomer contents was prepared by blending PLA1 and PLA2. The effect of the D-isomer content on (i) crystallization behavior, (ii) sorption/desorption of liquid CO_2 and (iii) foaming behavior was then investigated in order to assess the suitability of this approach for the particleboard process.

7.1 Thermal behavior of PLA blends with different D-isomer contents

Table 7.1 summarizes results from DSC heating scans from 25 to 230 °C at 10 K/min on as-extruded blends with different compositions and overall D-isomer contents, as shown in Figure 7.1. PLA1 and PLA2 were in each case blended in the extruder at 200 °C for 1 min and then cooled to 23 °C air to give predominantly amorphous extrudates. As seen from Figure 7.1, exothermic cold crystallization peaks were observed in the range 100 to 120 °C for D-isomer contents of up to 6.5 %, and melting endotherms were observed at about 170 °C for up to 9.05 % D-isomer, although at 9.05 % D-isomer there was no clear cold crystallization peak and the melting peak observed at 167.3 C was very weak. The nominally fully amorphous PLA2, which contained 11.6 % D-isomer did not crystallize under these conditions. The onset T for cold crystallization, T_{onset}, as well as the cold crystallization peak temperature, T_c, increased with D-isomer content, and the difference between T_{onset} and T_c also increased from about 11 to 21 °C as the D-isomer content increased from 1.4 to 6.5 %, while the enthalpy of fusion, ΔH, associated with the melting peak and the melting point, T_m, decreased. This implied a strong decrease in the degree of crystallinity and a decrease in the crystalline lamellar thickness associated with the cold crystallization of the as-extruded blends with increasing D-isomer content.

Table 7.1 Thermal characteristics of as-extruded PLA blends with different D-isomer contents as determined from DSC heating scans from 20 to 230 °C at 10 K/min.

Sample	D-isomer [%]	T_{onset} [°C]	T_c [°C]	T_m [°C]	ΔH [J/g]
PLA1	1.4	102.1	113.5	171.0	40.6
PLA1-25 % PLA2	3.95	109.8	128.7	170.7	32.7
PLA1-50 % PLA2	6.5	119.4	140.2	169.0	13.5
PLA1-75 % PLA2	9.05	-	-	167.3	0.7
PLA2	11.6	-	-	-	-
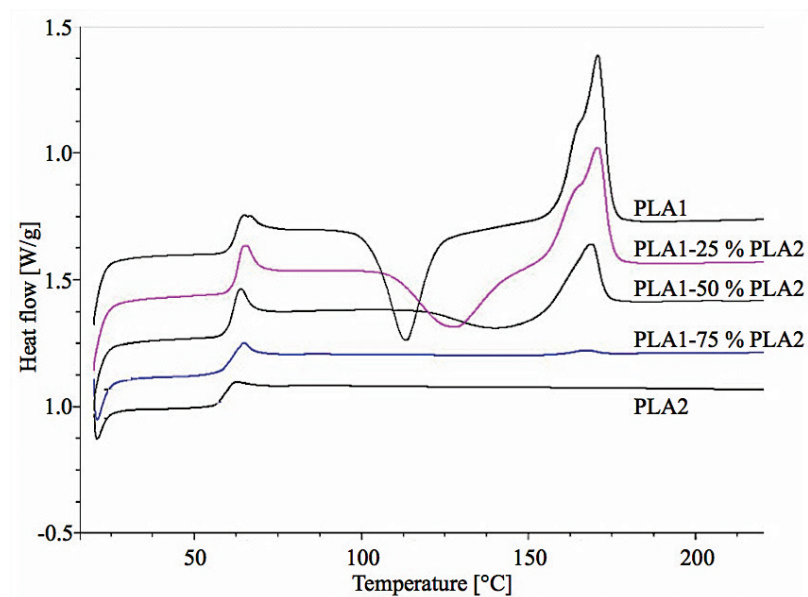
Figure 7.1 Results from DSC heating scans at 10 K/min on extrusion-blended PLA with the different mixing ratios indicated.

Figure 7.2 shows results from tensile DMA scans at 3 K/min in which 0.05 % strain was applied at 1 Hz to 0.2 mm thick amorphous films compression molded from the extruded blends. Consistent with the DSC results, an increase in storage modulus due to crystallization was observed at around 100 °C at 1.4 and 3.95 % D-isomer. However, at and above 6.5 % D-isomer there was little increase in the storage modulus in this temperature range in spite of the observation of crystallization in the DSC scans. However, the specimens containing 6.5 % and 9.05 % D-isomer showed an extended rubbery plateau compared with PLA2, from which it was concluded that the crystallinity was sufficient to hinder chain disentanglement at high T.
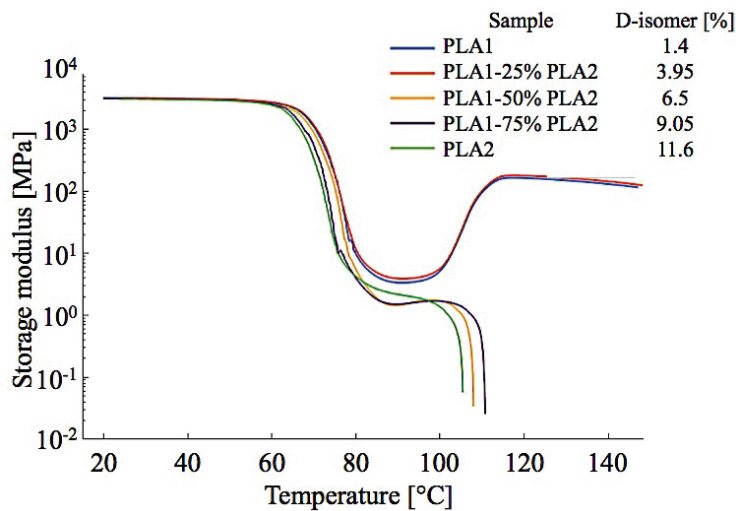
Figure 7.2 Results from DMA heating scans on 0.2 mm thick compression molded films with different D-isomer contents.

7.2 CO$_2$ absorption and foaming behaviors

Initially amorphous hot pressed 1 mm thick discs with a diameter of 25 mm were immersed in liquid CO$_2$ at 5 MPa and 10 °C for 3 hr in order to saturate them with CO$_2$. Figure 7.3 shows the subsequent CO$_2$ desorption as a function of time at ambient T and P. The highest desorption rates were observed at higher D-isomer contents of 9.05 and 11.6 %, for which the saturated specimens tended to foam at room temperature, as noted previously in the case of PLA2. On the other hand at higher D-isomer contents of 3.95 and 6.5 %, little expansion was observed and the desorption rates were similar to that of PLA1, the CO$_2$ content tending to about 0.15 g/g after 7000 s, suggesting the specimens to have been stabilized by crystallization during impregnation. As highlighted in the inset in Figure 7.3, the initial CO$_2$ content of the saturated specimens also decreased from 0.37 to 0.29 g/g as the D-isomer content decreased from 11.6 to 1.4 %, which was again assumed to reflect the presence of crystallinity, as discussed in Chapter 4.1.

Figure 7.4 and Table 7.2 show results from DSC heating scans for saturated specimens after subsequent desorption of the CO$_2$. The results confirmed PLAs with up to 9.05 % D-isomer to have crystallized at least to some extent on exposure to liquid CO$_2$ at 10 °C, sharp melting peaks being observed in each case, with little or no cold crystallization. Moreover the corresponding

values of *ΔH* were generally significantly greater those obtained after cold crystallization of the corresponding as-extruded specimens (Table 7.1).
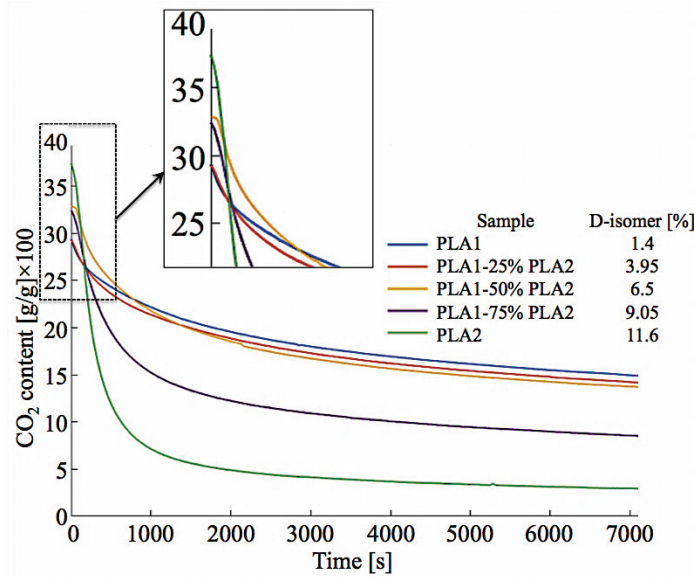
Figure 7.3 CO_2 desorption behavior measured from 3 hr liquid CO_2 treated 1 mm thick hot pressed initially amorphous discs
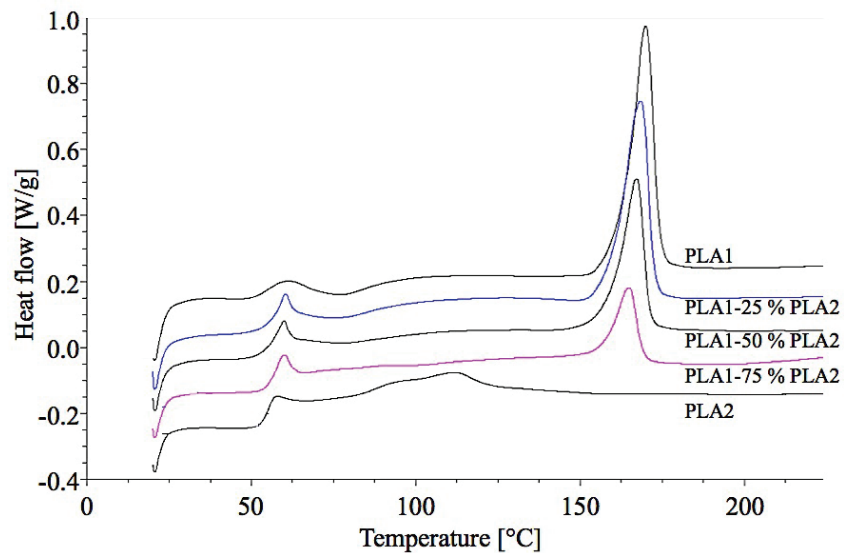
Figure 7.4 After desorption DSC measurement from 25 to 230 °C at 10 K/min

Table 7.2 Summary of after desorption DSC measurement from 25 to 230 °C at 10 K/min

Sample	D-isomer [%]	T_m [°C]	ΔH [°C]	χ_c [%]
PLA1	1.4	169.9	38.4	41.3
PLA1-25 % PLA2	3.95	168.4	33.1	35.6
PLA1-50 % PLA2	6.5	167.2	23.8	25.6
PLA1-75 % PLA2	9.05	164.9	10.7	11.5
PLA2	11.6	-	-	-

For further investigation, stable foam precursors containing about 0.2 g/g of CO_2 were prepared from initially amorphous compression molded discs of all the blends by 10 min impregnation in liquid CO_2 at 10 °C followed by conditioning for 2 hr at 10 °C, as described in Chapter 4.1.3. Free expansion of these precursors was carried out in a silicon oil bath at 80 and 100 °C for one minute, and the resulting cell structures are shown in Figures 7.5 and 7.6 respectively. A distinct skin-core structure was obtained at low D-isomer contents of 1.4 and 3.95 %. As argued previously in Chapter 4.4, the relative lack of expansion in the skin was caused by crystallization during partial impregnation, when the CO_2 content was locally high. In these specimens, the cellular morphology of the core was highly anisotropic, particularly in specimens foamed at 100 °C (Figure 7.6 (a), (b)), presumably because lateral expansion was blocked by the rigid, more highly crystalline skin layer, constraining the cells to grow in the through-thickness direction. Thus the thickness/diameter ratio increased from an initial value of 25 (25 mm/1 mm) to 7.7 (26.6/3.45) and 8.4 (40.45/4.8) at 1.4 and 3.95 % D-isomer, respectively, while values of 19 (46.6/2.45) and 16.9 (30.4/1.8) were obtained at 9.05 and 11.6 % D-isomer. The overall foam density obtained after expansion at 100 °C was about 340 kg/m^3 at 1.4 % D-isomer but fell to 100 kg/m^3 at 3.95 % D-isomer (Figure 7.7). These results indicate that that the geometry of low D-isomer foam precursors is likely to have a strong influence on the foaming step. More specifically, a plaque-like precursor morphology is likely to be more favorable to the production of low density foams at high D-isomer contents than a roughly spherical morphology (i.e. a pellet), in which the skin layer will presumably constrain expansion in all directions.

At 6.5 % D-isomer, a more uniform isotropic cellular structure was observed over most of the specimen thickness than at lower D-isomer contents, but also some significantly larger cavities

owing to rupture of the cell walls and consequent cell coalescence during expansion. This was qualitatively consistent with the reduced tendency to crystallize seen e.g. in the DMA scans (Figure 7.2), which implied reduced stability of the cell walls under these conditions, particularly at 100 °C. As the D-isomer content was increased further to 9.05 and 11.6 % not only was a more coalesced and open cell structure observed at both 80 and 100 °C, but also marked shrinkage, leading to relatively high foam densities, as shown in Figure 7.7.
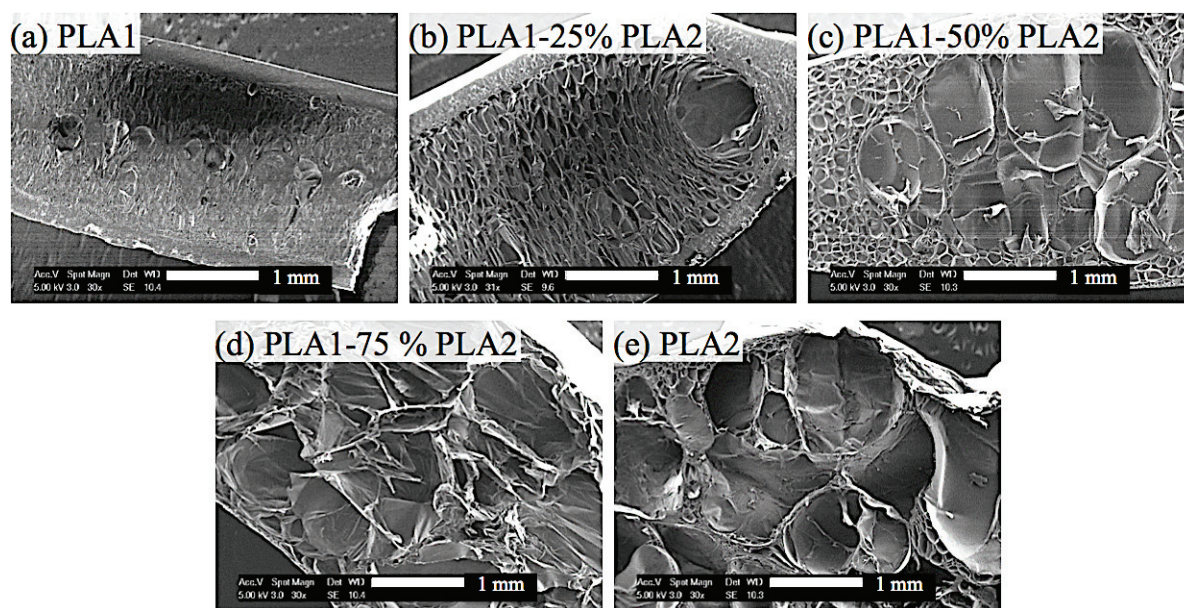
Figure 7.5 Cell structure observed by SEM in precursors containing 0.2 g/g CO_2 foamed for 1 min at 80 °C in a silicone oil bath: (a) 1.4, (b) 3.95, (c) 6.5, (d) 9.05 and (e) 11.6 % D-isomer.
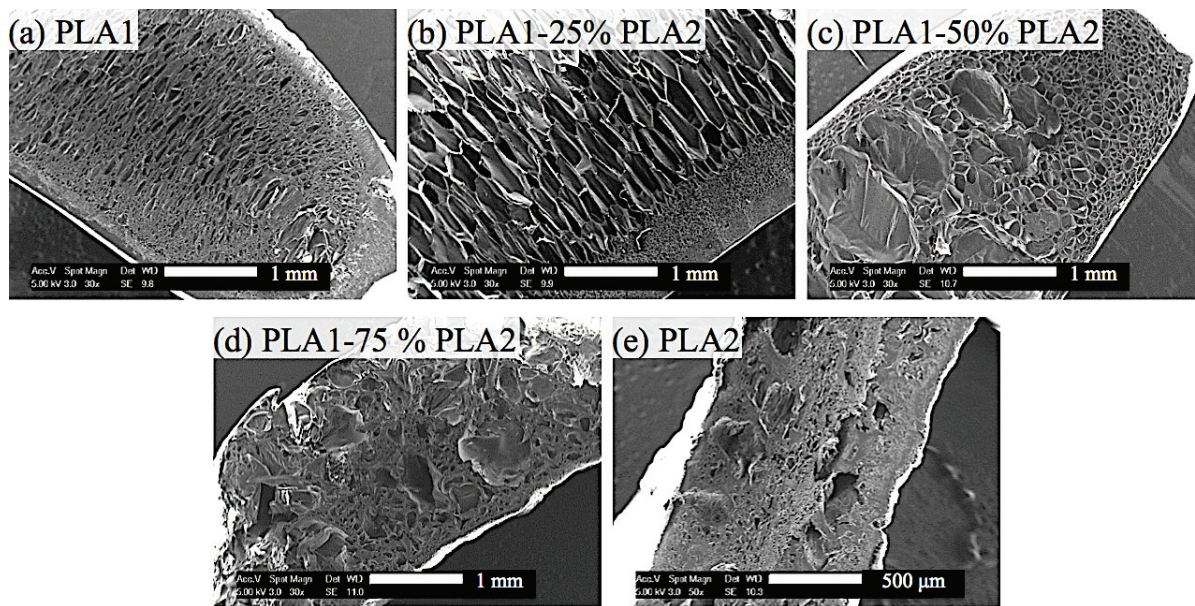
Figure 7.6 Cell structure observed by SEM in precursors containing 0.2 g/g CO_2 foamed for 1 min at 100 °C in a silicone oil bath: (a) 1.4, (b) 3.95, (c) 6.5, (d) 9.05 and (e) 11.6 % D-isomer.

Compressive DMA tests were carried out on $> 3 \times 3$ mm^2 cuboid specimens cut from discs foamed at 100 °C as described in Chapter 3.3.3. The relatively fine, regular cell morphology and high overall low density obtained for PLA1 was reflected by a high compressive modulus at low T, as shown in Figures 7.7 and 7.8. A small increase in storage modulus with temperature observed at around 70 °C, i.e. just above T_g, in all the foams was assumed to be caused by residual shrinkage during the measurements. However as T increased further the modulus dropped sharply to a value corresponding to the rubbery plateau. At 3.95 % D-isomer, the low T storage modulus remained relatively high at 6.5 MPa, in spite of the low density in this case (Figure 7.7), implying a particularly high specific stiffness. The low T storage modulus decreased significantly for the coalesced cell structures obtained at 6.5 and 9.05 % D-isomer, although their densities were similar to that for 3.95 % D-isomer. Finally, the foams obtained from PLA2, again showed a reduced low T storage modulus, in spite of its much higher density. It follows that foams produced from PLA/CO_2 precursors containing 3.95 % D-isomer showed particularly promising combinations of modulus and density at a foaming temperature of 100 °C, i.e. consistent with the particleboard process.
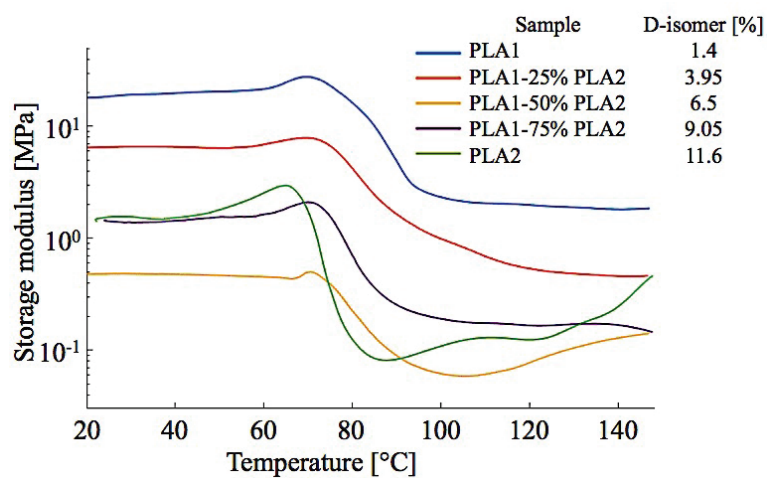
Figure 7.7 Storage modulus as a function of *T* from compressive DMA measurements on specimens foamed at 100 °C.
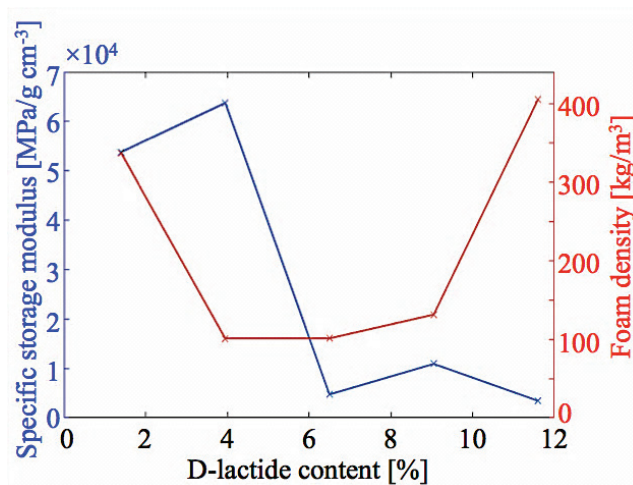
Figure 7.8 Foam density and specific modulus as a function of D-isomer content after 1 min expansion at a foaming temperature of 100 °C.

7.3 Conclusion

The present chapter describes an investigation of the possibility of obtaining heat expandable, partly crystallizable foam precursors by using blending to control the D-isomer content of the

117

PLA matrix and hence its tendency to crystallize. Foams with densities as low as 100 kg/m^3 could be prepared by free expansion of impregnated and conditioned precursors containing about 0.2 g/g of CO_2 at 100 °C for D-isomer contents in the range 3.95 to 9.05 %. However, the resulting foam cell structures were dependent on D-isomer content, more homogeneous with directional cell structures being obtained at a low D-isomer content of 3.95 %, where an unexpanded skin layer prevented lateral expansion of the discs, than at higher D-isomer contents, for which there was considerable cell coalescence.

The foaming observed at low D-isomer contents is expected to be influenced by two main factors: (i) CO_2 concentration dependent crystallization during impregnation and (ii) strain induced crystallization during the expansion step [44]. After 10 min impregnation in liquid CO_2, the high concentration of CO_2 in the surface layer of the 1 mm thick and 25 mm diameter low D-isomer content PLA discs may be assumed to result in a relatively high degree of crystallinity and limited expansibility in the temperature range of interest here, while the core layer undergoes little or no crystallization owing to the relatively low CO_2 content throughout impregnation and/or conditioning at 10 °C, as discussed in Section 4.4. The extent to which this skin layer forms is expected to be strongly dependent on the D-isomer content. Strain-induced crystallization may also take place in relatively weakly crystalline regions during subsequent foaming, as a result of the biaxial stretching of the foam cell walls, again depending on the D-isomer content. Although strain-induced crystallinity in the cell walls was not observed directly in the present work, initially amorphous PLA with comparable D-isomer contents is known to show considerable crystallization during mechanical stretching at 100 °C, e.g. ~17 % and ~6 % crystallinity at 2 and 4 % D-isomer respectively after biaxial stretching at 1 m/min up to a 5 × 5 stretch ratio [44]. This readily explains the improved stability of the intermediate high D-isomer content PLA with respect to elastic recovery immediately after expansion, which has been shown to severely limit the process windows corresponding to fully amorphous PLA.

However, while the expansibility and stability of foams produced from PLA containing 3.95 % D-isomer led to promising combinations of stiffness and density, a foreseeable practical concern is a lack of adhesion between individual foam precursors at processing temperatures below the melting point of the crystalline skin, as in the present case. This is generally known to be a major concern for the chest-molding of pre-expanded semicrystalline PLA precursors [180], and in the

present case is also likely to affect adhesion between the foam core and the particle facings in the particleboard process. Furthermore, the presence of a non-expandable skin layer may hinder expansion of the pellet-type foam precursors used for the fully amorphous materials considered up to now. It follows, therefore, that an extended planar foam precursor sheet (cf. the plaques used for the foaming studies described in this chapter), may be more appropriate to the particleboard process, because it should (a) reduce constraints on through thickness expansion and (b) eliminate the need to form internal fusion bonds between neighboring precursor pellets. The extent to which this approach is effective will be discussed further in Chapter 8.2.

Chapter 8

Implementation of the precursors

The following section describes trials aimed at implementing the foam precursors in a one-step foam core particleboard process with adhesive treated wood particles as the surface layers. A hot press with precise control of the pressure, platen height and cooling rate was employed. The emphasis was on investigating the feasibility of panel production using processing parameters, e.g. the press time and range of temperatures, which suit both the consolidation of the surface layers and foaming of the core layer. The trials were carried out in collaboration with BUAS.

8.1 Manufacturing the sandwich panel by hot pressing

The partial impregnation technique was applied to extruded and pelletized PLA2 and PLA2-50 wt% PMMA containing 1 wt% talc as a nucleating agent. The dimensions of the pellets were 1-1.5 mm in diameter and 2-3 mm in length. After a 15 min treatment in liquid CO_2 at 10 °C and storage for more than 1 hr at low T (<10 °C) at atmospheric pressure, the foam precursors contained approximately 0.12 g/g CO_2.

As shown in Figure 8.1, the initially transparent pellets became opaque after impregnation, suggesting some degree of expansion during depressurization and/or conditioning. Moreover, the precursors tended to aggregate owing to plasticization by the dissolved CO_2 during the impregnation step. The PLA2-50 wt% PMMA pellets could nevertheless easily be separated mechanically during lay-up of the three-layered mat used to produce the particleboard (Figure 8.2), whereas PLA2 pellets were more difficult to disaggregate. The target density and thickness of the foam layer and the final particleboard were 100 kg/m^3 and 13 mm, and 350 kg/m^3 and 19 mm, respectively, and the resulting particleboard density was 325 kg/m^3 when produced with the PLA2-50 wt% PMMA foam precursor. However, the target thickness could not be achieved using

pure PLA2 owing to shrinkage-induced collapse of the expanded foam core layer in the hot press during the cooling step.

Figure 8.1 PLA2-50 wt% PMMA foam precursors in pellet form containing 0.12 g/g CO_2.
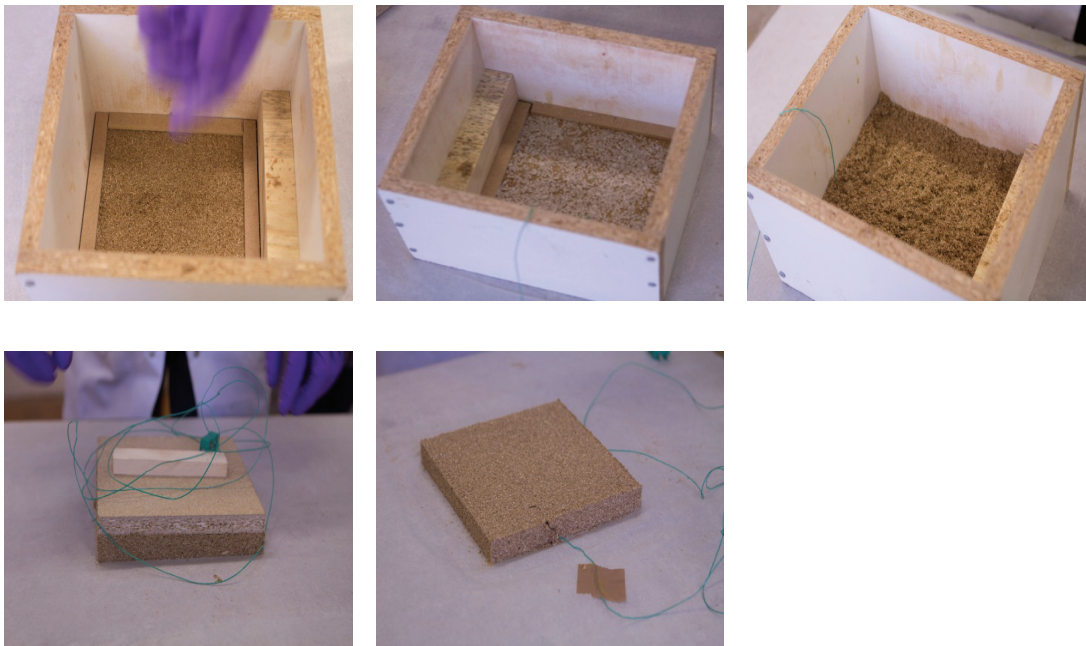
Figure 8.2 One example of the preparation of a three-layered mat with adhesive treated wood particles and foam precursors. Thermocouples were used to monitor the temperature of the bottom and middle layers of the mat *in situ*.

As shown in Figure 8.2, the three layer mat was prepared in a rectangular wooden frame. A first layer of wood particles treated with urea formaldehyde/ammonium persulfate adhesive was introduced into the frame and compressed manually. The foam precursor pellets were then evenly distributed on the first wood particle layer to within about 15 mm of the edges of this latter, leaving a foam precursor free perimeter that acted to confine the foam during processing. Finally, the top wood particle layer was added following same procedure as for the first layer. The wooden frame was carefully removed and the mat transferred to the hot press between two release films.

Data acquisition and control of the hot press (HLP210, Hōfer) was carried out using a PC. The platen temperature was set to 125 °C (cf. 160 °C for EPS and MS). The process consisted of three main stages. The first stage was to consolidate the surface layers under high T and P. The press was then opened to a pre-set height of 19 mm in order to allow the foam precursors to expand. Finally, an integrated water cooling system was activated to cool and stabilize the resulting structure. A typical set of operational parameters is shown in Figure 8.3.
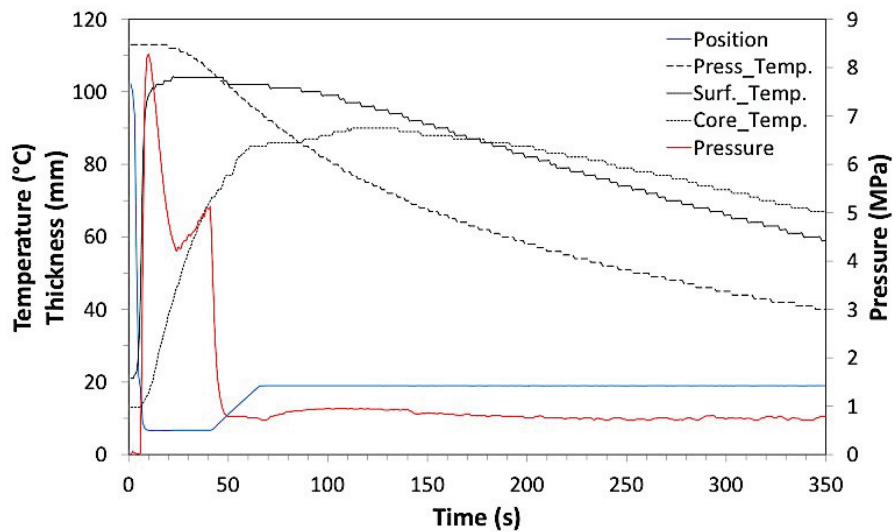
Figure 8.3 A typical press cycle for the production of foam core particleboard.

As inferred from the observed increase in pressure of about 1 MPa (red curve in Figure 7.3) at ~ 20 s after the start of the process cycle, foaming initiated at a core temperature of ~ 45 °C. The press was maintained closed until the cycle time reached 40 s, so that the pressure was maintained

at about 4 MPa for 20 s after the onset of foaming. Because the pressure decreased sharply when the press was opened, it was difficult to follow the subsequent evolution of the expansion force, but the slight increase in pressure between 70 and 140 s indicated the foaming time to be relatively long. The highest T reached in the core layer was ~90 °C, at 110 s. The cooling water was made to circulate starting at the same time as the onset of foaming, in order to stabilize the foam structure, and the core layer temperature decreased to below the T_g (70 °C) of PLA2-50 wt% PMMA after about 280 s. However, this method of cooling was not sufficient to decrease the core layer T to below the T_g of PLA2 (60 °C) prior to extensive collapse of the foam core (Figure 8.4).
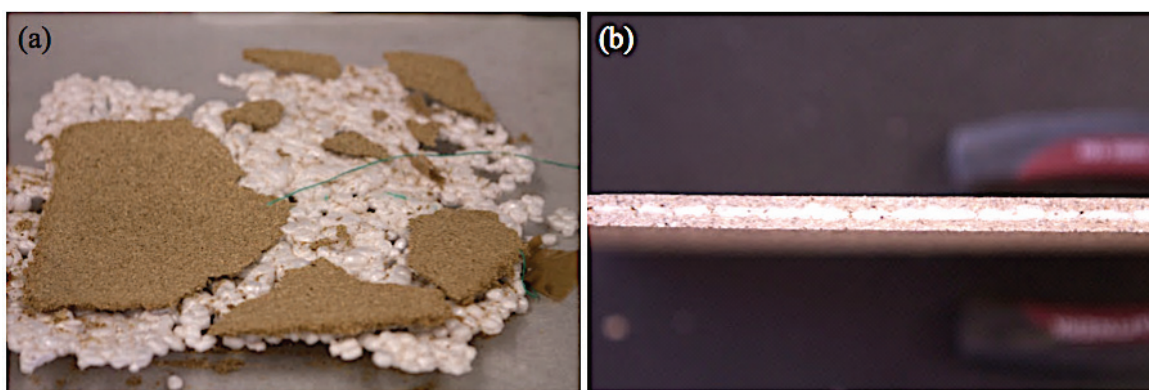
Figure 8.4 Failures in foam core particleboard production using PLA2 foam precursors: (a) poorly consolidated surface layers and (b) collapsed core layer

8.2 Feasibility test with a plaque-shaped foam precursor prepared from low D-isomer content PLA

First trials were also carried out in which a commercial 5 % D-isomer long chain branched PLA (Ingeo 8052D, Natureworks LLC) was used to produce plaque-shaped foam precursors. Transparent, amorphous 40×80 mm^2, 1 mm thick plaques were first prepared from this material without additives in the hot-press, as for the circular plaques used for the diffusion studies described in Chapter 4.1.3. They were then subjected to liquid CO_2 impregnation for 10 min at 5 MPa and 10 °C followed by conditioning at ambient P and < 10 °C to give overall CO_2 contents of 0.1 to 0.11 g/g. The resulting foam precursors remained transparent but were slightly swollen after impregnation. 160×160 mm^2 square three-layered mats were prepared using 8 of these

plaques placed side-by-side, and comparable hot press steps were applied as for the pellet precursors. As shown in Figure 8.5, individual precursor plaques processed in this way showed substantial and highly stable through-thickness expansion to give a final density of 121 kg/m^3 and final dimension of $41 \times 87 \times 10$ mm^3, with approximately 1.5 mm of a relatively unexpanded skin layer. However, there was no adhesion between the foam core and particleboard surfaces and attempts to produce foam-core particleboard from this material were not successful in spite of the excellent foaming characteristics of the core.

While further investigation of processing with intermediate D-isomer content PLA is clearly needed, some important and encouraging points arise from this study. First, *in situ* foaming to give core acceptable core densities under conditions representative of the particleboard process was greatly facilitated at 5 % D-isomer content. Moreover, the concept of a non-granulate plaque-type foam precursor was validated and indeed the potential for limiting foam expansion to the through-thickness direction thanks to the presence of the skin layer is particularly attractive for the particleboard process since it obviates the need for lateral confinement in the press. It may also be promising for higher output production, e.g. continuous production in a roll type hot press with a sheet-like foam precursor. There may also be advantages in terms of reduction of the impregnation time; it has reported previously that lower CO_2 contents are needed to foam low D-isomer PLA than for amorphous PLA [44]. Indeed, in the present case it was found that comparable foam densities could be achieved in the plaque geometry with only 0.05 g/g CO_2 (obtained by immersion in liquid CO_2 for 5 min at 5 MPa and 10 °C followed by conditioning at 10 °C). Moreover, if it is possible to increase the consolidation T owing to the relative lack of foam collapse, shorter consolidation cycles may be possible, and the cooling step may be attenuated or eliminated.

Nevertheless, the outstanding obstacle to use of PLA with 5 % D-isomer as a precursor is the lack of adhesion of the semi-crystalline skin to the wood particle facings. This may not be insurmountable, given the possibility of introducing an adhesion layer to the plaque surfaces. For example, a thin foil of amorphous PLA could be bonded to the 5 % D-isomer PLA during compression molding of the plaques. However, it had not been possible to schedule further trials at BUAS at the time of writing.
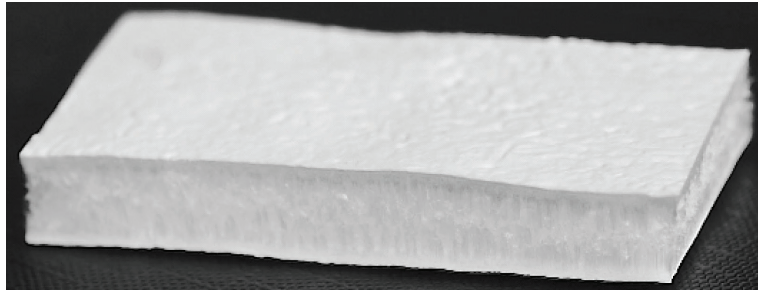
Figure 8.5 Foam core resulting from the one step particleboard process trial using a plaque-type long chain branched PLA foam precursor containing ~ 5 % D-isomer.

8.3 Mechanical property evaluation of the PLA-PMMA foam core (results from BUAS)

The foam core particleboard produced by the one-step press process described in the previous section is shown in Figure 8.5. To evaluate mechanical properties of the PLA-50 wt% PMMA foam, tensile and compression tests were carried out, and the elastic behavior was compared with that of core layer foams from EPS and MS sandwich panels [20].
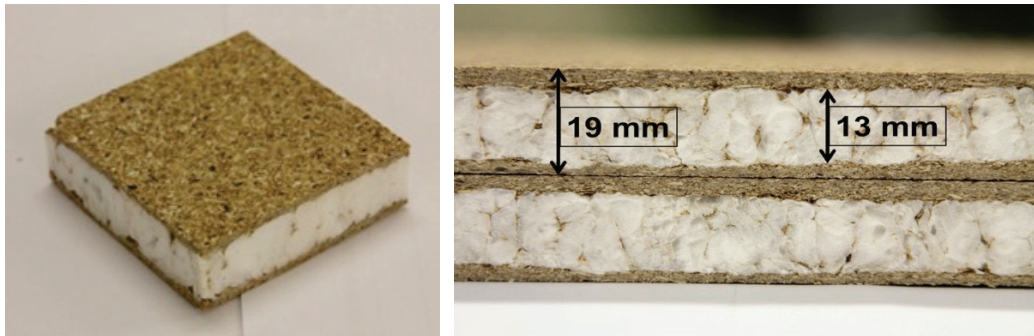
Figure 8.6 Foam core particleboard with a PLA2-50 wt% PMMA foam core produced using the one-step process.

Stress-strain curves and the corresponding Young's moduli are shown in Figure 8.6. In overall, the compressive stiffness and maximum strength were greater in compression than in tension. The PLA2-50 wt% PMMA foam showed intermediate values of the Young's modulus in tension and

compression at ~23 and ~32 MPa respectively, while the MS foam showed the highest values at ~32 and ~37 MPa. The SEM micrographs in Figure 8.7 indicate the MS foam to have the smallest cell size, and the EPS foam to have the largest cell size.
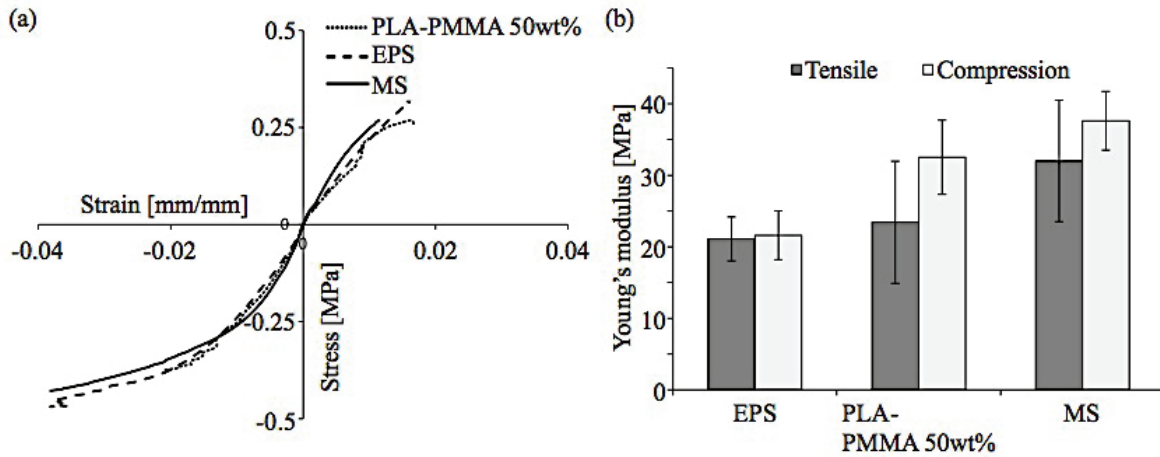
Figure 8.7 (a) Stress-strain curve from different particleboard foam cores and (b) the corresponding Young's moduli [19].
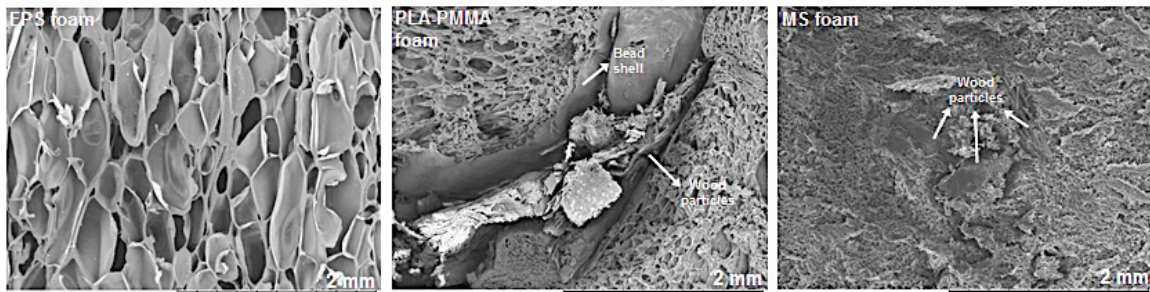
Figure 8.8 Micrograph of EPS, PLA-50wt% PMMA and MS foams from the respective particleboard structures [19].

The significant differences between the tensile and compressive behavior of the PLA-50 wt% PMMA foam was assumed to be due to less effective tensile load transfer, owing to imperfect bonding between the foam precursor beads. The poorly bonded boundaries, with interposed wood particles are seen for example in the SEM micrograph in Figure 8.7 (middle). The relatively large initial granule size (1-1.5 mm in diameter and 2-3 mm in length) of the PLA-50 wt% PMMA precursor (cf. diameters of 15 μm and 300-800 μm for MS and EPS respectively) may have

increased the effective local distances between neighboring granules allowing infiltration of the wood particles. The contribution of the granule boundaries to performance was further investigated by preparing a reference foam specimen hot pressed at 125 °C in a rectangular shaped mold without the wood particle surface layers. As seen from Figure 8.8, the reference specimen showed significantly different elastic behavior and morphology. The higher moduli, and the closer correlation between the compressive and tensile response in this case may be attributed to a more uniform cell size distribution as well as better bonding between the granules (Figure 8.8 bottom).
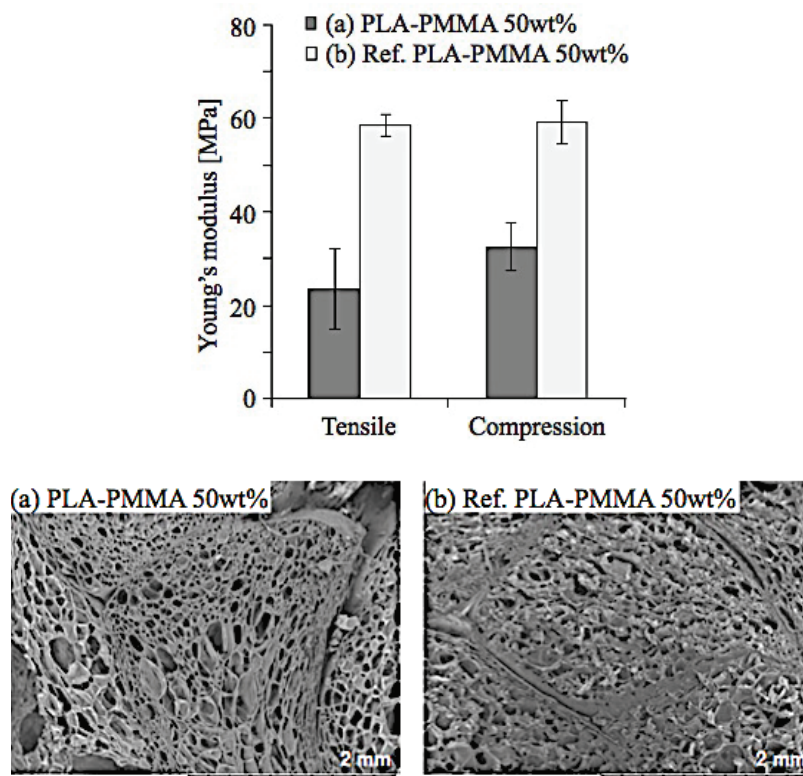
Figure 8.9 Comparison between PLA-50wt% PMMA foams produced by hot press (a) with wood particles and (b) without wood particles.

8.4 Conclusions

Production of PLA-based foam core particleboard using a one step process with the hot press was successfully demonstrated. Partial impregnation of PLA-50 wt% PMMA at 5 MPa and 10 °C for 10 min, followed by low T conditioning for 2 hr at ambient pressure resulted in foam precursors that could be integrated into the particleboard process, with adequate handling and storage properties, and acceptable foam density without collapse during hot pressing. 19 mm thick panels with well-consolidated wood particle facings were produced with a variety of foam cores and their mechanical properties evaluated. Relatively poor interfaces between the foam precursor granules was observed in PLA2-50 wt% PMMA and resulted in mismatch in tensile and compressive behavior. Reducing the size of the foam precursors may be beneficial for more uniform distribution and homogeneous foam structures. However it should be borne in mind that the size modification may be accompanied by more rapid CO_2 diffusion out of the granules. Optimization of the processing conditions should continue with emphasis on the relationship between mechanical properties and processing parameters. Moreover, modeling of the sandwich structures will permit establishment of target properties for each component, which can be verified with feedback from further mechanical testing.

Chapter 9

General conclusion

9.1 Main achievements

The main objective of this thesis has been to develop foam precursors for the in-line production of lightweight foam core particleboard sandwich structures, whose production costs and performance should remain comparable with those of conventional particleboard if they are to be commercially viable. A number of studies have shown that a single-step hot press process, in which consolidation of the particleboard facings and foaming of the core layer take place in a single operation, is feasible and could form the basis for a continuous production method. The challenge is to match the processing window of the particleboard facings, which is fixed by the curing characteristics of the adhesive and the presence of water in the wood particles, and that of the foam core. To date, all proofs of principle have been based on inflammable physical blowing agents for the foam core that are inconsistent with safety and environmental requirements associated with the use of an open press. The focus in the present work has been on understanding and controlling the stability and foaming behaviour of an alternative foam precursor system that not only meets these requirements, thanks to the use of a non-inflammable blowing agent, CO_2, but is also based on a bio-sourced, biodegradable polylactide (PLA) matrix, with clear benefits for sustainable development.

The PLA was impregnated by immersion in liquid CO_2 at 10 °C and a pressure of 5 MPa in order to avoid the premature foaming during the depressurization step that was generally observed during high temperature supercritical CO_2 processing. Systematic observations of the sorption/desorption behaviour of resulting the PLA/CO_2 solid solutions were made and on the basis of the desorption data, a concentration dependent diffusion model was established that could be used to predict CO_2 concentration profiles for different combinations of impregnation and

desorption times. On this basis, a novel protocol involving impregnation in liquid CO_2 followed by low temperature conditioning at ambient pressure was developed that permitted preparation of fully amorphous (11 % D-isomer) PLA precursors containing a relatively uniform CO_2 content of around 0.1 g/g from 1 mm thick compression moulded discs or pellets with comparable diameters. These were stable at room temperature with respect to both foaming and rapid CO_2 loss, but expanded to form foams with densities less than 100 kg/m^3 when heated to above the nominal glass transition temperature, T_g, of the PLA (about 55 °C). On the other hand, PLA with a low D-isomer content (1.4 %) was found to crystallize during impregnation and show little or no foaming when heated to above T_g. Subsequent efforts to develop PLA/CO_2 foam precursors for use in the particleboard process therefore initially focused on the amorphous PLA.

An immediate problem to be overcome was the mismatch between particleboard process temperature, which implied a core temperature of the order of 100 °C, and the optimum foaming temperature of the amorphous PLA/CO_2 of around 60 °C, pure PLA/CO_2 foam cores tending to collapse in preliminary trials with particleboard facings. In order to adjust the thermal properties of PLA, it was extrusion compounded with a relatively high T_g polymer, polymethylmethacrylate (PMMA). The solubility of the CO_2 was dependent on the mixing ratio between two polymers but the desorption behaviour of the blends was similar to that of unmodified PLA. The impregnation and conditioning technique developed for the amorphous PLA could hence be applied without significant modification to produce stable foam precursors from the blends. Moreover, PLA-50 wt% PMMA containing 0.13 g/g CO_2 gave foams with densities of less than 70 kg/m^3 and these showed far less tendency to collapse when foaming was carried out at 100 °C, consistent with the requirements of the particleboard process.

In an effort to develop a fully bio-based alternative to blending with PMMA, amorphous PLA-microcrystalline cellulose (MCC) and PLA-wood fibre (WF) were also investigated, based on previous reports of improved foam stability during supercritical processing of cellulose-modified PLA. These biocomposites showed some improvement in tensile modulus over the pure PLA, but a permeable interface between the PLA and the additives was suggested to lead to increased CO_2 diffusion rates at additive contents at or greater than about 10 wt%. While it was possible to prepare stable foam precursors containing more than 0.1 g/g of CO_2 from these materials, severe collapse of the foam structures was observed at high additive contents immediately after

expansion, particularly at high foaming temperatures. This effect was attributed to rapid CO_2 loss and subsequent elastic recovery, and made it difficult to produce low density foams from the highly loaded biocomposites, even at foaming temperatures where pure PLA/CO_2 showed a satisfactory response. Acceptable foam densities with significant increases in specific modulus were nevertheless obtained at 3 to 5 wt% WF, but it was concluded that cellulose-based additives were unlikely to have benefits for processing in the temperature range of interest for the particleboard process.

In a further effort to develop fully bio-based precursors, therefore, blending was used to vary the D-isomer content of the PLA systematically with the aim of producing materials that showed limited (or no) crystallization during impregnation with liquid CO_2, but sufficient crystallization during expansion to stabilize foam structures formed at and around 100 °C. A range of PLA blends with different overall D-isomer contents were prepared and it was confirmed that their tendency to crystallize decreased systematically as the D-isomer content increased. Thus, stable low density foams with acceptable specific properties could be obtained for D-isomer contents of 3.95 and 6.5 % under conditions representative of the particleboard process, i.e. free foaming at 100 °C with heating times of the order of minutes. Indeed these precursors were found to show improved foam stability compared with the PLA-PMMA blends.

The final implementation trials were mainly based on PLA-50 wt% PMMA foam precursors in pellet form, containing about 0.12 g/g CO_2, which showed negligible expansion at ambient temperature and pressure and showed little CO_2 loss during medium terms storage in a refrigerator, but readily underwent foaming in the hot press under conditions consistent with full consolidation of the particleboard facings. 19 mm thick foam core particleboard sandwich panels with high quality, well consolidated facings, were successfully produced using these precursors, after careful adjustment of the process conditions to ensure sufficiently rapid cooling of the foam core after the expansion step, this being crucial for stability of the core with respect to collapse of the foam structure. A 50 % density reduction was achieved in the final particleboard product. Moreover, the foam cores showed superior mechanical properties to EPS cores obtained under similar conditions, although they were markedly anisotropic and showed relatively coarse internal morphologies owing to the relatively large pellets used for these studies (diameters of around 2

mm). The results of these trials were considered to be a great success and a proof of principle for the processing route and materials proposed at the outset of this thesis.

9.2 Outlook

While the outcome of the work is considered to be highly positive, there remains considerable scope for further development and optimization of the foam core particleboard process. First, this work has been restricted to the laboratory scale, and industrial scale production using a continuous process has yet to be addressed in detail. One potential difficulty with an industrial scale foam core particleboard process is the need for a three-layered mat as the starting material. Because an even distribution of the foam precursor is important for mechanical properties, great care must be taken in the preparation of this mat, with consequences for the production cycle time. Different foam precursor geometries, e.g. smaller pellets or continuous sheets may therefore need to be considered, but modifying the precursor dimensions will also influence of the effective diffusion distance for the CO_2. Thus smaller pellets may lose CO_2 too rapidly for convenient handling or effective foaming to be possible, while much longer impregnation times may be needed for thick sheets, depending on their thickness. In the case of a continuous particleboard process, which should make use of a double belt press as in conventional particleboard manufacture, the 3-layered mat would be formed on a moving belt, and mat densification, skin layer consolidation, core layer foaming and cooling would subsequently take place in-line, e.g. by changing the belt spacing to allow expansion and introduction of a cooling bath. The foam precursors may again be introduced in the form of either pellets or sheets, but preparation of a flexible roll of PLA impregnated with CO_2 with the right thickness is expected to be problematic, so that it would be necessary to use discrete plates rather than a continuous sheet.

The precursor geometry is expected to be particularly important with regard to the formulation of the core layer precursor. If the excellent foaming properties of semicrystalline PLA with intermediate D-isomer contents are to be exploited, adhesion must be improved both between the precursor pellets and the foam core and between the particleboard facings, which the first trials showed to be inexistent. Clearly problems with adhesion between foam precursors can be at least partly avoided by use of a continuous and semi-continuous sheet precursor. This approach was

shown to be very promising for *in situ* foaming in the hot press, not only because it eliminates the need to form PLA-PLA interfaces within the foam core, but also because it releases constraints on expansion in the through thickness direction due to the formation of a highly crystalline skin layer during impregnation (and which may severely limit expansion of roughly spherical or cylindrical pellets). However, in future developments it will still be necessary to improve adhesion between the core and the facings, presumably by including an additional bonding layer, e.g. an amorphous PLA foil, or a (preferably bio-friendly) adhesive capable of interacting with both the PLA and the wood particles. This is obviously more practical for a sheet geometry. However, the additional processing steps would also increase production costs.

Further investigation of the functionality of the foam core particleboard will also be necessary for practical applications. For example, the panels may need to be cut and/or joined in furniture applications, which case the influence of the sandwich structure on these operations should be carefully assessed, and if necessary compensated e.g. by use of local reinforcements.

Finally, as well as fulfilling the immediate objective, i.e. validation of a potentially industrially viable lightweight foam core particleboard process, this work is significant in that it has also opened up novel possibilities for the use of CO_2 as a physical blowing agent for the *in situ* foaming of PLA during compression molding. The concept may easily be extended to other types of facing (aluminium, paper etc.) and it should also be borne in mind that the relatively strict constraints on the processing window in the particleboard process may be significantly relaxed in other applications.

References

[1]   I. Eastin, I. Brose, F. Maplesden, I. Novoselov, Forest Products: annual market review 2014-2015, 2015.

[2]   X. Li, Z. Cai, J.E. Winandy, A.H. Basta, Selected properties of particleboard panels manufactured from rice straws of different geometries, Bioresource Technology. 101 (2010) 4662–4666. doi:http://dx.doi.org/10.1016/j.biortech.2010.01.053.

[3]   C. Xing, S.Y. Zhang, J. Deng, S. Wang, Investigation of the effects of bark fiber as core material and its resin content on three-layer MDF performance by response surface methodology, Wood Science and Technology. 41 (2007) 585–595. doi:10.1007/s00226-007-0129-6.

[4]   C. Schopper, A. Kharazipour, C. Bohn, Production of innovative hemp based three-layered particleboards with reduced raw densities and low formaldehyde emissions, International Journal of Materials and Product Technology. 36 (2009) 358–371. doi:10.1504/IJMPT.2009.027842.

[5]   Z. Chen, N. Yan, J. Deng, G. Smith, Flexural creep behavior of sandwich panels containing Kraft paper honeycomb core and wood composite skins, Materials Science and Engineering: A. 528 (2011) 5621–5626. doi:http://dx.doi.org/10.1016/j.msea.2011.03.092.

[6]   T.H. Poppensieker, Untersuchung der Wirtschaftlichkeit von leichten Holzwerkstoffen, Univers. of Hamburg, 2010.

[7]   M.R.J. Witt, S. Shah, Methods of manufacture of polylactic acid foams, WO2008093284 A1, 2008.

[8]   Y. Yoon, C.J. Plummer, H. Thoemen, J. -a. E. Manson, Liquid CO2 processing of solid polylactide foam precursors, Journal of Cellular Plastics. (2014). doi:10.1177/0021955X14537662.

[9]   J.L. Eguiburu, J.J. Iruin, M.J. Fernandez-Berridi, J.S. Roman, Blends of amorphous and crystalline polylactides with poly(methyl methacrylate) and poly(methyl acrylate): a miscibility study, Polymer. 39 (1998) 6891–6897.

[10]   C. Boissard, Processing of Sustainable Cellular Biocomposites, École polytechnique fédérale de Lausanne, 2012. doi:10.5075/epfl-thesis-5499.

[11]   J.-P. Garancher, A. Fernyhough, Crystallinity effects in polylactic acid-based foams, Journal of Cellular Plastics. 48 (2012) 387–397. doi:10.1177/0021955X12448804.

[12]   S. Jarusombuti, S. Hiziroglu, P. Bauchongkol, V. Fueangvivat, Properties of Sandwich-Type Panels Made from Bamboo and Rice Straw, Forest Products Journal. 59 (2009) 52–57. doi:10.13073/0015-7473-59.10.52.

[13]   Z.A. Abdullah, B.-D. Park, Hydrolytic stability of cured urea-formaldehyde resins modified by additives, Journal of Applied Polymer Science. 114 (2009) 1011–1017. doi:10.1002/app.30713.

[14]   A. Despres, A. Pizzi, C. Vu, L. Delmotte, Colourless formaldehyde-free urea resin adhesives for wood panels, European Journal of Wood and Wood Products. 68 (2010) 13–20. doi:10.1007/s00107-009-0344-y.

[15]   D. Krug, S. Tobisch, Use of proteins as binders for wood-based panels, European Journal of Wood and Wood Products. 68 (2010) 289–301. doi:DOI: 10.1007/s00107-010-0464-4.

[16]   H.R. Mansouri, P. Navarrete, A. Pizzi, S. Tapin-Lingua, B. Benjelloun-Mlayah, H. Pasch, et al., Synthetic-resin-free wood panel adhesives from mixed low molecular mass lignin and tannin, European Journal of Wood and Wood Products. 69 (2011) 221–229. doi:10.1007/s00107-010-0423-0.

[17]   A. Shalbafan, J. Luedtke, J. Welling, H. Thoemen, Comparison of foam core materials in innovative lightweight wood-based panels, European Journal of Wood and Wood Products. 70 (2012) 287–292. doi:10.1007/s00107-011-0552-0.

[18]   J. Luedtke, H. Thoemen, J. Welling, C.M. Barbu, Lightweight wood-based board and process for producing it, WO2008071618 A3, 2008.

[19]   A. Shalbafan, M. Rhême, H. Thoemen, Ultra-light particleboard: characterization of foam core layer by digital image correlation, European Journal of Wood and Wood Products. (2016) 1–11. doi:10.1007/s00107-016-1088-0.

[20]   A. Shalbafan, O. Tackmann, J. Welling, Using of expandable fillers to produce low density particleboard, European Journal of Wood and Wood Products. 74 (2016) 15–22. doi:10.1007/s00107-015-0963-4.

[21]   A. Shalbafan, J. Luedtke, J. Welling, A. Fruehwald, Physiomechanical properties of ultra-lightweight foam core particleboard: different core densities, Holzforschung. 67 (2013) 169. doi:10.1515/hf-2012-0058.

[22]   A. Shalbafan, M.A. Dietenberger, J. Welling, Fire performances of foam core particleboards continuously produced in a one-step process, European Journal of Wood and Wood Products. 71 (2013) 49–59. doi:10.1007/s00107-012-0653-4.

[23]   A. Shalbafan, J. Welling, J. Luedtke, Effect of processing parameters on mechanical properties of lightweight foam core sandwich panels, Wood Material Science and Engineering. 7 (2012) 69–75. doi:10.1080/17480272.2012.661459.

138

[24]   A. Shalbafan, J.T. Benthien, J. Welling, M.C. Barbu, Flat pressed wood plastic composites made of milled foam core particleboard residues, European Journal of Wood and Wood Products. 71 (2013) 805–813. doi:10.1007/s00107-013-0745-9.

[25]   M.A. Dietenberger, A. Shalbafan, J. Welling, C. Boardman, Treated and untreated foam core particleboards with intumescent veneer: Comparative analysis using a cone calorimeter, Journal of Thermal Analysis and Calorimetry. 114 (2013) 979–987. doi:10.1007/s10973-013-3331-9.

[26]   S.-T. Lee, C.B. Park, N.S. Ramesh, Polymeric foams: Science and technology, CRC Press, 2006.

[27]   S.J.D. van Stralen, M.S. Sohal, R. Cole, W.M. Sluyter, Bubble growth rates in pure and binary systems; combined effect of relaxation and evaporation microlayers, International Journal of Heat and Mass Transfer. 18 (1975) 453–461.

[28]   S.P. Nalawade, F. Picchioni, L.P.B.M. Janssen, Supercritical carbon dioxide as a green solvent for processing polymer melts: Processing aspects and applications, Progress in Polymer   Science.   31   (2006)   19–43. doi:http://dx.doi.org/10.1016/j.progpolymsci.2005.08.002.

[29]   L.M. Matuana, Solid state microcellular foamed poly(lactic acid): Morphology and property   characterization,   Bioresource   Technology.   99   (2008)   3643–3650. doi:10.1016/j.biortech.2007.07.062.

[30]   D.L. Tomasko, H.B. Li, D.H. Liu, X.M. Han, M.J. Wingert, L.J. Lee, et al., A review of CO(2) applications in the processing of polymers, Industrial & Engineering Chemistry Research. 42 (2003) 6431–6456. doi:Doi 10.1021/Ie030199z.

[31]   L. Matuana-Malanda, C.B. Park, J.J. Balatinecz, Characterization of Microcellular Foamed PVC/Cellulosic-Fibre Composites, Journal of Cellular Plastics . 32 (1996) 449–469. doi:10.1177/0021955X9603200503.

[32]   Y. Sato, T. Takikawa, A. Sorakubo, S. Takishima, H. Masuoka, M. Imaizumi, Solubility and diffusion coefficient of carbon dioxide in biodegradable polymers, Industrial   &   Engineering   Chemistry   Research.   39   (2000)   4813–4819. doi:10.1016/S0378-3812(99)00153-3.

[33]   J. Von Schnitzler, R. Eggers, Mass transfer in polymers in a supercritical CO2-atmosphere, Journal of Supercritical Fluids. 16 (1999) 81–92. doi:10.1016/S0896-8446(99)00020-0.

[34]   G. Li, H. Li, L.S. Turng, S. Gong, C. Zhang, Measurement of gas solubility and diffusivity   in   polylactide,   Fluid   Phase   Equilibria.   246   (2006)   158–166. doi:10.1016/j.fluid.2006.05.030.

[35]   C.J.G. Plummer, Y. Yonghoon, L. Garin, J.-A.E. Månson, Crystallization of

polylactide during impregnation with liquid CO2, Polymer Bulletin. (2014). doi:10.1007/s00289-014-1262-7.

[36]   N.S. Oliveira, J. Dorgan, J. a. P. Coutinho, a. Ferreira, J.L. Daridon, I.M. Marrucho, Gas solubility of carbon dioxide in poly(lactic acid) at high pressures, Journal of Polymer Science Part B: Polymer Physics. 44 (2006) 1010–1019. doi:10.1002/polb.20746.

[37]   N.S. Oliveira, J. Oliveira, T. Gomes, A. Ferreira, J. Dorgan, I.M. Marrucho, Gas sorption in poly(lactic acid) and packaging materials, Fluid Phase Equilibria. 222–223 (2004) 317–324. doi:10.1016/j.fluid.2004.06.032.

[38]   E. Aionicesei, M. Škerget, Ž. Knez, Measurement of CO2 solubility and diffusivity in poly(l-lactide) and poly(d,l-lactide-co-glycolide) by magnetic suspension balance, Journal of Supercritical Fluids. 47 (2008) 296–301. doi:10.1016/j.supflu.2008.07.011.

[39]   M. O'neill, Q. Cao, M. Fang, Solubility of homopolymers and copolymers in carbon dioxide, Industrial & Engineering Chemistry Research. 5885 (1998) 3067–3079. doi:10.1021/ie980010x.

[40]   C. Boissard, P.-E. Bourban, C.J. Plummer, C. Neagu, J. -a. E. Manson, Cellular Biocomposites from Polylactide and Microfibrillated Cellulose, Journal of Cellular Plastics. 48 (2012) 445–458. doi:10.1177/0021955X12448190.

[41]   J.M.D. Srinivas Siripurapu Saad A. Khan, Richard J. Spontak, Controlled foaming of polymer films through restricted surface diffusion and addition of nanosilica particles of CO2 philic surfactants, Macromulecules. 38 (2005) 2271–2280.

[42]   J.S. Colton, N.P. Suh, The nucleation of microcellular thermoplastic foam with additives: Part I: Theoretical considerations, Polymer Engineering & Science. 27 (1987) 485–492. doi:10.1002/pen.760270702.

[43]   L.M. Mathieu, M.-O. Montjovent, P.-E. Bourban, D.P. Pioletti, J.E. Månson, Bioresorbable composites prepared by supercritical fluid foaming., Journal of Biomedical Materials Research. Part A. 75 (2005) 89–97. doi:10.1002/jbm.a.30385.

[44]   M. Mihai, M.A. Huneault, B.D. Favis, Crystallinity Development in Cellular Poly(lactic acid) in the Presence of Supercritical Carbon Dioxide, Journal of Applied Polymer Science. 113 (2009) 2920–2932. doi:10.1002/app.30338.

[45]   S.T. Chow, Molecular interpretation of glass transition temperature of polymer-diluent systems, Macromolecules. 364 (1980) 362–364.

[46]   E. kee Lee, Novel Manufacturing Processes for Polymer Bead Foams, University of Toronto, 2010.

[47]   J.J. Crevecoeur, L. Nelissen, P.J. Lemstra, Water expandable polystyrene (WEPS): Part 1. Strategy and procedures, Polymer. 40 (1999) 3685–3689.

doi:http://dx.doi.org/10.1016/S0032-3861(98)00617-X.

[48]   J.J. Crevecoeur, L. Nelissen, P.J. Lemstra, Water expandable polystyrene (WEPS): Part 2. In-situ synthesis of (block)copolymer surfactants, Polymer. 40 (1999) 3691–3696. doi:http://dx.doi.org/10.1016/S0032-3861(98)00619-3.

[49]   J.J. Crevecoeur, J.F. Coolegem, L. Nelissen, P.J. Lemstra, Water expandable polystyrene (WEPS): Part 3. Expansion behaviour, Polymer. 40 (1999) 3697–3702. doi:http://dx.doi.org/10.1016/S0032-3861(98)00621-1.

[50]   M. Jonsson, Thermally Expandable Microspheres Prepared Via Suspension Polymerization – Synthesis, characterization and application, KTH Royal Institute of Technology, 2010.

[51]   AkzoNobel,   Expancel   microspheres,   (n.d.) https://www.akzonobel.com/expancel/system/Images/A.

[52]   H. Thoemen, Lightweight panels for the European furniture industry: Some recent developments, in: S. Medved (Ed.), Lightweight Wood Based Composites: Production, Properties and Usage, University of Ljubljana, Ljubljana, 2008.

[53]   M.C. Barbu, J. Lüdtke, J. Welling, J. Heinrich, W. Technology, W. Biology, New Technology for the Continuous Production of Wood- based Lightweight Panels, (2010) 1–10.

[54]   Z. Que, T. Furuno, S. Katoh, Y. Nishino, Effects of urea-formaldehyde resin mole ratio on the properties of particleboard, Building and Environment. 42 (2007) 1257–1263. doi:10.1016/j.buildenv.2005.11.028.

[55]   A.J. Bolton, P.E. Humphrey, The Hot Pressing of Dry-formed Wood-based Composites: Part I. A Review of the Literature, Identifying the Primary Physical Processes and the Nature of their Interaction, Holzforschung. 42 (1988) 403–406. doi:10.1515/hfsg.1988.42.6.403.

[56]   H. Thoemen, P.E. Humphrey, Modeling the physical processes relevant during hot pressing of wood-based composites. Part I. Heat and mass transfer, Holz Als Roh- Und Werkstoff. 64 (2005) 1–10. doi:10.1007/s00107-005-0027-2.

[57]   M. Theis, B. Grohe, Biodegradable lightweight construction boards based on tannin/hexamine bonded hemp shaves, Holz Als Roh- Und Werkstoff. 60 (2002) 291–296. doi:10.1007/s00107-002-0306-0.

[58]   A.S. Herrmann, P.C. Zahlen, I. Zuardy, Sandwich Structures Technology in Commerical Aviation: Present Applications and Future Trends, Sandwich Structures: Advancing with Sandwich Structures and Materials. 7 (2005) 13–26. doi:10.1007/1-4020-3848-8_2.

[59]   ASTM, Space Simulation; Aerospace and Aircraft; Composite Materials, (2007).

[60]   S. a. Kumar, K.S. Ahmed, Flexural behavior of stiffened syntactic foam core sandwich composites, Journal of Sandwich Structures and Materials. 16 (2013) 195–209. doi:10.1177/1099636213512498.

[61]   P.D. Evans, O. Morrison, T.J. Senden, S. Vollmer, R.J. Roberts, A. Limaye, et al., Visualization and numerical analysis of adhesive distribution in particleboard using X-ray micro-computed tomography, International Journal of Adhesion and Adhesives. 30 (2010) 754–762. doi:10.1016/j.ijadhadh.2010.08.001.

[62]   G. Standfest, S. Kranzer, A. Petutschnigg, M. Dunky, Determination of the Microstructure of an Adhesive-Bonded Medium Density Fiberboard (MDF) using 3-D Sub-micrometer Computer Tomography, Journal of Adhesion Science and Technology. 24 (2010) 1501–1514. doi:10.1163/016942410X501052.

[63]   R. Stürzenbecher, K. Hofstetter, G. Schickhofer, J. Eberhardsteiner, Development of high-performance strand boards: multiscale modeling of anisotropic elasticity, Wood Science and Technology. 44 (2009) 205–223. doi:10.1007/s00226-009-0259-0.

[64]   M.F. Ashby, R.F.M. Medalist, The mechanical properties of cellular solids, Metallurgical Transactions A. 14 (1983) 1755–1769. doi:10.1007/BF02645546.

[65]   M.J. Silva, L.J. Gibson, The effects of non-periodic microstructure and defects on the compressive strength of two-dimensional cellular solids, International Journal of Mechanical Sciences. 39 (1997) 549–563. doi:10.1016/S0020-7403(96)00065-3.

[66]   a. E. Simone, L.J. Gibson, The effects of cell face curvature and corrugations on the stiffness and strength of metallic foams, Acta Materialia. 46 (1998) 3929–3935. doi:10.1016/S1359-6454(98)00072-X.

[67]   J.L. Grenestedt, K. Tanaka, Influence of cell shape variations on elastic stiffness of closed cell cellular solids, Scripta Materialia. 40 (1998) 71–77. doi:10.1016/S1359-6462(98)00401-1.

[68]   J.L. Grenestedt, F. Bassinet, Influence of cell wall thickness variations on elastic stiffness of closed-cell cellular solids, International Journal of Mechanical Sciences. 42 (2000) 1327–1338. doi:10.1016/S0020-7403(99)00054-5.

[69]   J.C. Halpin, J.L. Kardos, The Halpin-Tsai Equations: A Review, Polymer Engineering & Science. 16 (1976) 344–352.

[70]   R.C. Neagu, M. Cuenoud, F. Berthold, P.-E. Bourban, E.K. Gamstedt, M. Lindstrom, et al., The potential of wood fibers as reinforcement in cellular biopolymers, Journal of Cellular Plastics. 48 (2012) 71–103. doi:10.1177/0021955X11431172.

[71]   H. Ku, H. Wang, et al., A Review on the Tensile Properties of Natural Fibre Reinforced Polymer Composites, Igarss 2014. (2014) 1–5. doi:10.1007/s13398-014-0173-7.2.

[72]   A.G. Facca, M.T. Kortschot, N. Yan, Predicting the elastic modulus of natural fibre reinforced thermoplastics, Composites Part A: Applied Science and Manufacturing. 37 (2006) 1660–1671. doi:10.1016/j.compositesa.2005.10.006.

[73]   K. Parker, J.-P. Garancher, S. Shah, a. Fernyhough, Expanded polylactic acid - an eco-friendly alternative to polystyrene foam, Journal of Cellular Plastics. 47 (2011) 233–243. doi:10.1177/0021955X11404833.

[74]   D. Garlotta, A Literature Review of Poly(Lactic Acid), Journal of Polymers and the Environment. 9 (2001) 63–84. doi:10.1023/A:1020200822435.

[75]   B. Gupta, N. Revagade, J. Hilborn, Poly(lactic acid) fiber: An overview, Progress in Polymer Science. 32 (2007) 455–482. doi:10.1016/j.progpolymsci.2007.01.005.

[76]   a. P. Gupta, V. Kumar, New emerging trends in synthetic biodegradable polymers – Polylactide: A critique, European Polymer Journal. 43 (2007) 4053–4074. doi:10.1016/j.eurpolymj.2007.06.045.

[77]   B.R.E. Drumright, P.R. Gruber, D.E. Henton, Polylactic Acid Technology, Advanced Materials. 48674 (2000) 1841–1846.

[78]   J. Lunt, Large-scale production, properties and commercial applications of polylactic acid polymers, 3910 (1998) 145–152.

[79]   H. Tsuji, S. Miyauchi, Poly (l -lactide): VI E   ects of crystallinity on enzymatic hydrolysis of poly (l -lactide) without free amorphous region, Polymer Degradation and Stability. 71 (2001) 415–424.

[80]   K. Jamshidi, Y. Ikada, Thermal characterization of polylactides, 29 (1988) 2229–2234.

[81]   J.R. Dorgan, H. Lehermeier, M. Mang, Thermal and Rheological Properties of Commercial-Grade Poly (Lactic Acid) s, 8 (2000) 1–9.

[82]   Y. Di, S. Iannace, E. Di Maio, L. Nicolais, Reactively Modified Poly(lactic acid): Properties and Foam Processing, Macromolecular Materials and Engineering. 290 (2005) 1083–1090. doi:10.1002/mame.200500115.

[83]   T. Fujiwara, T. Yamaoka, Y. Kimura, K.J. Wynne, Biomacromolecules 2005, 6, 2370 - 2373 Poly(lactide) Swelling and Melting Behavior in Supercritical Carbon Dioxide and Post-Venting Porous Material, (2005) 2370–2373.

[84]   S.T. Lee, L. Kareko, J. Jun, Study of Thermoplastic PLA Foam Extrusion, Journal of Cellular Plastics. 44 (2008) 293–305. doi:10.1177/0021955X08088859.

[85]   J. Wang, W. Zhu, H. Zhang, C.B. Park, Continuous processing of low-density, microcellular poly(lactic acid) foams with controlled cell morphology and crystallinity, Chemical   Engineering   Science.   75   (2012)   390–399. doi:http://dx.doi.org/10.1016/j.ces.2012.02.051.

[86]   K. Taki, D. Kitano, M. Ohshima, Effect of growing crystalline phase on bubble nucleation in poly(L -lactide)/CO2 batch foaming, Industrial and Engineering Chemistry Research. 50 (2011) 3247–3252. doi:10.1021/ie101637f.

[87]   M. Nofar, A. Ameli, C.B. Park, Development of polylactide bead foams with double crystal melting peaks, Polymer (United Kingdom). 69 (2015) 83–94. doi:10.1016/j.polymer.2015.05.048.

[88]   M. Nofar, Y. Guo, C.B. Park, Double crystal melting peak generation for expanded polypropylene bead foam manufacturing, Industrial and Engineering Chemistry Research. 52 (2013) 2297–2303. doi:10.1021/ie302625e.

[89]   A. Ameli, D. Jahani, M. Nofar, P.U. Jung, C.B. Park, Processing and characterization of solid and foamed injection-molded polylactide with talc, Journal of Cellular Plastics. Online ver (2013) 1–24. doi:10.1177/0021955X13481993.

[90]   S. Pilla, S. Gong, E. O'Neill, L. Yang, R.M. Rowell, Polylactide-Recycled Wood Fiber Composites, Journal of Applied Polymer Science. 111 (2009) 37–47. doi:10.1002/app.28860.

[91]   S. Pilla, A. Kramschuster, J. Lee, G.K. Auer, S. Gong, L.-S. Turng, Microcellular and Solid Polylactide–Flax Fiber Composites, Composite Interfaces. 16 (2009) 869–890. doi:10.1163/092764409X12477467990283.

[92]   D.J. Kang, D. Xu, Z.X. Zhang, K. Pal, D.S. Bang, J.K. Kim, Well-controlled microcellular biodegradable PLA/Silk composite foams using supercritical CO2, Macromolecular Materials and Engineering. 294 (2009) 620–624. doi:10.1002/mame.200900103.

[93]   L.M. Matuana, O. Faruk, Effect of gas saturation conditions on the expansion ratio of microcellular poly (lactic acid)/wood-flour composites, Express Polymer Letters. 4 (2010) 621–631. doi:10.3144/expresspolymlett.2010.77.

[94]   C.B. Park, D.F. Baldwin, N.P. Suh, Effect of the pressure drop rate on cell nucleation in continuous processing of microcellular polymers, Polymer Engineering & Science. 35 (1995) 432–440. doi:10.1002/pen.760350509.

[95]   P. Rachtanapun, S.E.M. Selke, L.M. Matuana, Microcellular foam of polymer blends of HDPE/PP and their composites with wood fiber, Journal of Applied Polymer Science. 88 (2003) 2842–2850. doi:10.1002/app.12170.

[96]   M. Shimbo, I. Higashitani, Y. Miyano, Mechanism of strength improvement of foamed plastics having fine cell, Journal of Cellular Plastics. 43 (2007) 157–167. doi:10.1177/0021955x06075585.

[97]   K.A. Seeler, V. Kumar, Tension-Tension Fatigue of Microcellular Polycarbonate: Initial Results, Journal of Reinforced Plastics and Composites . 12 (1993) 359–376.

doi:10.1177/073168449301200308.

[98] J.A. Martinez-Diez, M.A. Rodriguez-Perez, O.A. Almanza, The Thermal Conductivity of a Polyethylene Foam Block Produced by a Compression Molding Process, Journal of Cellular Plastics. 37 (2001) 21–42. doi:10.1106/D0MJ-HJH8-5YDQ-H5VB.

[99] W.G. Zheng, Y.H. Lee, C.B. Park, Use of Nanoparticles for Improving the Foaming Behaviors of Linear PP, Journal of Applied Polymer Science. 117 (2010) 2972–2979.

[100] Y. Ema, M. Ikeya, M. Okamoto, Foam processing and cellular structure of polylactide-based nanocomposites, Polymer. 47 (2006) 5350–5359. doi:10.1016/j.polymer.2006.05.050.

[101] Y. Fujimoto, S. Sinha Ray, M. Okamoto, A. Ogami, K. Yamada, K. Ueda, Well-controlled biodegradable nanocomposite foams: From microcellular to nanocellular, Macromolecular Rapid Communications. 24 (2003) 457–461. doi:10.1002/marc.200390068.

[102] J. Reignier, R. Gendron, M.F. Champagne, Extrusion Foaming of Poly (Lactic acid) Blown with CO2 : Toward 100 % Green Material NRC Publications Archive (NPArC), Cellular Polymers. 26 (2007) 83–115.

[103] R. Auras, B. Harte, S. Selke, An overview of polylactides as packaging materials, Macromolecular Bioscience. 4 (2004) 835–864. doi:10.1002/mabi.200400043.

[104] M. Mihai, M.A. Huneault, D.B. Favis, Rheology and Extrusion Foaming of Chain-Branched Poly(lactic acid), Polymer Engineering & Science. (2009). doi:10.1002/pen.21561.

[105] S. Pilla, A. Kramschuster, J. Lee, C. Clemons, S. Gong, L.S. Turng, Microcellular processing of polylactide-hyperbranched polyester-nanoclay composites, Journal of Materials Science. 45 (2010) 2732–2746. doi:10.1007/s10853-010-4261-6.

[106] S.-S. Hwang, P.P. Hsu, J.-M. Yeh, K.-C. Chang, Y.-Z. Lai, The Mechanical/Thermal Properties of Microcellular Injection-Molded Poly-Lactic-Acid Nanocomposites, Polymer CompositesPolymer Composites. (2009). doi:10.1002/pc.20736.

[107] A. Ameli, M. Nofar, D. Jahani, G. Rizvi, C.B. Park, Development of high void fraction polylactide composite foams using injection molding: Crystallization and foaming behaviors, Chemical Engineering Journal. 262 (2015) 78–87. doi:10.1016/j.cej.2014.09.087.

[108] M. Cuenoud, P.-E. Bourban, C.J. Plummer, J. -a. E. Manson, Plasticization of polylactide foams for tissue engineering, Journal of Cellular Plastics. 48 (2012) 409–432. doi:10.1177/0021955X12447941.

[109] M. Cuénoud, P.-E. Bourban, C.J.G. Plummer, J.-A.E. Månson, Plasticization of poly-L-lactide for tissue engineering, Journal of Applied Polymer Science. 121 (2011)

2078–2088. doi:10.1002/app.33835.

[110] M. Cuénoud, Hybrid Polymer Foams for Osteochondral Tissue Engineering, EPFL, 2012. doi:10.5075/epfl-thesis-5495.

[111] L.M. Mathieu, T.L. Mueller, P.-E. Bourban, D.P. Pioletti, R. Müller, J.-A.E. Månson, Architecture and properties of anisotropic polymer composite scaffolds for bone tissue engineering., Biomaterials. 27 (2006) 905–16. doi:10.1016/j.biomaterials.2005.07.015.

[112] M. Bühler, P.-E. Bourban, J.-A.E. Månson, Cellular thermoplastic composites with microstructural gradients of fibres and porosity, Composites Science and Technology. 68 (2008) 820–828. doi:http://dx.doi.org/10.1016/j.compscitech.2007.08.028.

[113] M. Bühler, P.-E. Bourban, J.-A.E. Månson, Cellular composites based on continuous fibres and bioresorbable polymers, Composites Part A: Applied Science and Manufacturing. 39 (2008) 1779–1786. doi:http://dx.doi.org/10.1016/j.compositesa.2008.05.020.

[114] C. Delabarde, C.G. Plummer, P.-E. Bourban, J.-A. Månson, Biodegradable polylactide/hydroxyapatite nanocomposite foam scaffolds for bone tissue engineering applications, Journal of Materials Science: Materials in Medicine. 23 (2012) 1371–1385. doi:10.1007/s10856-012-4619-1.

[115] R.C. Neagu, M. Cuénoud, F. Berthold, P.-E. Bourban, E.K. Gamstedt, M. Lindström, et al., Processing and Mechanical Properties of Novel Wood Fibre Composites Foams, ICCM 17 Proceedings. (2009).

[116] S. Weal, Heat Stability of Polylactic Acid - Based Foams and its Measurement, in: Biofoams 2011 Conference, Capri, Italy, 2011.

[117] J. Noordegraaf, J. De Jong, P. De Bruijn, R. Hartmann, BIOFOAM ® : PLA PARTICLE FOAM (FURTHER) EXPANDING IN EUROPE, in: International Conference Particle Foam Conference, Berlin, Germany, 2012.

[118] R. Gendron, J. Reignier, J. Tatibouët, Effect of Dissolved Carbon Dioxide on the Glass Transition and Crystallization of Poly (lactic acid) as Probed by Ultrasonic Measurements, Journal of Applied Polymer Science. 112 (2009) 1345–1355. doi:10.1002/app.

[119] J. Crank, The mathematics of diffusion, 2nd ed., Oxford university press, London, 1975.

[120] J. Crank, G.S. Park, Diffusion in polymers, Academic Press, London and New York, 1968.

[121] S. Zhou, S.A. Stern, The effect of plasticization on the transport of gases in and through glassy polymers, Journal of Polymer Science Part B: Polymer Physics. 27 (1989) 205–222. doi:10.1002/polb.1989.090270201.

[122] J.-C. Huang, H. Liu, Y. Liu, Diffusion in Polymers with Concentration Dependent Diffusivity, International Journal of Polymeric Materials and Polymeric Biomaterials. 49 (2001) 15–24. doi:10.1080/00914030108035864.

[123] M. Minelli, G.C. Sarti, Permeability and diffusivity of CO2 in glassy polymers with and without plasticization, Journal of Membrane Science. 435 (2013) 176–185. doi:http://dx.doi.org/10.1016/j.memsci.2013.02.013.

[124] H. Hajova, J. Chmelar, A. Nistor, T. Gregor, J. Kosek, Experimental Study of Sorption and Diffusion of n-Pentane in Polystyrene, Journal of Chemical & Engineering Data. 58 (2013) 851–865. doi:10.1021/je300916f.

[125] R. Pini, G. Storti, M. Mazzotti, H. Tai, K.M. Shakesheff, S.M. Howdle, Sorption and swelling of poly(DL-lactic acid) and poly(lactic-co-glycolic acid) in supercritical CO2: An experimental and modeling study, Journal of Polymer Science Part B: Polymer Physics. 46 (2008) 483–496. doi:10.1002/polb.21382.

[126] J.D. Ferry, Viscoelastic properties of polymers, 3rd ed., John Wiley & Sons, Ltd, 1980.

[127] D. Ehlich, H. Sillescu, Tracer diffusion at the glass transition, Macromolecules. 23 (1990) 1600–1610. doi:10.1021/ma00208a008.

[128] W.J. Koros, Barrier Polymers and Structures: Overview, in: Barrier Polymers and Structures, American Chemical Society, 1990: p. 1. doi:doi:10.1021/bk-1990-0423.ch001.

[129] T. Alfrey, E.F. Gurnee, W.G. Lloyd, Diffusion in glassy polymers, Journal of Polymer Science Part C: Polymer Symposia. 12 (1966) 249–261. doi:10.1002/polc.5070120119.

[130] H.L. Frisch, T.T. Wang, T.K. Kwei, Diffusion in glassy polymers. II, Journal of Polymer Science Part A-2: Polymer Physics. 7 (1969) 879–887. doi:10.1002/pol.1969.160070512.

[131] A. Peterlin, Diffusion in a network with discontinuous swelling, Journal of Polymer Science Part B: Polymer Letters. 3 (1965) 1083–1087. doi:10.1002/pol.1965.110031222.

[132] N.L. Thomas, A.H. Windle, A theory of case II diffusion, Polymer. 23 (1982) 529–542. doi:http://dx.doi.org/10.1016/0032-3861(82)90093-3.

[133] M. Hedenqvist, U.W. Gedde, Diffusion of small-molecule penetrants in semicrystalline polymers, Progress in Polymer Science. 21 (1996) 299–333. doi:http://dx.doi.org/10.1016/0079-6700(95)00022-4.

[134] H.L. Frisch, Sorption and transport in glassy polymers–a review, Polymer Engineering & Science. 20 (1980) 2–13. doi:10.1002/pen.760200103.

[135] C.E. Rogers, Permeation of Gases and Vapours in Polymers, in: J. Comyn (Ed.),

Polymer Permeability SE - 2, Springer Netherlands, 1985: pp. 11–73. doi:10.1007/978-94-009-4858-7_2.

[136] T.M. Aminabhavi, U.S. Aithal, S.S. Shukla, An Overview of the Theoretical Models Used to Predict Transport of Small Molecules through Polymer Membranes, Journal of Macromolecular Science, Part C. 28 (1988) 421–474. doi:10.1080/15583728808085382.

[137] S. Alexander Stern, Polymers for gas separations: the next decade, Journal of Membrane Science. 94 (1994) 1–65. doi:http://dx.doi.org/10.1016/0376-7388(94)00141-3.

[138] M.H. Klopffer, B. Flaconneche, Transport Properdines of Gases in Polymers: Bibliographic Review, Oil & Gas Science and Technology - Rev. IFP 56 (2001) 223–244. doi:http://dx.doi.org/10.2516/ogst:2001021.

[139] C. Delabarde, C.J.G. Plummer, P.E. Bourban, J.A.E. Månson, Accelerated ageing and degradation in poly-L-lactide/hydroxyapatite nanocomposites, Polymer Degradation and Stability. 96 (2011) 595–607. doi:10.1016/j.polymdegradstab.2010.12.018.

[140] Y. Ikada, K. Jamshidi, H. Tsuji, S.H. Hyon, Stereocomplex formation between enantiomeric poly(lactides), Macromolecules. 20 (1987) 904–906. doi:10.1021/ma00170a034.

[141] R.M. Rasal, A. V. Janorkar, D.E. Hirt, Poly(lactic acid) modifications, Progress in Polymer Science. 35 (2010) 338–356. doi:10.1016/j.progpolymsci.2009.12.003.

[142] B. Imre, B. Pukánszky, Compatibilization in bio-based and biodegradable polymer blends, European Polymer Journal. 49 (2013) 1215–1233. doi:10.1016/j.eurpolymj.2013.01.019.

[143] B. Imre, K. Renner, B. Pukánszky, Interactions , structure and properties in poly (lactic acid)/ thermoplastic polymer blends, Express Polymer Letters. 8 (2014) 2–14. doi:10.3144/expresspolymlett.2014.

[144] G. Zhang, J. Zhang, S. Wang, D. Shen, Miscibility and phase structure of binary blends of polylactide and poly(methyl methacrylate), Journal of Polymer Science Part B: Polymer Physics. 41 (2003) 23–30. doi:10.1002/polb.10353.

[145] C. Samuel, J. Cayuela, I. Barakat, A.J. Müller, J.-M. Raquez, P. Dubois, Stereocomplexation of polylactide enhanced by poly(methyl methacrylate): improved processability and thermomechanical properties of stereocomplexable polylactide-based materials., ACS Applied Materials & Interfaces. 5 (2013) 11797–807. doi:10.1021/am403443m.

[146] S. Hirota, T. Sato, Y. Tominaga, S. Asai, M. Sumita, The effect of high-pressure carbon dioxide treatment on the crystallization behavior and mechanical properties of

poly(l-lactic acid)/poly(methyl methacrylate) blends, Polymer. 47 (2006) 3954–3960. doi:10.1016/j.polymer.2006.03.069.

[147] T. Shirahase, Y. Komatsu, Y. Tominaga, S. Asai, M. Sumita, Miscibility and hydrolytic degradation in alkaline solution of poly(l-lactide) and poly(methyl methacrylate) blends, Polymer. 47 (2006) 4839–4844. doi:10.1016/j.polymer.2006.04.012.

[148] B. Yao, A. V Nawaby, X. Liao, R. Burk, Physical Characteristics of PLLA/PMMA Blends and Their CO2 Blowing Foams, Journal of Cellular Plastics. 43 (2007) 385–398. doi:10.1177/0021955x07079209.

[149] S.-H. Li, E.M. Woo, Immiscibility–miscibility phase transitions in blends of poly(L-lactide) with poly(methyl methacrylate), Polymer International. 57 (2008) 1242–1251. doi:10.1002/pi.2469.

[150] S.-H. Li, E.M. Woo, Effects of chain configuration on UCST behavior in blends of poly(L-lactic acid) with tactic poly(methyl methacrylate)s, Journal of Polymer Science Part B: Polymer Physics. 46 (2008) 2355–2369. doi:10.1002/polb.21567.

[151] M. Canetti, A. Cacciamani, F. Bertini, Miscible blends of polylactide and poly(methyl methacrylate): Morphology, structure, and thermal behavior, Journal of Polymer Science Part B: Polymer Physics. 52 (2014) 1168–1177. doi:10.1002/polb.23544.

[152] C. Samuel, J.-M. Raquez, P. Dubois, PLLA/PMMA blends: A shear-induced miscibility with tunable morphologies and properties?, Polymer. 54 (2013) 3931–3939. doi:http://dx.doi.org/10.1016/j.polymer.2013.05.021.

[153] D. Velasco, L. Benito, M. Fernández-Gutiérrez, J. San Román, C. Elvira, Preparation in supercritical CO2 of porous poly(methyl methacrylate)–poly(l-lactic acid) (PMMA–PLA) scaffolds incorporating ibuprofen, The Journal of Supercritical Fluids. 54 (2010) 335–341. doi:10.1016/j.supflu.2010.05.012.

[154] E.W. Fischer, H. Sterzel, G. Wegner, Investigation of the structure of solution grown crystals of lactide copolymers by means of chemical reactions, Kolloid-Zeitschrift Und Zeitschrift Für Polymere. 251 (1973) 980–990. doi:10.1007/BF01498927.

[155] W. Brostow, R. Chiu, I.M. Kalogeras, A. Vassilikou-Dova, Prediction of glass transition temperatures: Binary blends and copolymers, Materials Letters. 62 (2008) 3152–3155. doi:10.1016/j.matlet.2008.02.008.

[156] D. Herrera, J.C. Zamora, A. Bello, M. Grimau, E. Laredo, A.J. Müller, et al., Miscibility and crystallization in polycarbonate/poly(ε-caprolactone) blends: Application of the self-concentration model, Macromolecules. 38 (2005) 5109–5117. doi:10.1021/ma050481c.

[157] M.-J. Brekner, H.A. Schneider, H.-J. Cantow, Approach to the composition

dependence of the glass transition temperature of compatible polymer blends: 1, Polymer. 29 (1988) 78–85. doi:10.1016/0032-3861(88)90203-0.

[158] T.P. Lodge, T.C.B. McLeish, Self-Concentrations and Effective Glass Transition Temperatures in Polymer Blends, Macromolecules. 33 (2000) 5278–5284. doi:10.1021/ma9921706.

[159] D.W. Grijpma, J.P. Penning, a. J. Pennings, Chain entanglement, mechanical properties and drawability of poly(lactide), Colloid & Polymer Science. 272 (1994) 1068–1081. doi:10.1007/BF00652375.

[160] V. Subramanian, P. Samuel Asirvatham, R. Balakrishnan, T. Ramasami, Molecular mechanics studies on polypropylene and polymethylmethacrylate polymers, Chemical Physics Letters. 342 (2001) 603–609. doi:10.1016/S0009-2614(01)00620-0.

[161] B. Krause, K. Diekmann, N.F. a. van der Vegt, M. Wessling, Open Nanoporous Morphologies from Polymeric Blends by Carbon Dioxide Foaming, Macromolecules. 35 (2002) 1738–1745. doi:10.1021/ma011672s.

[162] F. Yu, T. Liu, X. Zhao, X. Yu, Effects of talc on the mechanical and thermal properties of polylactide, Journal of Applied Polymer Science. 125 (2012) E99–E109. doi:10.1002/app.

[163] S. Bhattacharya, R.K. Gupta, S.N. Bhattacharya, Role of clay in compatibilization of immiscible high melt strength polypropylene and ethylene vinyl acetate copolymer blends, Polymer Engineering & Science. (2010) 1350–1357. doi:10.1002/pen.

[164] L.J. Gibson, M.F. Ashby, Cellular solids Structure and Properties, 2nd ed., Cambridge University Press, 1999.

[165] Y. Yoon, C.J.G. Plummer, J.-A.E. Månson, Solid heat-expandable polylactide-poly(methyl methacrylate) foam precursors prepared by immersion in liquid carbon dioxide, Journal of Materials Science. 50 (2015) 7208–7217. doi:10.1007/s10853-015-9275-7.

[166] M.S. Huda, L.T. Drzal, M. Misra, a. K. Mohanty, Wood-fiber-reinforced poly(lactic acid) composites: Evaluation of the physicomechanical and morphological properties, Journal of Applied Polymer Science. 102 (2006) 4856–4869. doi:10.1002/app.24829.

[167] A. IWATAKE, M. NOGI, H. YANO, Cellulose nanofiber-reinforced polylactic acid, Composites Science and Technology. 68 (2008) 2103–2106. doi:10.1016/j.compscitech.2008.03.006.

[168] A.K. Bledzki, A. Jaszkiewicz, D. Scherzer, Mechanical properties of PLA composites with man-made cellulose and abaca fibres, Composites Part A: Applied Science and Manufacturing. 40 (2009) 404–412. doi:10.1016/j.compositesa.2009.01.002.

[169] K.M. Bogren, E.K. Gamstedt, R.C. Neagu, M. AAkerholm, M. LindstroOm,

Dynamic-Mechanical Properties of Wood-Fiber Reinforced Polylactide: Experimental Characterization and Micromechanical Modeling, Journal of Thermoplastic Composite Materials. 19 (2006) 613–637. doi:10.1177/0892705706067480.

[170] A.P. Mathew, K. Oksman, M. Sain, The effect of morphology and chemical characteristics of cellulose reinforcements on the crystallinity of polylactic acid, Journal of Applied Polymer Science. 101 (2006) 300–310. doi:10.1002/app.23346.

[171] R.C. Neagu, Stiffness Contribution of Various Wood Fibers to Composite Materials, Journal of Composite Materials. 40 (2005) 663–699. doi:10.1177/0021998305055276.

[172] C. (Calvin) Sun, True density of microcrystalline cellulose, Journal of Pharmaceutical Sciences. 94 (2005) 2132–2134. doi:10.1002/jps.20459.

[173] S.J. Eichhorn, R.J. Young, The Young's modulus of a microcrystalline cellulose, Celluslose. 8 (2001) 197–207.

[174] B.S. Ndazi, S. Karlsson, Characterization of hydrolytic degradation of polylactic acid/rice hulls composites in water at different temperatures, Express Polymer Letters. 5 (2011) 119–131. doi:10.3144/expresspolymlett.2011.13.

[175] J.C. Halpin, J.L. Kardos, The Halpin-Tsai equations: A review, Polymer Engineering and Science. 16 (1976) 344–352. doi:10.1002/pen.760160512.

[176] A.P. Mathew, K. Oksman, M. Sain, Mechanical properties of biodegradable composites from poly lactic acid (PLA) and microcrystalline cellulose (MCC), Journal of Applied Polymer Science. 97 (2005) 2014–2025. doi:10.1002/app.21779.

[177] L. Avérous, C. Fringant, L. Moro, Plasticized starch-cellulose interactions in polysaccharide composites, Polymer. 42 (2001) 6565–6572. doi:10.1016/S0032-3861(01)00125-2.

[178] S. Doroudiani, C.E. Chaffey, M.T. Kortschot, Sorption and diffusion of carbon dioxide in wood-fiber/polystyrene composites, Journal of Polymer Science, Part B: Polymer Physics. 40 (2002) 723–735. doi:10.1002/polb.10129.

[179] M. Nofar, C.B. Park, Poly (lactic acid) foaming, Progress in Polymer Science. 39 (2014) 1721–1741. doi:10.1016/j.progpolymsci.2014.04.001.

[180] M. Nofar, Expanded PLA Bead Foaming : Analysis of Crystallization Kinetics and Development of a Novel Technology, University of Toronto, 2013.

Appendix 1

Following Huang J.-C. *et al.* [122], for sorption into a semi-infinite plate with $c[t, 0] = c_o$ and $c[0, x > 0] = 0$, equations (4.1) and (4.2) may be rewritten as

$$u \frac{d^2 u}{d\xi^2} = -2\xi \frac{du}{d\xi} \qquad \text{(A1)}$$

where

$$D = D[0] \exp[Ac_0] u; \quad u = \exp[A(c - c_0)]; \quad \xi = \frac{x}{\sqrt{D[0]t}} \exp\left[-\frac{Ac_0}{2}\right] \qquad \text{(A2)}$$

so that $u \rightarrow exp[-Ac_0]$ in the limit $\xi \rightarrow \infty$, and the initial and boundary conditions are

$$u[0] = 1; \quad \frac{du}{d\xi}[0] = -u'[0] \qquad \text{(A3)}$$

$u'[0]$ may be related to Ac_0 by solving equation (A1) for different $u'[0]$, and determining the limiting value of u at large ξ. $u'[0]$ obtained using the Euler method could be interpolated in the range 0–8, i.e. the range of interest for the present work, using a fourth-order polynomial, $u'[0]=-0.001(Ac_o)^4 + 0.0213(Ac_0)^3 - 0.1842(Ac_0)^2 + 1.1064(Ac_0)$. The amount of solute that has entered the semiinfinite plate after time t was then calculated from [122]

$$\int_0^t J dt = \frac{\sqrt{D[0]}}{A} u'[0] exp\left[\frac{Ac_0}{2}\right] t^{1/2} \qquad \text{(A4)}$$

Hence, for times very much less than the time to reach saturation, $X[t]$ as defined by equation (4.3) for a wide specimen of finite thickness l, normalized with respect to $X[t]$ at saturation, is approximately

$$\frac{X[t]}{X[\infty]} = \frac{2\sqrt{D[0]}}{Ac_0 l} u'[0] \exp\left[\frac{Ac_0}{2}\right] t^{1/2} \qquad \text{(A5)}$$

Assuming that the overall concentration dependence of the diffusion coefficient depends on the CO_2 concentration of the amorphous phase, i.e. the crystalline phase contributes to $D[0]$ only (via the tortuosity effect), and Ac_0 in equation (A5) should be independent of the degree of crystallinity.

Publications related to this work

Journal papers

1. <u>Yoon, Y.</u>, Plummer, C. J., Thoemen, H. & Manson, J.-A. E. Liquid CO_2 processing of solid polylactide foam precursors. Journal of Cellular Plastics. 2014. doi:10.1177/0021955X14537662

2. Christopher J.G. Plummer, <u>Yoon Yonghoon</u>, Léo Garin, Jan-Anders E. Månson. Crystallization of polylactide during impregnation with liquid CO_2, Polymer bulletin. 72 (2015) 103-116

3. <u>Yoon, Y.</u>, Plummer, C. J. & Manson, J.-A. E. Solid state polylactide-poly (methyl methacrylate) foam precursors prepared by immersion in liquid CO_2, Journal of Materials Science. 50 (2015) 7208-

Conferences

1. <u>Yonghoon Yoon</u>, Christopher J.G. Plummer, Heiko Thömen, Jan-Anders E. Månson, Solid bio-based precursors for one-step processing of foam sandwich composites. Society for the advancement of material and process engineering (SAMPE) Europe student conference 2014, Paris (2014)

2. <u>Yonghoon Yoon</u>, Jože Smole, Martin Rhême, Heiko Thömen, Christopher J.G. Plummer, Jan-Anders E. Månson, Solid state poly(lactide)-poly(methyl methacrylate) precursors for the in-line production of foam core sandwich structures, 20th International Conference on Composite Materials (ICCM), Copenhagen (2015).

Curriculum vitae

Yonghoon Yoon   Date of birth: 9th March 1980

Av. Louis-Ruchonnet 20 1003 Lausanne   Nationality: Korean

toughmo@gmail.com   Language: Korean and English

Education

10/2012-09/2016	**Swiss Federal Institute of Technology in Lausanne (EPFL)**, Lausanne Switzeralnd

- Laboratory of Polymer and Composite Technology (LTC)
- Prof. Jan-Anders Månson
- PhD thesis: CO_2 foamed biopolymers for sandwich structures

03/2003-02/2005	**Seoul National University (SNU)**, Seoul, Korea

- Textile & Composites Laboratory
- Prof. Tae Jin Kang
- Master thesis: Low velocity impact properties of 3-D braided glass/epoxy composites

03/1999-02/2003	**Seoul National University (SNU)**, Seoul, Korea

- Department of Materials science and Engineering (MSE)

Work experience

01/2005-09/2016	**LG Hausys** (spin-off from LG Chem in 2009) R&D center, Anyang, Korea

- Automotive component project

LG Chem Ltd. R&D center, Daejeon, Korea

- Automotive component project